TRACK DETECTOR STUDIES USING CR-39, OPT AND X-RAY FILMS

Thesis submitted to the University of Calicut

In partial fulfillment of the requirements

for the Degree of

DOCTOR OF PHILOSOPHY

IN PHYSICS

By

SR. LILLY.C.M.

DEPARTMENT OF PHYSICS

UNIVERSITY OF CALICUT

2003

TO

MY PARENTS

AND

TEACHERS

Dr. K. M. Varier
Department of Physics
Professor
University of Calicut

CERTIFICATE

This is to certify that this thesis entitled `Track Detector studies using CR-39, OPT and X-ray films' is a bonafide record of research work carried out by Sr. Lilly. C.M. under my supervision for the award of the Ph. D degree of University of Calicut and that no part of this thesis has been presented elsewhere for the award of any degree, diploma or other similar title.

Calicut University

K. M. Varier

30th April 2003

(Dr. K. M. Varier)

DECLARATION

I hereby declare that this thesis entitled ` Track Detector studies using CR-39, OPT and X-ray films' is a bonafide record of research work done by me and that no part of this thesis has been presented before for the award of any degree or diploma.

Calicut University
30th April 2003

Sr. Lilly. C. M.
(Sr. Lilly. C. M.)

ACKNOWLEDGEMENTS

I express my deep and sincere gratitude to Dr. K. Muraleedhara Varier, Professor, Dept. of Physics, for suggesting this problem and for guiding me throughout the research work. He has always been a source of inspiration and encouragement to me.

I wish to express my sincere thanks to Dr. K. Neelakandan, Professor and Head of the Department of Physics, for providing the necessary facilities during the research period, and for his encouragement.

I am also thankful to my provincial superior and other sisters who inspired me to do this work..

I owe my thanks to all members of the teaching and non-teaching staff and friends in the department for their cooperation.

I am indebted to Sr. Valsa A.T., Principal Carmel College, Mala for deputing me for Ph.. D course and to the University Grants Commission, Govt. of India, for providing the financial assistance under the FIP scheme.

Sr.Lilly.C.M.

LIST OF FIGURES

LIST OF TABLES

Papers Presented at Conferences etc.

1. "Neutron Slowing down Studies in Paraffin using CR-39 Track Detector.", **Sr. C. M. Lilly**, Antony Joseph and K. M. Varier.
Proceedings of 13th National Symposium on Radiation Physics, Dec21-23,1999 at Mangalore University. P. 527-530.

2. "Some Numerical Calculations on Etched Track Properties in SSNTDs.", **Sr. C. M. Lilly**, Antony Joseph and K. M. Varier.
Book of Abstracts, 12th National Symposium on Solid State Nuclear Track Detectors (SSNTDs), Oct 29-31,2001 at D.A.V. collage, Jalandhar.p.30

3. "Neutron Induced Reaction Studies in Boron and Copper using CR-39 Track Detector.", **Sr. C. M. Lilly**, Antony Joseph and K. M. Varier.
Book of Abstracts, 12th National Symposium on Solid State Nuclear Track Detectors (SSNTDs), Oct 29-31,2001 at D.A.V. collage, Jalandhar.p.59

4. "Use of Overhead Transparency Sheet as a Heavy ion Track Detector.", **Sr. C. M. Lilly**, K. M. Varier and Antony Joseph
Communicated to Indian Journal of Physics.

CONTENTS

CHAPTER I

INTRODUCTION

The field of Solid State Nuclear Track Detection (SSNTD) had its origin in the year 1958 when first observations were reported by Young [1] at AERE Harwell. He noticed that when lithium fluoride crystals, held 1 mm away from uranium oxide film, were irradiated, a number of shallow etch pits appeared after treatment with a chemical reagent (HF + CH_3 COOH), saturated with FeF_3. Further, the number of these pits, as seen under the optical and electron microscope, had a one to one correspondence with the theoretically estimated number of fission fragments recoiling into the crystal from the uranium foil. A particle detector was thus born but its potential was not realized until three years later. In this short paper in Nature [1], Young had recognized the existence of tracks, demonstrated that they could be etched and made optically visible and explained their formation as resulting from the trails of damage left behind by the passage of fission fragments.

The direct observation of these damaged regions, produced by fission fragments, in thin sheets of mica, under a transmission electron microscope was reported in 1959 by Silk and Barnes [2], also of AERE, Harwell. They were unaware of the work published earlier by Young.

The credit for the development of a new particle detector, from above observations, goes to Fleischer, Price and Walker [3], who began in 1961 where Silk and Barnes left off. Since then, the field has grown to such an extent that now there is hardly any field of science and technology where it does not have an actual or potential application.

1.1 CR-39 Track Detector.

CR-39 is a recently discovered versatile plastic track detector. Its discovery by Cartwright et al [4] in 1978 has ushered in a new era of important applications of SSNTDs. The superiority of this thermo set plastic in many respects over other polymeric thermo plastics were reported by Cassou and Benton [5] in the same year.

Thermo plastics are inherently heterogeneous, composed of mixture of amorphous zones and crystalline regions of different chemical etchability. CR-39 is an amorphous homogeneous detector. Several investigators have used this in detecting charged particles ranging from protons to heavy nuclei [4]. CR-39 is highly transparent and its optical properties are comparable to those of optical glass. It maintains the excellent optical properties through a wide variety of conditions of use and even after prolonged etching. The mechanical and physical properties are better than that of other plastic detectors. It does not crack internally or at the surface as a result of age, stress or contact with solvents. It is isotropic and highly sensitive to radiations. The cross linking of chemical bonds broken by radiation damage is negligible. Light weight and flexibility are also attractive characteristics. It can be preferentially etched with a non solvent etchant.

The CR-39 track detector is developed by polymerizing the liquid monomer di ethylene glycol bis (allyl carbonate), commercially known as allyl glycol carbonate having the molecular structure as shown below.

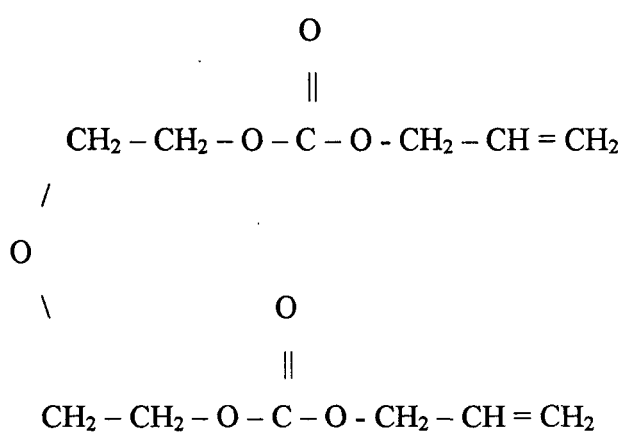

As we can see, contains two allyl functional groups $CH_2 = CH - CH_2$ -. Each allyl group can be incorporated into a different chain. This leads to the polymerization resulting in a network consisting of poly allyl chains connected by diethyl glycol dicarbonate links. Since the monomer repeat can be joined with upto four neighbours, the monomer is tetrafunctional and this cross linking makes it a thermoset plastic. So this plastic is essentially a macro molecule and that is the reason for its insolubility in ordinary solvents. Hence it neither softens on heating nor hardens on cooling. The monomer can be polymerized into a homopolymer or a copolymer. Homopolymer sheets are cast from pure monomer. If some additives such as vinyl acetate, methyl methacrylate or unsaturated alkyl resins are added to the monomer, they cast into copolymers [6].

For the development of both homopolymers and copolymers, certain initiators are added to the monomer. Commonly used initiators with CR-39 monomer are benzoil peroxide, dicyclohexyl peroxi dicarbonate (CHPC) and isopropyl peroxi dicarbonate (IPP). During the casting period, called the curing cycle, the temperature of the oven is changed step by step or gradually until the hardening of the polymer is completed [7].

1.2. New Detectors

1.2.1. CR-73 Detector

CR-73 monomer has chemical structure between CR-39 monomer and Lexan polycarbonate. This detector was the result of an investigation carried out by the Price and Tarle [8] in search of a new high resolution plastic track detector. CR-73 has the diallyl functionality of CR-39 with the aromatic ring structure of Lexan polycarbonate. Due to the energy absorbing properties of these aromatic rings, the Lexan polycarbonate is more resistant to radiation damage. Thus CR-73 plastic has high uniformity like CR-39 and yet have the low radiation sensitivity of Lexan polycarbonate. This new detector has resulted in lowering of Z^*/β value of 52 for Tuffak polycarbonate detector to 40 in

case of CR-73 detector. It is preferable to Tuffak when the maximum resolution for $Z^*/\beta >= 50$ is demanded. Comparative study of the chemical structure of CR-39, Tuffak polymer and CR-73 are given in fig1.1.

1.2.2. SR-86 Detector

To make applications of CR-39 polymers more extensive, higher sensitivities with still lower Z^*/β were considered desirable. Attention was therefore paid to linkage within the CR-39 molecule ie, to its molecular structure. Simultaneously a search for weaker linkages that are easily broken by charged particles where also initiated that could be finally introduced in CR-39. The efforts have yielded a new polymer SR-86. Here sulphonate (SO_3^-) linkages have been introduced to certain extent by co-polymerization of CR-39 monomer by diethylene glycol bis allyl sulphonate (DEAS). CR-39 has carbonate (CO_3^{--}) linkages. The sensitivity of SR-86 is three times higher than that of CR-39 for alphas and high energy ions. The sensitivity for protons has however not increased.

The investigations to be described in this thesis has been carried out mainly with CR-39 detector. Some investigations have been carried out with overhead projector transparency sheets as well as with X-ray films.

In the following chapters, a review of the previous studies related to track detector is given along with details about the present measurements and the results. In chapter II, a detailed review is given on the different investigations carried out by various scientists on track detectors in general and in particular the CR-39 track detector. In chapter III, the details of the set up used for etching studies on CR-39 and the preliminary measurements carried out for characterizing the CR-39 detector are enumerated. Chapter IV describes the details and results of some numerical calculations of the etched track profiles, track diameters and track lengths for CR-39 irradiated by protons, deuterons and alpha particles of various energies and for Makrofol irradiated

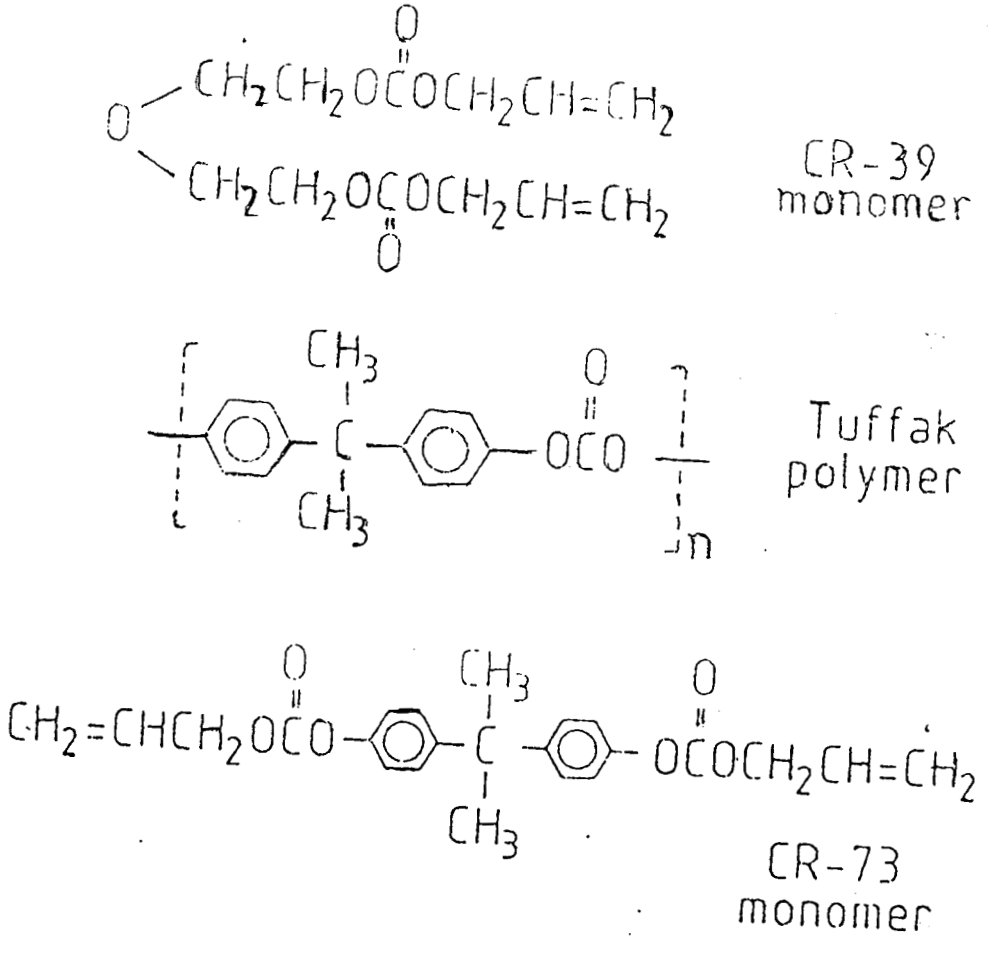

Fig1.1 Structure of CR-39 Monomer, Tuffak Polymer and CR-73 Monomer.

by heavy ions. The results are compared with experimental values wherever possible. The agreement with the measured values is reasonably good. In chapter V, some measurements using CR-39 detector on neutron slowing down in paraffin, using a neutron Howitzer are described. Chapter VI presents the details of the setup used for neutron irradiation studies on boron and copper targets and some of the results obtained there-from. Finally, in Chapter VII, the use of commercially available overhead projection transparency sheet and X-ray films as track detectors is discussed. Some results on the investigations carried out on these track detector materials are presented.

References

1. D.A. Young, Nature 182 (1958) 375.
2. E.C.H. Silk and R.S. Barnes, Phil. Mag 4 (1959) 970.
3. R.L. Fleischer, P.B. Price and R.M. Walker (1975) Nuclear Tracks in Solids: Principles and Applications, University of California Press, Berkeley.
4. B.G. Cartwright, E.K. Shirk and P.B. Price (1978) Nucl.Instr.andMeth.153, 457.
5. R.M. Cassou and E.V Benton (1978) Nucl. Track Detection 2, 173-179 Pergammon Press Ltd.
6. A.K. Ganguly and B.B. Baliga (1986) Proc. 4th Nat. Sem. Cum. Workshop on SSNTDs, Dehradun ed: K.K. Sharma 207.
7. G. Somogyi, `Solid State Nuclear Track Detector' (1981) Proc. 11th Int. Conf. SSNTD, Bristol ed: P.H. Fowler and U.M. Clapham 101-113.
8. P.B. Price and G. Tarle, Nucl. Instr. Meth. In the Phys. Res. Vol. B6 (1985) 513-516.

CHAPTER II

REVIEW OF PREVIOUS WORKS

Any energetic charged particle passing through a material medium interacts with it, producing ionisation and excitation of the atoms. This results in the formation of free charge carriers and photons. If the medium is a conducting one, these charge carriers soon recombine themselves unless drifted away by proper methods. In dielectric media the mobility of the charge carriers is very low and therefore a submicroscopic trail of damage is produced along the path of the incident particle. The permanent record of the trajectory is termed as hidden or latent nuclear track[1]. In some dielectric materials, these damaged regions are attacked preferentially by strong acid or base solutions leading to the formation of particle tracks when suitably etched with these solutions[2]. The materials which can be used to detect particles in this manner are called track etch detectors or Solid State Nuclear Track Detctors (SSNTDs).

There are inorganic and organic track detectors. Crystalline minerals and amorphous glasses belong to the inorganic group while plastics and polymers belong to the organic group[3]. In earlier days crystalline minerals were used as track detectors, but now a days plastics and galsses are preferred because their registration and development properties are better understood. Among the plastic track detctors, polycarbonate foils (PCs) (Lexan, Makrofol-I, Merlon, Kimfol) are very common and these are generally used for registering fissin fragments and alpha particles. Though not as sensitive as polycarbonate, sheets of poly ethylene terephthalate(PETs) (Mylar, Chronar, Melinex, Terphane) are also used for detecting fission fragments and alpha particles. The cellulose derivatives (Cellulose nitrate, Cellulose acetate, Cellulose acetate butyrate) are another class of very common plastic detectors, used mainly for

detecting alpha particles and recoil tracks. Kodak-pathe type LR-115 film, another member of cellulose nitrate family, is largely used in dosimetric applications. Another highly versatile and very sensitive track detector material is the thermoset plastic CR-39 [4]. All these are available commercially and are easy to handle.

2.1 Track formation models.

The track detector technique is based on the particle detection as a track in dielectic solids. The track is formed due to radiation damage caused in the solid by the incident charged particle and is clearly visible under in optical microscope, if amplified by a suitable etching process. For selecting a proper detector for a particular application and for choosing a suitable developing process, one must know the nature of radiation damage responsible for the formation of latent tracks in dielectrics.

2.1.1 Primary Ionisation (P.I) model or ionic explosion spike model [5].

When a charged particle traverses a material it losses energy upto immobilization following several mechanisms. The total energy loss rate can be represented in the form

$$(dE/dx)_{tot} = (dE/dx)_{nuc} + (dE/dx)_{el} \qquad \text{.....(2.1)}$$

where the terms on the rhs correspond to the nuclear and electron interactions.

2.1.1.1 Energy loss by Ionisation arising from electronic stopping

At energies greater than 0.1 Mev/n, the major part of the energy loss of the primary ions is due to interation with target electrons. This interaction is called electronic stopping. The energy loss of heavy charged particle is mainly governed by the particle velocity. The velocity determines firstly the charge and secondly the

interaction mechanism between the projectile and the charged particle. While passing close to an atom, an incident charged particle can pull out an electron and correspondingly create a positive ion either by capturing the electron or by ejecting it into the lattice. At each of such interactions the particle losses a part of its energy. The electron component of energy loss increases as $E^{1/2}$, where E is the ion energy, reaching a maximum depending on the ion species between 1 and 10 Mev/n and there decreasing as 1/E with increasing energy.

2.1.1.2 Energy loss by atomic collisions arising from nuclear stopping

At low velocities corresponding to particle energies as low as 10 keV/n, nuclear stopping dominates the stopping process. The nuclear stopping represents the scattering of the projectile at the screened columb potential of the target atoms. The nuclear stopping process is characterised by a large energy and angular momentum transfer, especially if the masses of the incident particle and the atom are not different. The probability of such an interaction is very small at high energy and increases when the energy of the particle decreases, since the atomic cross-section is inversely proportional to the energy. In this case the incident particle enters into direct collision with the atom as a whole and is able to eject it from its lattic site.

Thus nuclear stopping is only of importance at extremely low energies. At higher energies nuclear stopping contributes only a few percent of the total stopping cross-section. There are two arguments which point towards the almost exclusive contribution and ionisation in the formation of tracks in insulators:

a) Tracks are observed practically at full length, whereas atomic collisions principally occur at the end of the path;

b) No tracks are formed in conductors, where only atomic collisions are able to produce stable tracks. In these solids ionisation is typically a transient

phenomenon since the number of free electrons is large enough to compensate very quickly on electronic defect.

Starting from these considerations, Walker et al[6] introduced the idea of ionic explosion spike. The charged particle ionises a large number of atoms along its trajectory by ejection of electrons into the lattice thus creating a channel containing a large concentration of poistively charged ions. Since the material is an insulator there are only a few electrons available for neutralising these ions; hence the ions are subject to a strong Coulomb repulsion which eject them from their sites. This yields a channel of large vacancy concentrations surrounded by a region containing many interstitials. The preferential etching of tracks is then explained by the fact that their path is strongly disturbed and hence shows up a much greater chemical reativity than the bulk material.

If this theory can be applied to all insulators, for plastics another physo-chemical phenomenon may occur. The electrons ejected by ionisation (primary electron) as well as the secondary electrons (those ejected by the primaries, sometimes called delta rays) may break the polymeric chains and give rise to free radicals and the degradation of the polymers. The damaged region thus consists of polymeric chains with a mean molecular weight which is smaller than in the original polymers. Since the reactivity and the behaviour of a polymer with respect to a solvent usually vary with the inverse of its molecular weight the preferential etching of radiation damaged region is explained. Thus in inorganic SSNTDs, (crystals and glasses) secondary electrons do not play significant role in latent track formation.

2.1.2. Delta ray model [7]

Here it is assumed that the density of primary events has no direct influence in track formation. Most of the secondary elecrons created in the primary interactions by a fast moving ion of energy E possess energy E^{-n} where $2 < n < 3$. As this energy is small, the interaction of these electrons extends only to a very narrow region near

the path of the incident ion. The secondary dose D produced by an ion of effective charge Z^* depends on radius 'r' as

$$D(r) = a(Z^* / \beta)^2 (1/r) (1/r - 1/R) \quad \text{..... (2.2)}$$

where 'R' is the maximum track width and 'a' is a constant. According to Katz[7], the average energy density produced by secondary electrons at r = 17A° decides the preferential etchability.

In organic solids, the primary ionisation appears to be the major source of damage, the secondary effects of delta rays are not of much importance in such materials. In plastics both primary and secondary interactions contribute to the formation of tracks[8,9].

2.1.2.1 The effective charge Z^* [9]

If the velocity of the particle exceeds the orbital velocity of its own electrons, these electrons are stripped off in the first few collisions and only the stronger bound electrons of inner shells stay with the projectile. As the projectile slows down, more and more electrons are captured and the charge state of the projectile is reduced until it comes to rest and is neutralised. The dependence of projectile charge and velocity has been approximated as[9]

$$Z^* = Z[1 - \exp(-130\beta / Z^{2/3}) \ ] \quad \text{..... (2.3)}$$

Where 'Z' is the charge state of the projectile at its entry into the detector and β the velocity of the projectile relative to that of light.

2.1.3 Restricted Energy Loss(REL) model [10,11,12]

The restricted energy loss model, put forward by Benton, considers the combined effect of primary and secondary electron events. The total energy loss rate dE/dx can be represented as[13]

$$(dE/dx)_{W > W_o} = C_1 Z^{*2} \beta^2\{\ln(W_{max}/ W_o)-\beta^2\} \quad \text{..... (2.4a)}$$

$$(dE/dx)_{W < W_o} = C_1 Z^{*2}/ \beta^2\{\ln(W_{max}/ W_o /I_a^2)- \delta - U\} \quad \text{..... (2.4b)}$$

where $W_{max} = 4M_1 M_2 E/(M_1 + M_2)$, the maximum energy transfer,
I_a, the mean ionisation potential of the atomic electrons of the stopping medium U - takes into account the properties of the interaction with electrons in inner shells.
$(dE/dx) = (dE/dx)_{W>W_o} + (dE/dx)_{W<W_o}$. Where $(dE/dx)_{W>W_o}$ is the energy loss in near interactions in which electrons with energy $W>W_o$ are knocked out and $(dE/dx)_{W<W_o}$ is the energy loss in distant interactions for which $W<W_o$. The parameter W_o determines the boundary between the electron energies that are not taken into account in track formation.

The model makes allowance for the energy removed from the track core by high energy delta rays. It is assumed that only that part of energy loss is relevant to track formation where the energy carried by delta ray electrons is less than W_o . The value of W_o is around 350 eV.

In this model, all events of electrons ejected with energy transfer above the limit W_o are completely ignored though many of them may be located very near the ion path. All events of electrons with energy below the limit are considered efficient.

This model is easily applicable to most of the practical cases, but it fails in certain cases. In this model, all events of electrons ejected with energy transfer above the limit W_o is completely ignored though many of them may be located very near to the ion path. Also, all events of electrons with energy below the limit are considered efficient. But it was found that even 300 eV electrons can well deposit energy even beyond 100A° away from the ion path. In order to overcome this problem, another concept, the radius restricted energy loss $(dE/dx)_{r < r_o}$ was suggested by Bonfigloli et al (14).

2.1.4 Radius restricted energy loss model

This model considers all energy deposition events within a certain radial distance r_o as effective. To a good approximation it is represented as

$$(dE/dx) = (dE/dx)_{total} - a(Z^*/\beta)^2 \left[\ln(R/r) - (1-r/R)\right] \quad \text{.....(2.5)}$$

where R is the maximum track width.

2.1.5. Linear event denisty(LED) model [15].

In both restricted energy loss (REL) model and radius restricted energy loss model the density of relevant events is assumed to be strictly proportional to the local energy density. This assumption is useful for primary events due to incident particles, but not for secondary events from delta rays. So another model was put forward by Paretzke[15]. In this model, we basically consider the events and not energy as in REL concept. Here the event densities corrected for the overlapping of primary and secondary ionisations within a certain radial distance around the path of the incident particle is taken to be relevant for the increase of etching speed in plastic detectors.

2.2 Criteria for latent track formation

It is observed that almost all materials used as track detectors have resistivity about 20 ohm.m[16]. But resistivity is not the only criterian for the formation of track in a material. Fleischer et al[5] has suggested four necessary conditions for the formation of tracks by the ion explosion mechanism.

2.2.1 Mechanical strength of the material

It is observed that tracks are formed most easily in materials of low mechanical strength, low dielectric constant and close inter atomic spacing.

2.2.2 Intensity of ionization

The incident particle should possess at its entry into the detector an energy and a mass such that its energy loss rate dE/dx is larger than some critical value $(dE/dx)_{crit}$, which is characteristic for each of the material used. To verify this, Mory[17] carried out the following investigations. Various detector sheets were hit by different kinds of ions accelerated to a given energy. The recording efficiency (the ratio of the number of tracks to the number of ions which hit the target) is determined by counting the tracks. Also the quality of the tracks were examined, eg. their length. In another purely theoretical study, the variation of the primary ionisation rate is calculated for a given insulation and a given ion, as a function of the ion energy. Afterwards the experimental data were plotted. It was found that for each of the investigated solids, there exists a critical value of dJ/dx, above which the tracks are perfectly etched, and recorded with a 100% efficiency. Below this value no tracks are observed.

The dJ/dx – curves have been established from the Bethe[18] equation.

$$(dJ/dx) = (\alpha Z^{*2}/I_0\beta^2)[\ln\{2mc^2\beta^2/(1-\beta^2)I_0\} - \beta^2 + 3.04] \quad \text{.....(2.6)}$$

where dJ/dx = the number of ion pairs formed per unit length.

Z^* = the effective charge of the ionising particle,

β = v/c,

m = mass of electron,

I_o = the ionisation energy of the peripheric electron of the material (nearly 2 ev for plastics) and

α = a constant depending on the material.

It was also found that for the formation of microscopically and macro scopically continuous tracks there must be at least one ionisation per atomic plane crossed by the incident particle. If they are discontinous, the etch pit profile would be

rough and shape would be irregular. This is a criterion mostly imposed for tracks, which are to be revealed by chemical etching.

2.2.3 Availability of electrons near the track

This criterion is related to the supply of electrons near the ionised track. If other electrons replace those ejected by the incident charged particle before ionised atoms are forced into adjacent material, no track could be formed. The ions take around 10^{-4} nano seconds to get displaced from the normal sites. So if electrons can be drained from a cylindrical region around the ionised core in less than this time, the track formation can be prevented. In some of the semicondctors and most of the insulators this condition is fulfilled and therefore no track can be formed. In metals, unless the density of free electrons is less than $10^{26}/m^3$ tracks will not be formed.

2.2.4 Hole mobility

Along the ionised region in the track core, there is a high concentration of holes. These holes may move away, preventing the formation of permanent tracks. Calculations on hole mobility show that, if the hole mobility in a material at room temperature is more than 0.2 cm^2/V-sec, no track can be formed in that material. This criterion also leads to the conclusion that metals and most of semi conductors cannot be used as track storing materials.

2.3 Track Revelation Techniques

Several methods are in use for the visualization of the latent damage trails. The commonly used methods are chemical etching and electrochemical etching.

2.3.1 Chemical etching [19]

In a track etch detector a suitable chemical reagent preferentially attacks the damaged region to enlarge tracks. During the etching, the bulk of the material is also attacked but at a much slower rate. The final geometry of the etched tracks is therefore determined in the simplest case by the simultaneous action of these two etching processes. The rate of these two etching processes are respectively designated as V_T and V_G. While the track etch rate V_T depends on the specific ionization, both V_G and V_T are also dependent on the detector material, the etchant, its concentration and temperatre of etching. Initially, the track grows with its familiar cone like structure, characterised by the two etch velocities V_T and V_G. However, because of an increase in track etch rate near the end of the particle track, the track walls develop small curvature. Once the track etching reaches the end of the particle range, further etching only enlarges the track at the bulk etching rate and the track structure becomes progressively lost. Therefore for a determination of the partcile range from a measurement of the etched track length, it is necessary that etching time is just sufficient to fully etch the particle trajectory but not too much beyond that. Also corrections for the track enlargements due to the bulk etching have to be made.

2.3.2 Electrochemical etching [20]

Using this method tracks in plastics can be enlarged upto a size where they can be observed even with naked eye. An alternating voltage of several KV and frequency upto several KHz is applied between two electrodes placed on either side of the detector during the etching process. The resulting electric field enhances the penetration of the etching reagent both into the latent track and into the bulk of the polymer.

2.3.3 Grafting [21]

It is possible to graft an appropriate copolymer on chemical active site of the dielectric material. The chemically active sites consist of free radicals and chain ends produced on the original polymer along the trajectory of the nuclear particles. If the grafting reaction is performed with a monomer of acidic property, then a basic fluorescent dye can be fixed to the damaged trails. The tracks can be visualised under a microscope with ultraviolet light illumination as thin bright lines in dark field of view.

2.4 Registration and Development - Characteristics of Track Detectors leading to Particle Identification.

2.4.1 Track Formation Scheme.

The progressive steps for obtaining etchable tracks are (i) irradiation of track detector with charged particles (ii) chemical or electro chemical etching of the detector using appropriate etchant (iii) sensitivity of etching (V_T and V_G) (iv) observtion of visible tracks. The depending parameters for visible tracks for chemical etching are the energy loss rate (dE/dx), the charge of the ion(Z), the energy of the ionic particle (E), range (R) and angle (θ) of entry of the projectile into the detector, concentration (C) and temperature (T) of the solution, the thickness of the etched layer (h), the time of etching (t), etched track length (L), semi major (a) and semi minor (b) axes of the entrance opening of the track channel and the range (Ro) of the particle in the detecting medium.

The development of a track by chemical etching can be represented as resulting from two competing processes that take place practically simultaneously i) etching of the detector material at a rate V_G and ii) etching of the material in the region of the track at rate V_T . The first is determined by the ratio h/t where h is the thickness of the etched layer and t is the etching duration, while V_T is determined

from the relation $V_T = L/t$ where L is the track length during time 't'. In general V_T , is a function of the point on the track axis. The sensitivity of the track etching process is characterised by the relative etching rate $V = V_T / V_G$ at the given point of the track. Consequently, this ratio determines the geometrical shape of the track. The boundary condition for the track formation due to a particle that enters the detector of an angle θ has the form $L \sin\theta = 1$. So a track is developed if the angle of entry satisfies $\theta > \theta_{cr} = \text{arc Sin } (V_G / V_T)$. The angle θ_{cr} is called the critical angle for etchig. The etching rate depends on the temperature, the concentration of the etchant and the duration of the process.

The ratioV_G / V_T determines θ_{cr} which in turn determines not only the detection efficiency but also the track shape.

The sensitivity of the track etching increases with increasing specific energy loss.

2.4.2 Detection Efficiency

The detection efficiency is one of the most important criteria in the choice of a detector for physics experiments. The total detection efficiency can be defined as

$$\varepsilon_{tot} = \varepsilon\varepsilon_s \qquad \text{.....(2.7)}$$

The first factor ε of the product depends on the detection threshold of the SSNTD and for particles entering at 90° it is determined by comparison with the detection efficiency of another more sensitive SSNTD (For example, the efficiency of phosphate glass and mica for Ne ions entering normally with energy near ionization maximum is about 25% of the detection efficiency of PET in which all Ne ions of that efficiency are revealed by etching).

Above the detection threshold, ε is near unity. The geometrical factor ε_s is determined by the critical angle θ_{cr} of energy of the ion into the detector.

The critical angle θ_{cr} = arc Sin (V_G / V_T) ..... (2.8)

In this case of homogeneous particles and a thin source, $\varepsilon_s = 1 - \text{Sin}(\theta_{cr})$.

2.4.3. Sensitivity of SSNTDs.

The Sensitivity of all SSNTDs have a threshold nature. The threshold is characterised by the minimum ionization density produced by the charged particle in the matter at which (and above) the track can be developed by etching, ie when $V_T >> V_G$.

For polymers the sensitivity can be expressed as $V_T / V_G = 1 + a(x)^b$ or $V_T / V_G = a(x)^b$ where 'a' and 'b' are emperical coefficients.

Instead of x one may have dJ/dx, dE/dx or Z^*/β etc. Taking $V_T / V_G = Z$ at the beginning of the sensitive range, one can find the ionisation at which tracks are developed with 100% efficiency. The coefficients a and b are found on the basis of calibration.

Sensitivity is significant for REL > 2 x 10^{-3} MeV/cm. In another study Bhattacharya et al[22] have established the relationship between V_T / V_G and REL for Fe, Kr, La, Au and U on CR –39 Dop. For these heavy ions the least square fit to the measured data gave

$$V_T/V_G = 2.94654 + 0.00333592\ REL + 3.16746 \times 10^{-6}(REL)^2 - 7.50249 \times 10^{-10}(REL)^3 + 6.17989 \times 10^{-14}(REL)^4 \quad \ldots\ldots\ldots \quad (2.9)$$

This shows a short increase in etch rate ratio with REL for projectiles of charge Z≥ 79.

Variation of normalized etch rate ($V = V_T/V_G$) with energy is useful in developing appropriate models for track formation. For particles with Z > 2, the mechanism is slightly complicated. The result of an experimental study by Yadav[23]

shows the variation of V_T/V_G with energy of ^{12}C, ^{14}N and ^{20}Ne on CR – 39 Dop. These ions are very important as the products of exotic decay of heavy nuclei.

Poly carbonate detectors can be very well used to detect various heavy ions. ^{20}Ne ions of 65 MeV/n[24] energy generate tracks with $V_T/V_G > 2$ and hence can be detected. The same effect is found on CN(R) for 10 MeV/n ^{20}Ne[25].

In the case of proton, V_T/V_G increased at low energies and reaches maximum at about 0.5 to 0.8 MeV and then decreases with further increase in energy. This is in agreement with the trend of the variation of the rate of energy loss (ie stopping power of protons in samples) which shows a Bragg peak. The critical angle also varies with proton energy. Corresponding to the above changes, the detection efficiency also varies with energy.

Doping with plasticiser increases the reduced track etch rate ($V_T/V_G - 1$). It is generally proportional to Z^*/β, but the proportionality is not the same at all energies. It varies with the effective charge and velocity of the particle. Price and Sullivan[26] studied the effect on CR-39 doped with different plasticisers (DIDP : diisodecylphathalate, DOTP : dioctyle teraphthalate, DOP : Dioctyl phthalate). Instead of V_T/V_G , V_T also shows a direct correlation with dE/dx.

Another important parameter on which the sensitivity of a track detector depends is the residual energy of the particle. V_T/V_G or V_T at any point along the trajectory depends on the residual energy of the particle. The residual energy of the particle will be maximum at the point of entry into the detector and decreases as it proceeds into medium. Rao et al[27] successfully detected 10MeV protons, 70MeV ^3He and 52 MeV ^4He ions in CR-39 detector. The normalised etchig rate as a function of residual range for these particles has been obtained. This also showed that clear discrimination is possible between ^3He and ^4He in these energy bands. In this study the experimental data has been filted with the function

$$V_T/V_G = AJ^n \qquad \ldots\ldots \qquad (2.10)$$

Where $J = (Z^*/\beta)^2 \left[k + \ln\beta^2\gamma^2 - \beta\right]$ .... (2.11)

Here A and n are constants.

The results of this study showed that the response of 10MeV protons, 70MeV ^{3}He can be represented as a function of

$$V_T/V_G = (Z^*/\beta)^2 \left[1+0.05 \ln\beta^2\gamma^2 - 0.05 \beta^2\right] \quad .... \quad (2.12)$$

For the above ions they have got a smooth variation of normalised track etching rate as a function of residual range. This study also shows that CR-39 will register normally incident particles with value of Z/β as low as 8.

Knowing the etch rate ratio we can estimate the residual range R using the relation[28].

where A and B are fitting parameters.

Variation of track etch rate V_T with distance along the track shows a high resemblance with Bragg curve.This is also useful in particle identification.

2.4.4. Particle Identification.

Near the sensitivity threshold for small value of $V(= V_T/V_G)$,it is difficult to measure the track parameters except the diameter.Therefore for $V \leq 3$ the etched length and V are determined from the diameter D of the ions that enter the detector at 90°[12].

$$V = (1 + D^2/h^2) / (1 - D^2/h^2) \quad ..... \quad (2.14)$$

where D is the diameter of the ion track and h is the thickness of the layer removed during the etching time, from which L = Vh. The error in the determination of L of individual tracks is $\pm$ 3μm.

Khan et al[29] have carried out extensive studies on the track registration and development characteristics of CR-39 track detector. They have tested this detector for its response to light particles and heavy ions having a wide spectrum of energies.

Very useful information regarding energy loss and its reflection in the measured track diameter are well studied here.

When SSNTDs are used in nuclear reactions, for the precise estimation of the cross section for emission of particles having wide energy spectra, knowledge of the critical angel θ_{cr} is pre-requisite. For 1.2MeV protons, the critical angle of etching θ_{cr} is $(27.4 \pm 1.5)^{\circ}$. Higher energy protns are expected to yield higher values of θ_{cr} (for lower values of the track registration efficiencies). It is shown that θ_{cr} corresponds to the maximum value of θ allowed for production of etchable tracks, the maximum efficiency of CR-39 for the production of etchable tracks (in 2π geometry) comes out to be[30]

$$\varepsilon(\text{efficiency in } 2\pi \text{ geometry}) = 1 - \text{Sin}\,\theta_{cr} . \qquad \ldots\ldots\ldots (2.15)$$

The critical angles of etching of CR39 increases with increasing energy whereas efficiency decreases with increasing energy.

The etch pit diameter is a fairly useful parameter in studying the characteristic of charged particles producing damage trails. A knowledge of the variation of the etch pit diameter as a function of the etching time for tracks due to particles of known energies and charges can be great help in characterising the incoming particles. Etch pit diameter and its depth are particularly useful in determining (a) etch pit cone angle and (b) V_T , the etching velocity along the track. The results of the experiments carried out by Khan et al[29] were encouraging.

Mukherji et al[31] also conducted a study on variation of track diameter with etching time for alpha particles and heavy ions(boron). They also obtained similar results.

Jolly Raju and Dwivedi[32] measured the track diameter of 17.0 MeV/n ^{132}Xe in CR 39. Other heavy ions also showed linearity of the diameter growth with etching time.

Farid and Sharma studied heavy ion interactions on Cellulose nitrate (CN) and Makrofol – E polycarbonate (PC) [33,34,35] and found that track diameter linearly increases with etching duration. The computed values of energy losses in CN and PC detectors have been correlated with track diameters. The experimental results indicate the exponential dependence of diameter on energy loss. The track registration sensitivity ($V= V_T/V_G$) of track detectors was found to increase and cone angle was found to decrease towards higher temperatures. The maximum etched trak length is compared with the theoretical range. The heavy ions used were $_{10}Ne^{20}$, $_{26}Fe^{56}$, $_{36}Kr^{84}$, $_{8}O^{16}$. From the calibration curve the critical energy loss – $(dE/dx)_{crit}$ was also determined.

Using commercially available over head projector transperancy(OPT) sheets as track detector Ghosh et al[36] have measured track length of ^{132} Xe ions. Basu et al[37] carried out a systematic study on comparative basis with the standard plastic detector CR-39.

Polycarbonate also show similar behaviour for diameter growth with etching time. To verify this Bhattacharya et al[38] irradiated the polycarbonates – Makrofol-N, Makrofol-E and Makrofol-KG-with ^{252}Cf ions. The growth of diameter and the corresponding etched out layers at different times were noted. It is very useful in deducing the track length L, and track and bulk etch rates.

The variation of Etch Rate Ratio ($ERR = V_T/V_G$) is a function of REL. The distribution clearly indicated two distinct regions:

a). Low slope region (10^2MeV cm^2 g^{-1} $\leq$ REL $\leq$ 1.5 x 10^3 MeV cm^2 g^{-1}) and

b). High slope region REL $\geq$ 1.5 x 10^3 MeV cm^2 g^{-1} . The latter seems to be very significant for CR-39. In high slope region the two parameters are related as follows:

$$ERR = (V_T/V_G) = 7.51 \times 10^{-8} (REL)^{2.36} \quad \ldots\ldots\ldots\ldots \quad (2.16)$$

It is worth noting that a value of about 2 for ERR is obtained even for a light particle having REL value as low as 10^2 MeV cm^2 g^{-1}. This REL value may be compared with REL values of cellulose nitrate (1.1×10^3 MeV cm^2 g^{-1}) and Lexan (3.3×10^3 MeV cm^2 g^{-1}) reported by Benton and Nix[11]. This indicates the exceptionally high sensitivity of CR-39. Another important feature is that no saturation effect occurs even for an ERR of around 80. Still higher ERR values are expected for partilces with higher REL rates.

The existence of two slopes are found in ERR $vs(Z^*/\beta)^2$ graph. For $(Z^*/\beta)^2$ values exceeding 3×10^3, the two parameters are related as follows:

$$ERR\ (=V_T/V_G) = 7.24 \times 10^{-7}\ (Z^{*2}/\beta^2)^{1.92} \qquad \text{.....(2.17)}$$

Since the parameters (Z^{*2}/β^2) is proportional to the ionization rate of the particle, even lightly ionizing particles produce ERR values of about 2. This value of ERR corresponds to ~30° for θ_{cr}, which is comparable to that obtained for alpha particles of 40 MeV.

Khan et al[29] arrived at the following relation between Z^{*2}/β^2 of a particle and its REL value (MeV cm^2 g^{-1}) calculated for W_o = 200 eV) in CR-39 having the form

$$(REL)_{wo=200eV} = 2.62(Z^{*2}/\beta^2)^{0.81} \qquad \text{..... (2.18)}$$

Knowing the Z and Z/β thresholds of track detectors is thus important while choosing a detector for a particular application. It also gives the values of Z and Z/β thresholds and of the critical angle of etching of different plastics, mica and glass track detectors. There is an appreciable range in the Z and Z/β thresholds values. Among the glass track detectors, phosphate glass has the lowest threshold for track registration. The CR-39 has shown the highest sensitivity among all the detectors studied. It may be pointed out that certain Z/β are such that the ranges of the particles are very short. These short range particles, however, produce etchable tracks. This is because the

charged particles at this stage of their range are mostly highly ionizing and thus produce etchable damage regions.

The critical angles of etching increase with increasing value of the Z/β thresholds of the detector above.

Track detectors are the ideal detectors for detecting the fragments from spontaneous fission and exotic decay of heavier nuclei. In a study conducted on the spontaneous fission of ^{252}Cf, Ganguly et al[39] were able to detect several light and heavy fragments. Another important information from their study is the track diameter calibration curve for various charged products involved in this decay. The diameter corresponding to alpha, the most probable light and heavy fragments are also given.

2.5 Track Registration and Development efficiencies [40]

In order to make use of solid state nuclear track detectors(SSNTDs) in quantitative measurements, one needs to have precise values of their track registration and development efficiencies[9,41]. The experience gained until now shows that (a) the exposure geometry, (b) the effective charge of incident particles, (c) the degree of crystallization of the detectors, (d) the etching conditions, and (e) the environmental conditions existing before, during and after the exposure stage play an important role in controlling the track registration and development properties of SSNTDs.

The track formation effeciency η =

Number of tracks/ number of incident particles .... (2.19)

It is believed that charged particles like protons and heavier than protons produce latent damage trails in almost all the insulating materials. Therefore as far as the formation of latent damage trails is concerned, the efficiency is practically 100%. On the other hand, the experience with etched track formation shows that the

efficiency may not always be 100%. In some cases, it is even zero percent. The formation of an etchable track, besides being a function of the detecting material and the nature of the incoming particle, depends upon the exposure geometry[9,42] and the environemtnal conditions.

2.5.1 Collimated beams – perpendicular impacts

This is the simplest geometry to be considered. The efficiency determinations are the easiest to carry out. The "dE/dx vs range" curve for fission fragments shows that the maximum energy loss takes place in the early stages of their journey[43]. As the distance traversed in the medium increases, the energy loss decreases (except at the end where there is a small increase in dE/dx due to nuclear collisions). The parameter total energy loss can be assumed (to simplify the case) to represent the intensity of damage along the range of the particle[9]. Arguing on these lines, it can be concluded that in the above cited case, maximum damage exists at the start of the journey of a fission fragment. The topmost region is the easiest to etch. This means that in this case, the probabilty of enlarging the trail by etching is the maximum at the top of the detector surface. If the trail cannot be etched at the top of the detector surface, it cannot be etched at any other point lying inside the detector body. Therefore, it can be safely concluded that for a perpendicularly falling collimated beam of mono energetic particles (belonging to the fission fragments group) the etched track formation efficiency is either one hundred percent or zero percent.

The "effective charge" (Z^*) of these particles decreases as they continue their journey inside the medium. With the decrease of dE/dx, the damage density inside the core of the trail decreases. At a certain limiting value of Z^*, the trail remains no longer etchable. This limitations restricts the "etchable length" to a value smaller than the physical range of the particle. As the "etchability" of a damage trail is expected to vary with the etching conditions, they may be defined while quoting the efficiency value. The etch pits due to perpendicularly falling collimated particles have been found to have the most symmetric opening on the detector surface. Further

more, the "etched trail" so obtained is conical in shape. The ratio of the length to the diameter of the base of the core is quite high for most of the plastics and crystals like quartz, olivine, fieldspar, etc, where we get thin etched trails. On the other hand, this ratio is small for most of the glasses, which appear as circular or elliptic etch pits, when viewed from the top under an optical microscope [9,42,22].

2.5.2 Collimated beams – slanting impacts

2.5.2.1 The crtical angle of etching.

Exposures carried out under these conditions are slightly complicated. These studies exploit the use of critical angle of etching [9,42,44]. This is an important parameter and can be well understood if we first define a few parameters. Let the etching velocity of an etchant along the damage trail be V_T, and along the general surface be V_G. It can be easily shown that the component V_T along V_G is V_T Sin θ. During this time interval the detector surface will be etched away up to a thickness equal to $V_G t$.Now for the etch pit to be visible on the finally obtained detector surface (after etching), we have condition:

$$V_T t \, \mathrm{Sin}\theta > V_G t \text{ , or}$$

$$\mathrm{Sin}\theta > V_G / V_T \text{, or}$$

$$\theta > \mathrm{Sin}^{-1}(V_G/V_T)$$

If $\mathrm{Sin}^{-1}(V_G/V_T) = \theta_c$ is a critical value of angle θ , for etchable track formation, we have the condition that $\theta > \theta_c$.

This critical angle, at or below which the damage trail of an impinging particle is not etchable, is known as the critical angle of etching. This is an important parameter in the process of latent trail development by etching, and strongly governs the ultimate obtainable efficiencies of the detector systems.

2.5.2.2 Variation of efficiency as a function of the angle of impact.

If etched tracks are obtained for the detector exposed to a collimate beam of mono energetic particles belonging to the fission fragment group, the efficiency will be 100%. The efficiency may remain 100% up to certain stage when the angle of impact (with respect to the detector surface) is lowered from 90°. This response will be maintained till the angle is lowered to such an extend that it equals the critical angle of etching. For particles having lower Z^* the tracks will cease to appear at higher values of the angle of impact. This increase in the critical angle of etching will continue with decreasing value of Z^* of the particles present in the beam. The 100% efficiency value will start showing a decrease at angle close to 90%, and will ultimately fall to zero. The fall will be gradual, if the beam contains particles having a spectrum of charges and energies instead of having monoenergic singly charged particles. This is true when carrying out experiments with fission fragments obtained from spontaneous fissing of ^{252}Cf, or induced fission of ^{235}U, ^{239}Pu etc.

2.5.3. Some important properties of non crystalline solid state nuclear track detectors for registration and development of damage trail due to fission fragment like particles.

a) The critical angles.

Almost all the plastics have been found to possess low critical angles of etching (from 2° to 5°) for the registration of fission-fragements like particles[42]. Most of the glass detectors (like soda lime glass, tektite glass, etc), on the other hand, have critical angles in the range 25° – 40°[42].

b) The track registration and development efficiencies.

In this case due to θ_c – limitations there exists a maximum permissible core, which will contribute etchable tracks on the detector surface. Another cone is defined by the minimum angle made by particles falling just along the detector edges. The detection efficiency η is then equal to the solid angle subtended by the area circumscribed by the critical angle limitation, expressed as a

fraction of the total solid angle (which is 2π in the present case) subtended by the detector on the source

$$\eta = 1 - \mathrm{Sin}\theta_c$$

which shows that normally the plastics have high registration efficiencies (85-95%), while the efficiencies of most of the glasses range between 40-60%.

c) **Etch pit shape**.

Angular impacts on etching are revealed as completely circular etch pits. The slanting impacts, on the otherhand, result in long needle-like tracks in plastics and elliptic etch pits in glasses. The etch pit opening in all these non-crystalline detectors are either complete circles or ellipses.

d) **Degree of angular isotropy in track production**.

The experience gained until now in studying the dependence of track production in various directions in a fixed plane of non-crystalline detectors shows that all the directions have equal probability of track registration and enlargement through etching. Khan[45] carried out a number of experiments for studying this effect in Makrofol N, Makrofol-E, Lexan, soda lime glass and fused silica. No isotropy could be observed in these non-crystalline detectors.

2.5.4 Important factors affecting the track registration characteristics of solid state nuclear track detectors[46].

2.5.4.1 Pre-Irradiation and Post-irradiation annealing of plastics, glasses and crystals.

2.5.4.1.1 Effect of Pre-irradiation annealing.

Usually some water is obsorbed during the cleansing period of the detector. If this water is not removed completely and one goes ahead with the irradiation step, the tracks produced are found to differ in quality when compared with those produced in the same material but irradiated in dry state. Also, it is found that the etching

characteristics of "dry" and "wet" detectors are quite different. It has been found that the water problem can be solved by carrying out an initial thermal annealing of the platic detectors. Another advantage of this step is to anneal out all the pre-existing background tracks (fossil tracks, tracks produced by back ground radio activity and affected by environment u.v. etc.). Care must be taken not to overheat the detctors. Over heating produces some structural changes in the detector body and in extreme conditions may even disfigure it.

It is found that the maximum etched track length (l_{max}) increases with annealing temperature which indicates that the average length of etchable latent damage trail is effetively extended if "moderate annealing conditions" prevail before the irradiation stage. The experiment carried out to study the causes of enhancement in l_{max} caused by pre-irradiation annealing indicated that, as the temperature of a cellulose nitrate sheet is increased, an increase in the degree of polymerizatin is achieved, and due to cross linking etc. the hardness of the material increases and this results in a decrease of V_G. Apparently, V_T of a damage trail (produced after annealing) is not affected due to this increase in the hardness of the plastic. The improvement in the efficiency η, is principally due to a decrease in V_G. This explains the rise in l_{max} up to about 80°C. After about 80°C (region near to its softening point of 105°C) some structural changes take place, like a general break down of the material. These decrease the hardness of the material. An increase in V_G is also observed.

2.5.4.1.2. Effect of post irradiation annealing on latent damage trails.

A latent damage trail can be visualized to be consisting of a physical vacancy surrounded by a high density region under strain. This surrounding denser region contains extra atoms, which migrated from the central vacant region after the passage of the particle. These extra atoms are in comparatively unstable state and have a tendency to move towards the central vacant place originally occupied by them. All they need is a jolt, strong enough to make them leave the unstable positions occupied

them. This required jolt can be achieved by providing a heat treatment before etching, which "anneals out" the latent damage, partially or fully, depending upon the severeness of the heating step[9,47].

It has been observed that if the detectors containing latent damage trails are exposed to heat and etched afterwards, the "etched tracks" have dimensions smaller than those produced in the unannealed detectors. One advantage of the annealing step is that most of the background produced by light ionizing particles is eliminated. But the disadvantage is that the parameters of the genuine damage trails are also modified. An apparent "reduction" in track registration and developing efficiency is observed, which is to be accurately known before carrying out quantitative measurements using SSNTDs.

The results of works concerning the annealing of latent trails indicate that either the exposure to heat should be completely avoided or an accurate correction curve for the particular detector-particle combination should be obtained for making the necessary corrections.

2.5.4.2 Presence of oxygen, hydrogen peroxide, humidity and sources producing ultraviolet and ozone and light charged particles.

2.5.4.2.1 The effect of oxygen.

It was found that remarkable differences existed in the number and size of visible tracks in the oxygen-free detector and the detector exposed in air or oxygen. It was concluded that the presence of oxygen is necessary factor for track registration and development of the etched tracks.

2.5.4.2.2 The effect of humidity and hydrogen peroxide.

It was observed that the etching speed (maximum etch pit diameter) is considerably larger in the detectors exposed in humid air or in water than in those detectors which had been kept in dry air or in the laboratory air. It was also observed that the hydrogen peroxide treatment drastically increases the etching speed. It was also found that the etch pits appear sooner in H_2O_2- treated or dry plastic detectors.

On the otherhand, the presence of water increases the etching speed, but has only little effect, if any on the sensitivity. The saturation level of water is already obtained in humid air, and immersion in water does not increase the effect. Unlike the oxygen effect, pre-as well as post-treatment of exposed detectors has the same effect indicating that it is based on a "softening" ie a decrease of the detector resistance against the attack of the etchant. It is expected that the humidity effect is less pronounced or absent in plastics that do not absorb water.

Hydrogen peroxide also increases the sensitivity only slightly (the some what higher countable track density may be simulated by the easier visibility of the larger etch pits), but has an even more pronounced softening effect on the plastic either before or after exposure. Depending on the concentration and/or the time of immersion, the etchability of the plastic is considerably increased.

2.5.4.2.3 The effect of ultraviolet radiation on the sensitivity of a plastic track detector.

The results obtained after experiments in Lexan (which is also true for many other plastics) are [48].

1). greatly reduce the etching times for making the tracks visible;

2). Significantly lower the threshold for track registration;

3) Continuously vary the detector sensitivity to suit the particular experiment, thus aiding the identification of particles.

It would be worth mentioning at this stage that the effect of the presence of ozone is quite similar to the presence of oxygen and ultraviolet.

2.5.4..2.4 Effect of lightly ionizing radiations on the response of plastic track detectors.

It has been observed that when the doses of protons, gamma rays and electrons etc. exceed a few Mrad, the density of damage along the latent damage trail is enhanced. On etching the detectors exposed to the above radiations, longer and thicker etch pits are obtained as compared to the unexposed ones[49-53].

2.6. Dependence of track velocity on the shape of the track profile.

2.6.1 Tracks velocity for constant V_T.

The following discussions are based on two assumptions 1) V_T is constant along the track and 2) V_G is constant and isotropic. Therefore V_T/V_G is also constant. Hence down to the end of the track, the etch pit must be conical.

The simplest case of normal incidence is considered here. This is because in all our studies we made the geometries in such a manner as to detect only the normally incident particles.

Let φ be the cone angle often assumed to be small. From fig.2.1

$$\text{Sin } \varphi = OB / AB \simeq OB / OA = V_G t / V_T t = V_G / V_T \quad \text{..... (2.20)}$$

The visible track length $l = V_T t - V_G t$

$$\text{i.e. } l = (V_T - V_G)t \quad \text{..... (2.21)}$$

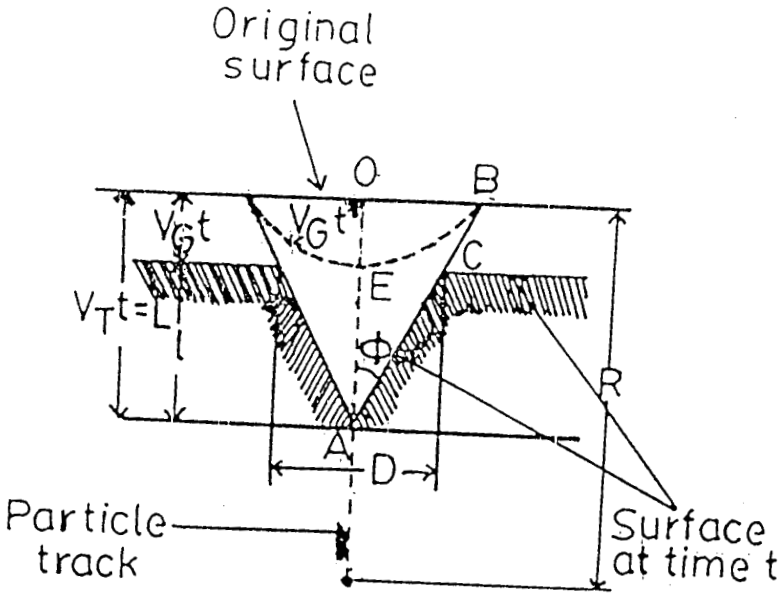

Fig 2.1. Track geometry for constant V_T

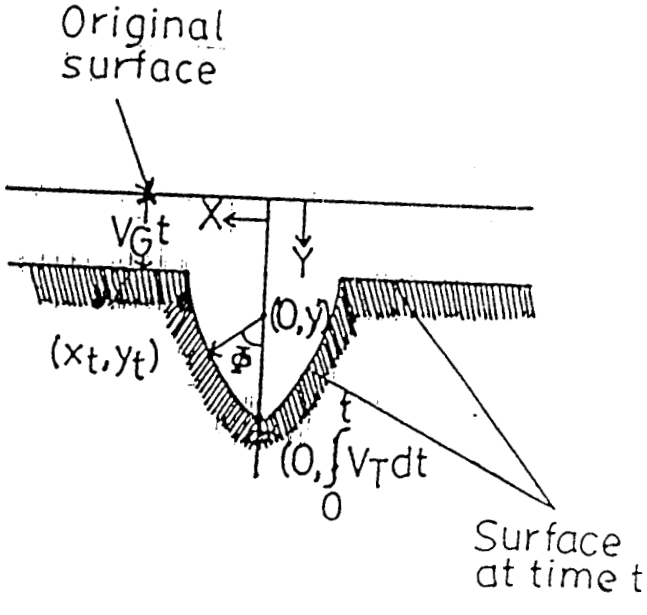

Fig 2.2. Track geometry for varying V_T

From Δ ECA,2EC = D, the track diameter

$$(D/2)^2 + l^2 = AC^2 = (l / \cos\varphi)^2 = l^2/ (1 - \sin^2\varphi)$$

substituting for $\sin\varphi$ and l from equations (2.20) and (2.21) we get

$$D = 2V_G t \left[(V_T - V_G) / (V_T + V_G) \right]^{1/2} \quad \ldots\ldots\ldots (2.22)$$

From eqautions (2.21) and (2.22) it is seen that if $V_T = V_G$, both l and D vanish. From the above equations we get

$$V_G t = D / 2 \left[D / 2l + \{(D / 2)^2 + l^2\}^{1/2} / l \right]$$
$$= D / 2 \left[\tan\varphi + \sec\varphi\right] \quad \ldots\ldots\ldots (2.23)$$

$$V_T t = \left[(D / 2)^2 + l^2 \right]^{1/2} \left[D / 2l + \{(D / 2)^2 + l^2\}^{1/2} / l \right]$$
$$= D / 2 \operatorname{Cosec}\varphi \left(\tan\varphi + \sec\varphi \right) \quad \ldots\ldots\ldots (2.24)$$

$$V_T / V_G = 2 / D \{(D / 2)^2 + l^2 \}^{1/2}$$
$$= \operatorname{Cosec}\varphi \quad \ldots\ldots\ldots (2.25)$$

2.6.2 Track geometry for vaying V_T

The etched track geometry is more complicated when V_T varies along the length of the track. It was experimentally verified that V_T in general varies along the track irrespective of the type of the detector [9,54,55].

The time required to etch through the measurable track length L is given by

$$t = \int_0^L dy / V_T(y) \quad \ldots\ldots\ldots (2.26)$$

If $V_T(y)$ is known, we can determine the track length L, diameter D and track profile (x_t,y_t) as a function of etching time. On the other hand, by measuring the track parameters L,D and (x_t,y_t) one can estimate $V_T(y)$.

The track profile (x_t,y_t) can be estimated as follows using the method suggested by Fleischer et al[56] and later by Paretzke et al[54]. Each point on the profile can be calculated by Huygen's (least time)[9] construction. Twice the value of x_t,, when $y_t = V_G t$, gives the diameter of the track after time t. The etching time to reach a point (o,y`) is $\int_0^{Y`} dy/V_T(y)$ and etching time to reach a point (x_t,y_t) from (o,y') is

$$[x_t^2 + (y_t - y`)^2]^{1/2}/ V_G$$

the total time to reach the point (x_t,y_t) is

$$t = \int_0^{y`} dy / V_T(y) + \sqrt{[x_t^2 + (y_t - y`)^2]} / V_G \qquad .....(2.27)$$

The actual path from origin (0,0) to (x_t,y_t) is the one corresponding to the least time. So taking the derivative of the above and setting it to zero we get

$$y` = y_t - (x_t / \sqrt{[(V_T(y`)/V_G)^2 - 1]} \qquad ..... (2.28)$$

This expression together with equation (2.27) defines x_t and y_t for a given t, y` and $V_T(y)$.

Since from fig(2.2) $\varphi = \mathrm{Sin}^{-1} (x_t / (y_t - y`))$, we can write equation (2.27) and (2.28) in y` as follows

$$x_t = [(y_t - y`)^2 + x_t^2]^{1/2} \mathrm{Sin}\theta \qquad ..... (2.29)$$

$$y_t = y` + [ (y_t - y`)^2 + x_t^2]^{1/2} \mathrm{Cos}\theta \qquad ..... (2.30)$$

Substituting for $(y_t - y`)^2 + x_t^2$ from equation (2.27) and for $(y_t - y`)$ from equation (2.28), we can write equations (2.29) and (2.30) as

$$x_t = V_G\left[t - \int_0^{y'} dy/ V_T(y) \right] [\, 1 - (V_G^2 / V_T(y`)^2)]^{1/2} \quad \ldots\ldots\ldots (2.31)$$

and

$$y_t = y` + (V_G^2/V_T(y`)) \left[t - \int_0^{y`} dy/V_T(y)\right] \quad \ldots\ldots\ldots (2.32)$$

These equations are valid for all y` and t. The procedure for calculating D(t) is as follows. Values of y` are substituted in equation (2.32) until the values of y` for which $y_t = V_G t$ is obtained. This value of y` in (2.31) gives D/2 correctly. Twice this value gives the diameter. The diameter is a function of V_T. V_T in turn depends on the energy of the incident particle and hence depends on the stopping power. Thus diameter depends on the stopping power in the detector.

Though several modifications of the above considerations have been suggested by several groups, the basic principle involved remain valid even now.

Diameter measurements on CN using H nd He isotopes have shown that by this method it is possible to distinguish various groups of H and He [57,58,59]. Subsequent studies have revealed that CN can distinguish alpha particles with a resolution of 300-400KeV at an energy of 2 - 4 MeV and with about 100 keV at 6 - 9MeV. Paretzke et al[54] observed that track diameter method is more sensitive for particles with lowest Z since the ionization rate changes drastically with distance in the detector medium.

Track diameter method in glass have been found more effective in the case of heavy particles like fission fragments[60]. With the discovery by Somogyi and Schlenk [61] that polycarbonates can very well be employed for identifyig particles by track diameter measurements, a new era of the use of plastic track detectors for particle identification was started.

The model suggested by Fleischer and Price[62] has been modified by Somogyi and Szalay[63] in 1973, to develop the diameter kinetics based on the parameters:- etch rate ratio, etchable range Ro and the angle of incidence φ. This model was also found suitable for understanding the etching kinetics of heavy ion tracks.

Though this model had satisfactorily explained many experimental data, it did not take into account the local changes of the etch rate along the trajectory. So Somogyi and Szalay[63] after a series of theoretical and experimental studies have found that the parameters etchable range Ro, critical range Rc, etch rate-ratio V(x) and angle of incidence φ are sufficient for most general details of the diameter kinetics. The variation of the etch rate ratio V(x) along the trajectory taken along the x axis based on these assumptions is shown in fig.2.3.

The criterion for the etch pit formation is that a chemically reactive defect density higher than a critical one should be produced by the particle along its trajectory. Hence Somogyi and Szalay [63] has introduced a residual range R_s at which the condition $V > 1$ is satisfied.

2.7. Mechanism of particle Track Etching in Polymeric Nuclear Track detector[64].

2.7.1 Mechanism and kinetics of chemical etching on cellulose nitrate

2.7.1.1 Mechanism of surface etching.

For tight polymers like pure cellulose nitrate[65] polycarbonate (Lexan, Makrofol) [66-68] poly (allyl) diglycol carbonate (CR-39)[68] and polyethyleneterephthte(Lavsan,Melinex, Mylar)[69], it can be supposed that the etching process is

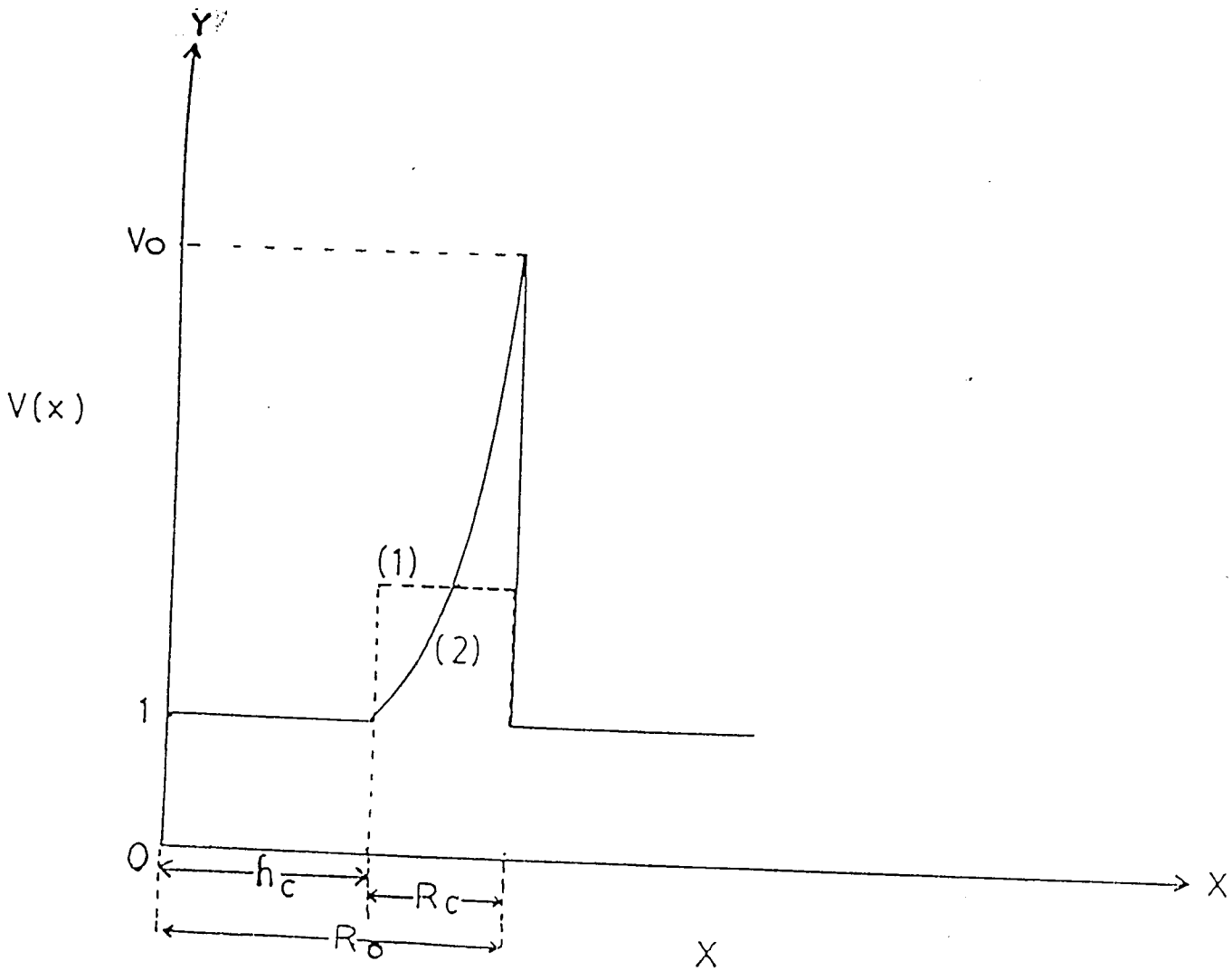

Fig 2.3. Schematic representation of the variation of the etch rate ratio along the trajectory, taking into account a critical layer removal h_c.

limited to the surface. This can be attributed to the fact that ions prefer to remain in a high dielectric constant medium, such as water, rather than to pass into a tight, low dielectric constant medium, such as a polymer film for electrostatic reasons[70-72].

The first stage in hydrolysis is the attack of a hydroxide ion at the central carbon atom of the ester group resulting in an intermediate. These intermediates were identified for polycarbonate (or PC), CR39[73,74] and poly ethyleneterphthalate (or PETP)[75]. The decay of the intermediate leads to a cleavage of a link in the polymer chain. In the hydrolysis of PETP a water molecule is involved in the decomposition of the Intermediate[76].

Since it is easier for the terminal monomer unit to turn into the right position for a successful attack of a hydroxide ion than for a monomer unit within the chain, the polymer chains are preferentially degraded from the chain end. This statement is confirmed by the appearance of a linear term in the response functions of bulk-irradiated polymers[77], which indicates a linear correlation between the radiation-induced surface density of chain ends and the enhanced surface etch rate after a bulk irradiation with gamma rays or electrons.

2.7.1.2 Mechanism of track etching.

The same hydrolysis reaction is supposed to be responsible for the degradation at the surface as well as in the particle track. However, in contrast to surface etching where the intermediate can expand into the solution in track etching a free reaction volume is required for the intermediate to be formed. In addition, the accessibility of the central carbon atom is influenced by the mobility of the monomer unit, which is dependent on the free volume[78].

Therefore the excess track etch rate (V_T -V_G) is assumed to be governed by the availability of the free reaction volume V^*, which can be formed from adjacent holes. These holes were produced within the particle track by release of gaseous radiolysis

products or of gaseous products of post-irradiation reactions. The free volume of such a hole V_f is determined by the volume of the escaped product. The main gaseous products of radiolysis of PC, CR-39 and PETP are CO_2 and CO[79,80] while NO_2 is released in addition in cellulose nitrate (or CN)[81]. Principally, the radiation damage will be most effective to V_T when the generation of a hole is accompanied by a chain cleavage.

The fact that no linear term was found in the response functions of CN,PC and PETP[82,83] for track etching in contrast to surface etching after a bulk irradiation[77] suggests the assumption that the rate determining step in the track etching is associated with the participation of more than one radiation product.

Based on the concept of a free reaction volume a linear correlation between the formation probability of the free reaction volume $P(V^*)$ and the track etch rate enhancement $(V_T - V_G)$ is supposed.

$$(V_T - V_G) = k.P(V^*), \qquad \ldots\ldots \quad (2.33)$$

where k is the specific rate constant, P(V*) can be derived from the formation probability $P(V_f)$ of a single hole with the free volume V_f. Taking into account that the number of holes required to form V* is determined by the ratio V^*/V_f, (P(V*) can be expressed in terms of $P(V_f)$,

$$P(V^*) = P^b(V_f) \qquad \ldots\ldots\ldots\ldots \quad (2.34)$$

By inserting (2.34) into (2.33)

$$V_T - V_G = k.P^b(V_f) \qquad \ldots\ldots\ldots \quad (2.35)$$

2.7.1.3 Response of organic polymers to ionizing radiations.

Organic polymers exhibit a basic difference in their reponse to ionizing particles compared to the response of biological cells or photographic emulsion. For the latter the assumption of a matrix of isolated targets with any energy transfer between the sensitive elements can be applied to describe their response by a multi-hit or multi-target model. Hence the response is saturating in nature and the excess energy is wasted.

This concept is not valid for polymeric nuclear track detectors, because of the energy transfer in polymer chains[87]. The distance of an effective energy transfer depends on the molecular structure. The distance is shortest for aliphatic hydrocarbons, increases with the amount of aromatic groups containing delocalized π - electrons, and becomes large for conjugated systems of aromatic groups and alternating double bonds in the main chain. For example, only a negligible increase in the radical yield in polyester was noticed after gamma-irradiation when the number of CH_2 – groups per monomer unit was increased upto 7[88]. The marked increase in radical yield for polymer containing 8 CH_2 – groups per monomer unit indicates that the radio protective effect of the terephthalic group covers $7CH_2$ – groups per monomer unit at maximum. Because of this, an effective energy transfer over several monomer units in PETP can be assumed, since it contains only 2 CH_2 – groups per monomer unit.

For polymer chains the waste of energy is supposed to be substantially reduced through an energy transfer resulting in an activation of adjacent elements in the chain. The cleavage yield of polymer chains is expected to vary linearly with the deposited energy upto a high dose.

The response pattern for very high values of deposited energy cannot be predicted. Experimental results of normally processed particle tracks appear to be far from a region of saturation. Even the track etch rate of fission fragment tracks in PC

can be further increased by an UV-exposure in the presence of oxygen. Through this treatment the etch rate ratio can be enhanced upto 10^4[89].

As a consequence of the very rapid energy transfer on the molecular level[90-93] the deposited energy is dissipated over a limited number of monomers resulting in an excited electronic system predominantly of valence electrons[92] before the first bond will be cleaved. Bond cleavage is not a random process. Besides geometric effects bonds are assumed to be cleaved in the order of their dissociation energies. Hence, in general only one or two different types of primary radicals can be identified in polymers after a bulk-irradiation[94].

These considerations suggests that (V_T -V_G) should be correlated with that energy fraction which is deposited within a cylinder of a certain radius around the particle trajectory[95]. The radius of the cylinder is dependent on the size and the number of monomer units involved in the formation of the free reaction volume. The size of the monomer unit is about 1 nm If a participation of two or three monomers in the formation of the free reaction volume is assumed the radius of the cylinder amounts to 2 - 3 nm. The smallest effective pore diameter in etched fission fragment tracks in PC[89] was found to be 5 nm, which can be considered as an upper limit of the radius.

From a practical point of view the (dI/dx) and REL values have been preferred so far, because they are easier to calculate and sufficient accuracy can be provided by fitting the adjustable parameters.

2.7.1.4 Discussion of the empirical response function

Based on the assumption that only the track etch rate enchacement (V_T -V_G) is the result of the radiation damage the following expression was experimentally derived for CN[96] using the model of "primary ionization" dI/dx.

$$V_T = V_G + a^* (dI/dx)^b \quad \ldots\ldots\ldots\ldots \quad (2.36)$$

The general form of the response function obtained by noramalization of V_G[65].

$$V_T/V_G) = 1 + a(x)^b \quad \ldots\ldots\ldots\ldots \quad (2.37)$$

where x can be replaced by (dI/dx), REL or L_r (radius restricted energy loss)[82,83]. According to the proposed concept of a free reaction volume the exponent in the response function represents the ratio V^*/V_f, while the factor a is K/V_G.

On the basis of this concept the influence of etchant activity, etching temperature and the degree of substitution on the response function of CN will be discussed in the following. A correlation between factor and exponent of the response functions obtained with alpha particles for different registration conditions[97]. Using the (dI/dx) values given in ref[98] for CN the correlation between the factor a and the exponent b has the following form.

$$a = 19.4 \times 0.0308^b \quad \ldots\ldots\ldots\ldots \quad (2.38)$$

By inserting (2.38) into (2.37) a general response function for CN in (dI/dx) values can be obtained.

$$(V_T/V_G)_{CN} = 1 + 19.4[0.0308\ (dI/dx)]^b \quad \ldots\ldots\ldots (2.39)$$

The term 19.4 represents the reduced specific rate constant K/V_G, while the term 0.0308 includes the formation probability $P(V_f)$ and a factor to correct for post-irradiation reactions which have an effect on the hole concentration. The value of 0.0308 depends on the applied model (REL, (dI/dx), L_r). The exponent covers an interval form 2 to 5.4 for the experimental conditions used. The results indicate that the exponent is strongly influenced by the water activity of the etchant. Based on the concept of a free reaction volume this effect can be explained as follows:

Although the absolute value is unkown, it can be assumed that the diffusion rate of water in the CN studied is higher than the track etch rate of alpha particle tracks[99]. Thus, an equilibrium water concentration is established in the latent track and in the surrounding material in front of the etch channel. The observed water acts like a plasticizer resulting in an elevated chain mobility. Because of this, the stability of the latent track structure is reduced and the thermodynamically non equilibrium state of a high concentration of holes and chain ends initiates a diffusion of holes and chain ends cut off the latent track region into the surrounding bulk material. A new concentration of holes and chain ends are established in the latent track at a lower level, which is a function of the chain mobility in the bulk material which depends eventually on the water activity in the etchant.

With respect to the lowest exponent found in the response function of CN two holes assumed to be required in the formation of the free reaction volume at minimum. It appears reasonable that only holes within a volume element of a critical radius are capable of generating the free reaction volume. Under the condition that the hole concentration in the latent track is depleted by diffusion, the free reaction volume can be formed only in such a volume element which contains at least two holes after diffusion. The original number of holes required to ensure that two holes will be available in the volume element at the moment of hydrolysis increases with the mobility, that means with the water activity in the etchant. The exponent in the response function represents the original number of holes per volume element.

As shown in fig.2.4 the points exhibit the tendency to cluster around natural numbers, but there are also some exponents outside these clusters suggesting that also volume elements with different hole numbers can contribute to the enhanced etchability. For an unaffected track structure this effect might be attributed to a variation of V_f and V^*. On the other hand, for a latent track which has lost some hole by diffusion the necessary number of holes in a volume element can be reached from different original numbers. Consequently, two terms with different exponents can be

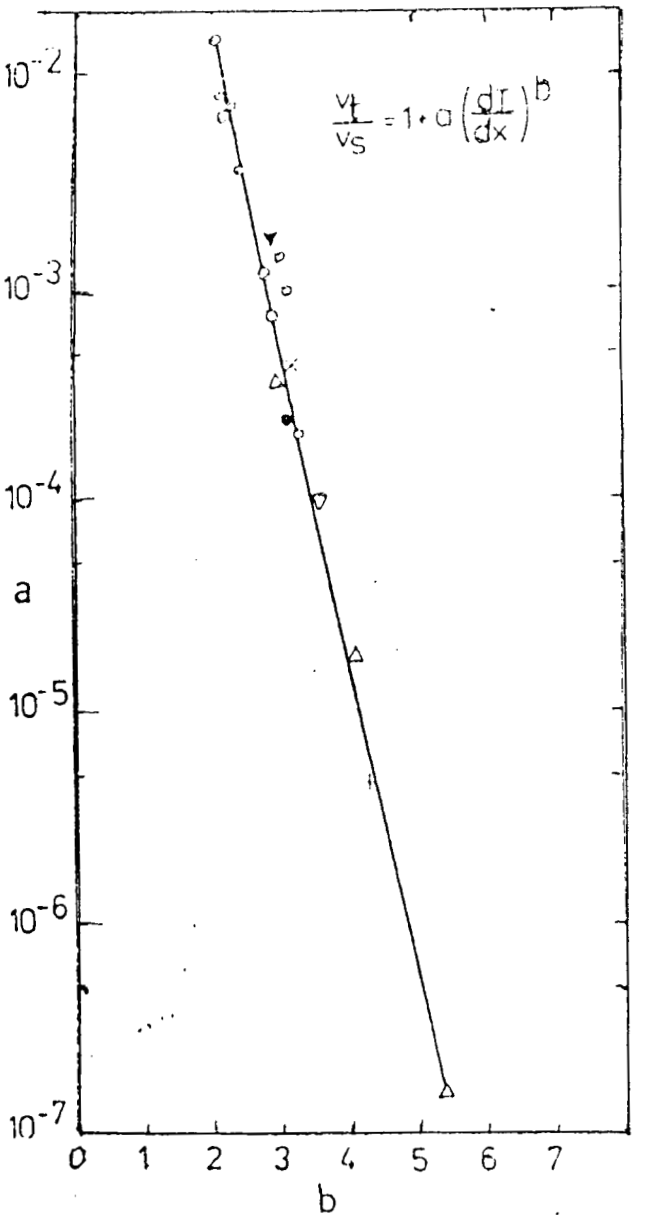

Fig 2.4. Plot of factor 'a' versus exponent 'b' of the response function for CN.

expected. However, for a narrow interval of V_T the two terms appear as one term with an averaged exponent.

2.7.2 Response of the light particles on cellulose nitrate [100].

2.7.2.1 Effect of particle parameters.

The response of the detector sheets prepared from CN material of various DS were generally studies with alpha particles in an energy interval from 1.7 to 8.5 MeV[98]. With reference to its high sensitivity to alpha particles detector sheets made from CN-88 were chosen to check the response to protons and deuterons in the energy interval of 0.3 – 1.2 MeV and 0.45 – 1.95 MeV, respectively. In fig.2.5 the noramlized excess track etch rate (V_T/V_G) - 1 is given as a function of the radius-restricted energy loss L_r, ie. The energy which is deposited within a cylinder of r = 3 nm around the particle trajectory[101]. Particle etching was performed in 5N KOH at 70°C. The response function (RF) obtained by least – squares fit has the following form.

$$V_T / V_G = 1 + 5.49 \times 10^{-4} L_r^{2.13} \quad \ldots\ldots\ldots \quad (2.40)$$

The standard deviation of the coefficient and the exponent in eqn.2.40 are 0.7×10^{-4} and 0.036 respectively. Transformed to $(REL)_{200}$ values [MeV cm^2g^{-1}] often used for CR-39[102] eqn.(2.40) takes the form

$$V_T / V_G = 1 + 7.22 \times 10^{-6} (REL)_{200}^{2.15} \quad \ldots\ldots\ldots \quad (2.41)$$

On a [keV/μm] basis the factor in eqn.(2.41) turns into 3.93×10^{-4}.

Although a steady approach of V_T / V_G to 1 can be expected as consequence of the form of the RF[103,104,82] it appeared reasonable to define a practical detection threshold which is influenced by the thickness of the etched surface layer Δ h and the

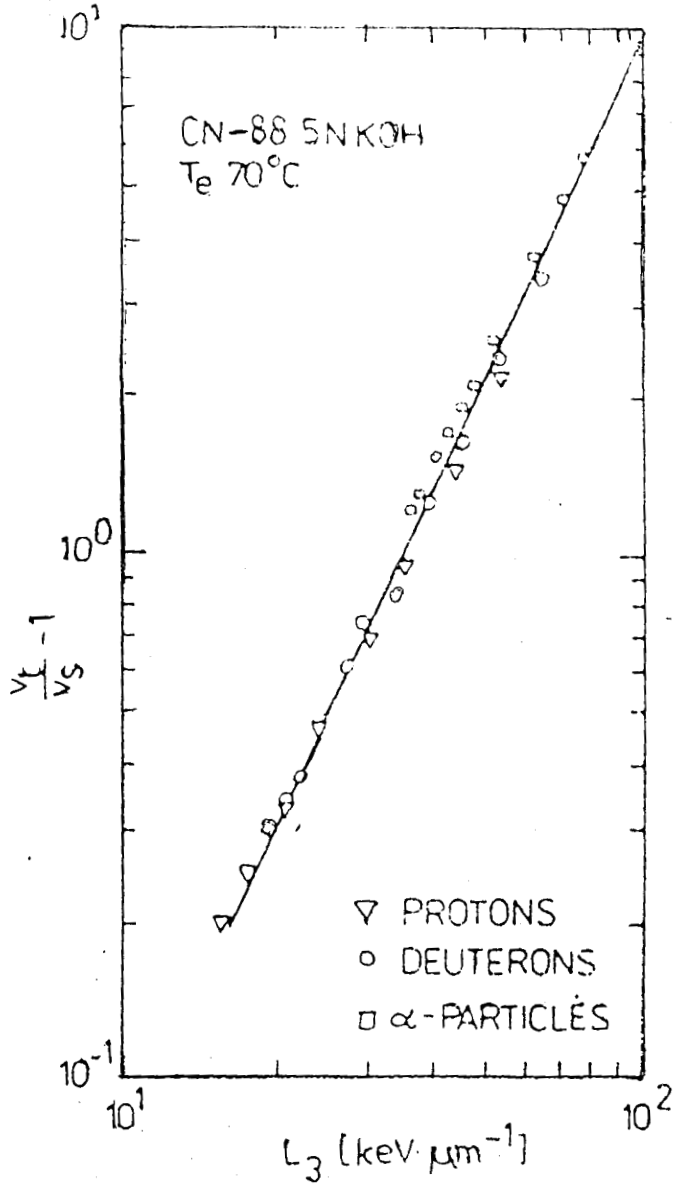

Fig 2.5. Response of CN-88 to protons, deuterons and α particles.

smoothness of the detector surface after etching[98]. With the present material an etch rate ratio of 1.2 was found to be sufficient for the identification of an etched particle track at $\Delta h = 4$ μm. The resulting practical threshold energies E_c with protons, deuterons and alpha particles are 1.2, 2.4 and 22.4 MeV, respectively. The critical $(REL)_{200}$ values associated with E_c amounts to 115 MeV cm^2g^{-1}. For comparison the E_c value obtained with alpha particles in Kodak CA80-15 cellulose nitrate is 3.1 ± 0.4MeV (2.5 N NaOH at 60°C). This E_c published by Hayashi and Iwata[105] is nearly consistent with the E_c of 3.8 MeV reported for Daicel Cellulose nitrate[106].

2.7.2.2 Material effects on the R.F.

The experiments with CN sheets of different DS and DP (degree of polymerisation) revealed a marked effect of these parameters on the RF. It is apparent that the sample CN-63/4000 which has the lowest DS and DP[107] delivered the lower registration sensitivity in the low L_r region for the given etching conditions. The lowest threshold value of $(L_r)_{1.2}$ associated with the lowest exponent was obtained with the material CN-88.

2.7.2.3 Effect of etching conditions.

The influence of the etchant concentration on alpha particle response was tested with CN-63 and CN88. The results indicated that the registration sensitivity increases with C_{KOH} or in other words with a decreasing water activity in the etchant. Apart from the 6.4N KOH the sensitivity of CN-88 was generally higher compared to CN-63. The concentration of 5 mol/l appeared to be an optimum etching condition for CN-88.

From the the RFs of CN-88 obtained at serveral etching temperatures in 5N KOH, the optimum etching temperature was found to be 70°C.

2.7.2.4 Correlation between factor and exponent of the RF.

Taking into account all RFs obtained with CN in a DS interval of 2.63 – 2.97 and various etching conditions a correlation between a and b of the RFs can be established as shown in fig.2.6. A least-squares fit of 28 experimental points delivered the following relation with a correlation factor of 0.988

$$a = 8.12(0.0111)^b \quad \ldots\ldots \quad (2.42)$$

Eqn.(2.42) indicates that the factor of a RF consists of a constant term which is independent of material parameters and etchig conditions, and a second term which has the same exponent as L_r. Thus a general RF can be formulated for CN which takes the following form when L_r is given in keV/μm.

$$V_T/V_G = 1 + 8.12(0.0111L_r)^b \quad \ldots\ldots \quad (2.43)$$

Principally, the individual RFs obey the general form in the whole factor interval studied (10^{-9} – 10^{-3}) which corresponds to an exponent interval from 5 to 2. Scattering of the experimental points around the line in (fig.2.6) is perhaps attributable to varying structural parameters of the detector sheets.

The response of the studied CN detectors to alpha particles is characterised by a large variation of the exponent of the RFs which cannot be explained in terms of a varying radiation sensitivity of CN. The effect of the water activity in the etchant on the exponent suggests that the exponent of the RF is rather governed by post-irradiation processes.

According to the concept of free reaction volume outlined in ref[108] the prefered etching along the latent track is considered to be attached to the availability

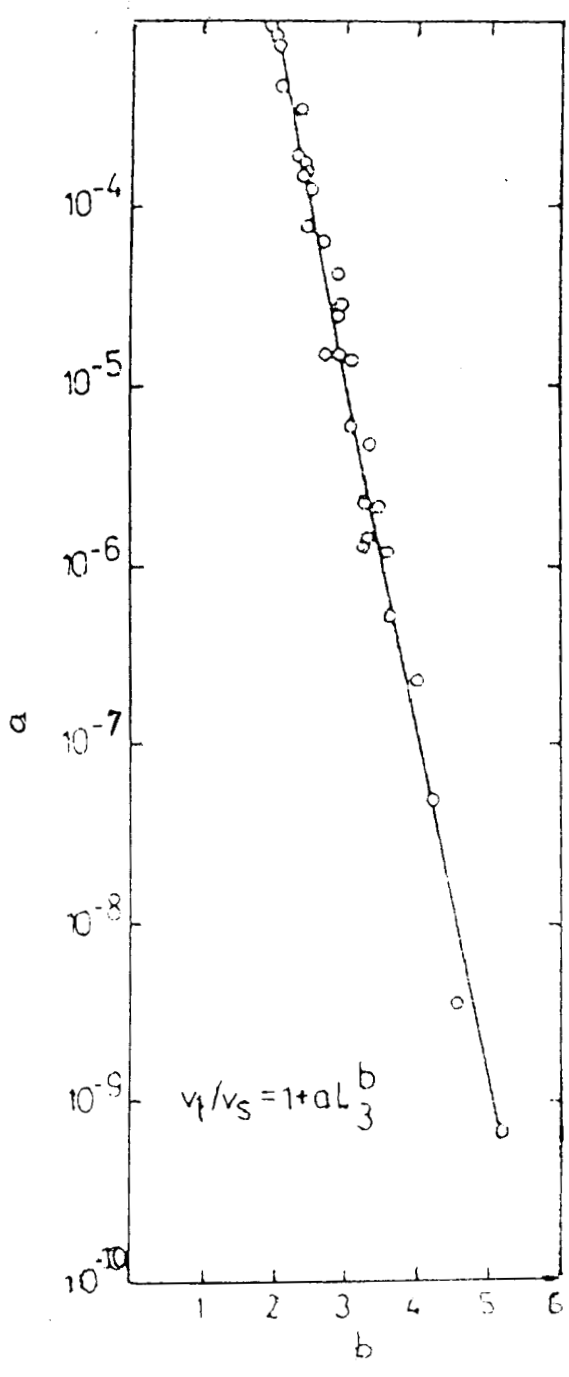

Fig 2.6. Correlation between factor 'a' and exponent 'b' of 28 different RFs obtained for various DS and several etching conditions. The standard deviations of the values are equal to the circle diameter.

of a free volume of molecular size which facilities the attack of the etchant and enables the formation of the activated complex or intermediate. The free reaction volume can be formed from adjacent molecular holes located in a critical volume. These holes are generated by release of gaseous radiolysis product. According to this concept the exponent of the RF presents the number of molecular holes needs for the free reaction volume[108].

In CN the holes are mainly created by release of CO_2, CO and NO_2[109]. The holes can be trapped in the latent track provided the temperature is lower than the glass transition temperature Tg of the bulk material, otherwise fading of the latent track would occur. The temporal stability of the latent track is a result of the "frozen in" mobility of polymer chains below Tg. The stability is lessened or even lost if the detector is subjected to a temperature above Tg.

The effect of the water activity on the exponent of the RF can be understood in terms of the following mechanism. For unplasticized CN the Tg is approximately 56°C[110]. Once the detector is immersed into the aqueous etchant water can quickly penetrate into the latent track and the bulk material[111,112] resulting in a plasticizing effect. Especially in a diluted etchant with a high water activity the absorbed water may cause a significant decrease in Tg. As a result a number of holes can escape from the latent track into the bulk by enhanced difffusion before the etchant can reach that region. With respect to the lowest exponent b = 2 (fig.2.6) it is supposed that 2 holes are required for the formation of the free reaction volume.

When holes can escape from the latent track only those volume elements can facilitate track etching which contain at least 2 holes even at the moment of chemical attack. It is obvious that the original number of holes required to satisfy this condition will increase with increasing chain mobility which, in turn, is a function of the difference between the etching temperature and the actual Tg. Therefore higher exponents in the RFs can be expected with the diluted etchants due to its higher water activity.

2.7.3 Response Function of the Plastic Track Detector CR-39.

Since the discovery of the unique sensitivity of the polymer CR-39 (Poly (allyl) diglycol carbonate) to ionizing partiles[4,113] intense efforts have been made to investigate its properties and to develop its practical application in numerous fields. The status of development has been reviewed very recently[114,115]. The ratio between the track etch are V_T and the surface etch rate V_G was found to vary with the restricted energy loss REL^n, where n = 2.5 was noticed for high values of REL[4], while n = 1.6 was reported for low values of REL[116]. In a study by Henshaw et al[117] the V_T curve (V_T Vs $(REL)_{200}$) exhibits a progressive change in slope, which becomes steeper with increasing $(REL)_{200}$. It was the aim of the present study to derive a response function from the availabel experimental data, which can be used to describe the track response of CR-39 in the entire $(REL)_{200}$ interval employed in particle track studies.

2.7.3.1 General Response Function of CR-39.

Based on the assumption that only the difference $V_T - V_G$ is caused by the radiation damage[96,98], which has been confirmed by the track response of numerous plastic track detectors[82,118], available V_T and V_G data of CR-39 reported in refs[117,119,120,121] were transformed into the normalised excess track etch rate $(V_T/V_G)^{-1}$. In order to cover a wide $(REL)_{200}$ range data had to utilized, which were obtained from CR-39 samples of different origin[117,119,120,121]. In spite of this shortcoming the data shown in fig.2.7 give evidence for a combination of linear and supra linear response, which can be described by the following general response function

$$V_T / V_G = 1 + a_1(REL)_{200} + a_3(REL)^3_{200} \quad \ldots\ldots\ldots\ldots \quad (2.44)$$

where a_3 is 1.25×10^{-3} and a_3 is 0.22×10^{-9} for the curve shown in (fig.2.7). The calculated curve correlates well with the experimental data. Although the general

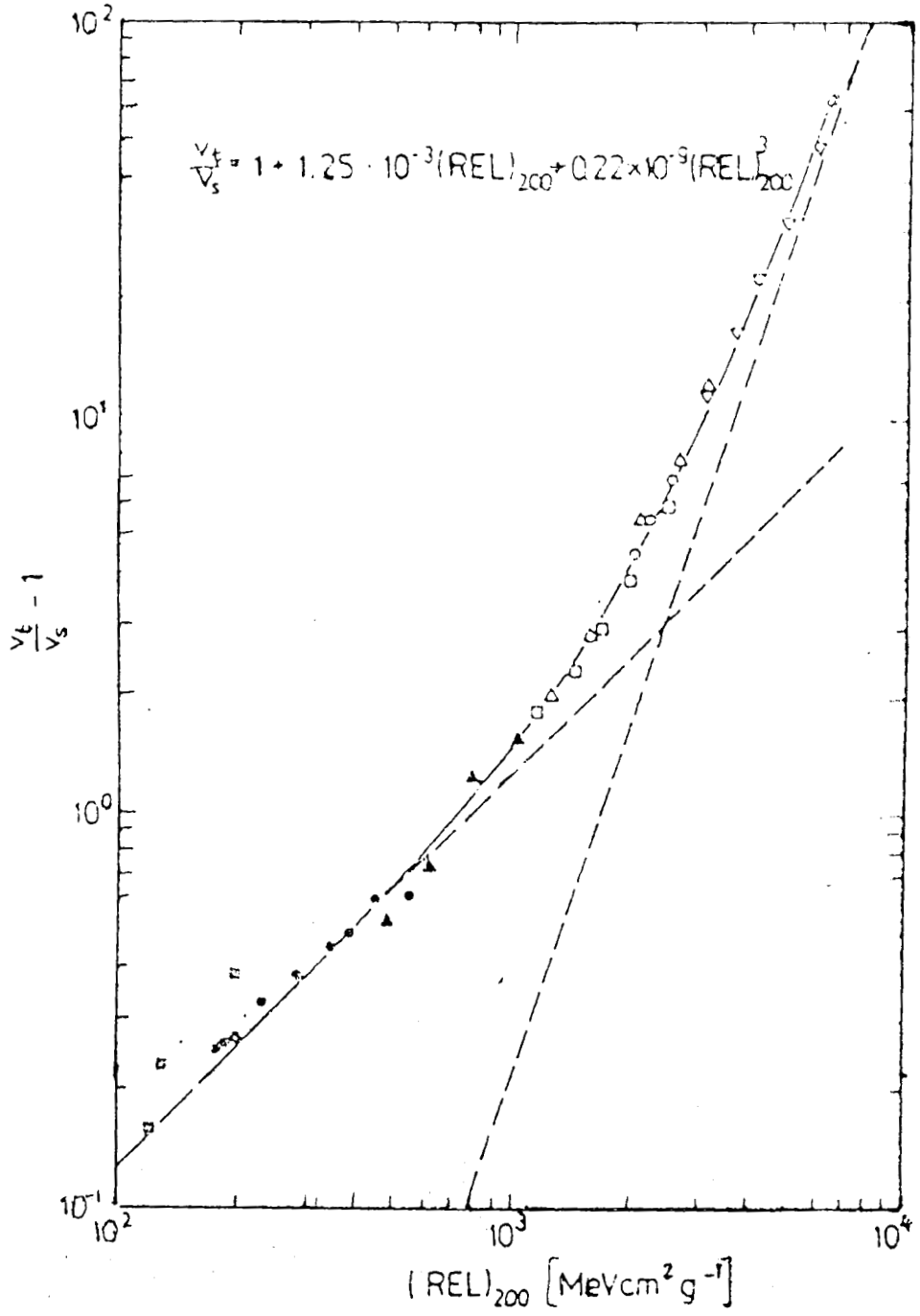

Fig 2.7. The response curve of CR-39 calculated from equation (2.44) compared to Experimental Data Selected from refs 116,117,119,120. Etching conditions : 6.25N NaOH at 343 K.

character of the response function in the form of eqn.(2.44) is confirmed by the results given in fig.2.8 and Table (2.1) the factor a_1 and a_3 can vary due to differences in the curing process used to produce the cross linked plastic.

At present CR-39 is the only plastic track detector which exhibits a combined linear and supra linear response. The response functions of detectors made from cellulose acetate, cellulose nitrate, poly carbonate, and polyethylena terephathalate have only one supralinear term with an exponent equal to or higher than two [82,118].

Table (2.1) Temperature Dependence of the Factor a_1 and a_3 of the response curves shown in fig.(2.8).

Temp K	$a_1 \times 10^3$	$a_3 \times 10^9$
300	0.56	0.040
313	0.65	0.069
327	0.75	0.121
343	0.88	0.216

2.7.3.2 Temperature Dependence of the Response Function.

Track etch data reported by Flower et al[119] for four etching temperatures were used to establish the temperature dependence of the response function. As shown in (fig.2.8) the data redrawn in the form of (V_T/V_G)-1 can be well described by response functions in the form of eqn(2.44). The corresponding factors are listed in Table 2.1. The temperature dependence of a_1 and a_3 indicates a difference in the temperature dependence of V_T and V_G). In an ARRHENIUS plot, however, straight line can be drawn from the values given in table 2.1. Therefore, it was possible to calculate the difference between the apparent activation energy of the rate determining processes in track etching and surface etching for a_1 and a_3, respectively.

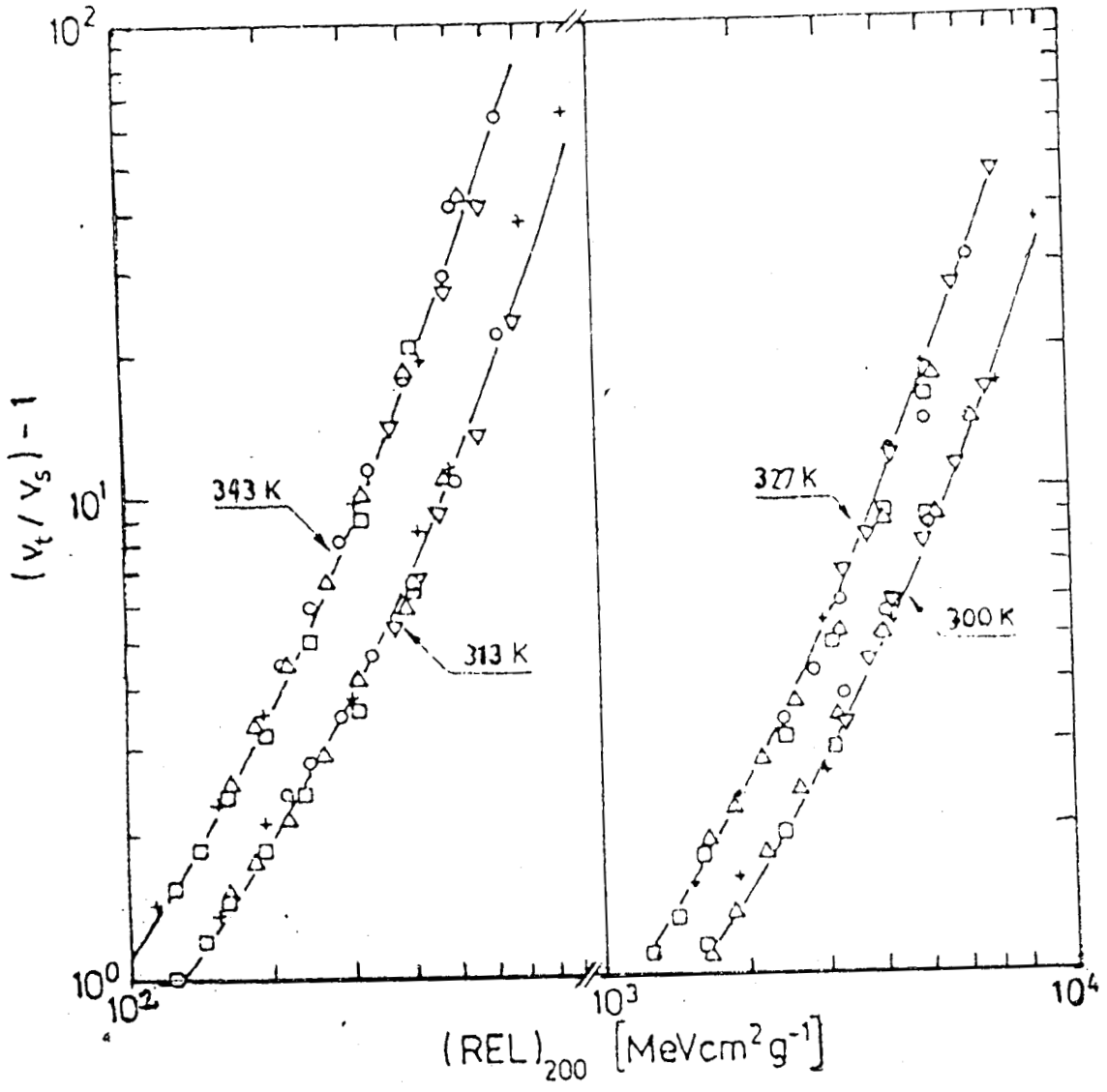

Fig 2.8. Response curves of CR-39 obtained from equation (2.45) compared to Experimental Data Reported by Fowler et al [119] for four Etching Temperatures 6.25N NaOH)

Taking into account the pre-exponential factor obtained from the same lines the temperature dependence of the track response can be expressed by the followig response function.

$$V_T / V_G = 1 + 2.06 \times 10^{-3} (REL)_{200} \exp(-9.0/RT) + 2.82 \times 10^{-5} (REL)^3_{200} \exp(-33.6/RT) \quad \ldots\ldots\ldots \quad (2.45)$$

R is the molar gas constant (8.314×10^{-3} KJ/mole K). The low value of 9.0 kJ/moleK in the first term is agreement with the observed weak temperature dependence of the track response in the case of alpha particles, while the higher value of 33.6 kJ/moleK in the second term is responsible for the marked temperature effect on the etch rate ratio of heavy ion tracks[114,115].

Taking into account the temperture dependence of the factors the following relation between a_3 and a_1 was found.

$$a_3 = 3.258\, a_1^3 \exp(-6.64/RT) \quad \ldots\ldots\ldots\ldots \quad (2.46)$$

By inserting eqn(2.46) into eqn(2.44) the factor of supralinear term can be replaced.

$$V_T / V_G = 1 + a_1(REL)_{200} + 3.258\left[a_1(REL)_{200}\right]^3 \exp(-6.64 / RT) \ldots\ldots\ldots \quad (2.47)$$

This form of the response function is of practical importance, because a_1 can be determined experimentally with alpha particles emitted from radio isotope sources. In this way it is possible to establish a response function which can be used to calculate the track response of CR-39 upto the heavy ion range of about $(REL)_{200} = 8 \times 10^3$ MeV/cm^{2}g^{-1}.

The correlation beween the normalised excess track etch rate and the restricted energy loss gives evidence for a response function of CR-39 which includes a linear and a supralinear term with an exponent of 3. The mixed response is considered as the reason for the appearance of various exponents in response functions reported for

small REL intervals. The observed different temperature dependence of the factor of the linear and the supralinear term suggests that the track etching mechanism may be different in the low and in the high REL region. The correlation between a_1 and a_3 indicates on the other hand that the yield of radiation induced damage relevant to the rate determining process responsible for a_1 and a_3, respectively, may be generated in a fixed ratio.

2.7.4 A Track Development Models for CR-39 for low Energy Alpha Particles.

Chemical etching is an important technique for the revelation of latent tracks of ionising particles in track detectors. In this technique, the latent tracks are amplified and made visible (under a microscope) by etching with appropriate reagents[9]. The success of this technique depends on the preferential attack of the damaged region along the track by the etchant. The surrounding undamaged material is affected less rapidly, resulting in an enlargement of the etched holes.

Fleischer et al[56] suggested a method to obtain the track profiles at various etching times. It was Somogyi[28] who was chiefly responsoble for developing a theoretical basis for the evolution of etched nuclear tracks for different initial conditions. In his treatement, the parameters of the etched track profile, track length and diameter are related to the etching response V_T/V_G. (where V_T = track etch rate, V_G = bulk etch rate), which, in turn, is related to the damage response S and finally to the particle parameters Z, M, E and range. Thus, the measurement of the track parameters gives information on the particle parameters for identifyiing the particles.

Antony et al[122] have developed a model for finding the track profile and other parameters using a numerical method. This has been successfully applied to low energy alpha particles in CR-39 detector.

A numerical method has been developed for determining the etched track profile and its parameters like track diameter and track length for CR-39 track

detector for low energy alpha particles. The track etch rate is assumed to vary along the track and etching is assumed to take place normal to the etched surface at any time. The results agree well with the measurements.

2.8. Method of Measuring Various Track Parameters.

2.8.1 Measurment of V_G.

The methods commonly adopted for the determination of V_G are the following:

2.8.1.1 Thickness change method[38].

In this case the bulk etch rate V_G is given by

V_G = Reduction in the detector thickness after etching/twice etching time.

= $x/2t$

where $x/2 = h$, the thickness of the bulk material removed from one surface of the detector.

This method is capable of accuracy of 0.1μm when the most accurate instruments are used to measure the detector thicknes (eg. Michelson interferometer etc.) before and after the etching. After etching, detectors are usually cleaned with alcohol to remove the greasy material if any.

2.8.1.2. Track diameter method[24].

For normally incident particles, the track diameter D after etching for a time t is given by

$$D = 2V_G t \left[(V_T - V_G) / (V_T + V_G) \right]^{1/2}$$

For heavily ionising charged particles $V_T >> V_G$.

$D = 2V_Gt$

Usually bulk etch rates are calculated from measurements of the diameters for normally incident ^{252}Cf fission tracks.

2.8.1.3 Mass change method (Gravimetric method)

If M_o and M_t are the Mass values of detector respectively before and after etching for a time t, and A and ρ are respectively the surface area and density of the detector, the expression for the bulk etch rate V_G is

$$V_G = (M_o - M_t)/2A\rho t \quad \ldots\ldots\ldots\ldots \quad (2.48)$$

This method has a potential of 0.001μm accuracy if samples are weighed with an analytical balance of 0.01 mg sensitivity.

2.8.2 Measurement of V_T.

The projected track length l is measured from the centre of the track ellipse at the etched surface to the end of the track tip. The true track length L (the length from the original surface to the terminal end of the track) is then obtained from the relation[38] as

$$L = l/\cos\theta + V_Gt/\sin\theta - V_G(t-tc) \quad \ldots\ldots \quad (2.49)$$

where θ = angle of incidence

t = etching time.

$V_Gt/\sin\theta$ = surface etching correction

$V_G(t-tc)$ = over etching correction

tc = ectching time required to etch the tracks upto the points where they stop (etched) until the track ends become round). Then $V_T = \Delta L/\Delta T$, where ΔL is the track length increase in etching time ΔT.

2.8.3 Measurement of residual range.

Knowing the etch rate relation V ($=V_T/V_G$), we can estimate the residual range R using the relation[123].

$V = 1 + \exp(-AR + B)$ where A and B are fitting parameters.

2.8.4. Determination of specific energy loss dE/dx[28].

From the relationship $V = 1 + \alpha(dE/dx)^{\beta}$ ..... (2.50)

Where α and β are fitting parameters characterising the detector materials and the track etching conditions employed, one can estimate the specific energy loss.

2.8.5 Measurments of activation energies.

2.8.5.1 Activation energy for bulk etching.

Determination the bulk etch rate V_G at different etching temperatures T. Plot a graph between $\log(V_G)$ and 1/T. The graph will be a straight line with negative slope. So the bulk etch rate V_G depends exponentially on the etching temperatures[124] as given below.

$V_G = A \exp(-E_G/kT)$ ..... (2.51)

Where A is a constant depending on the nature of the etching reaction, E_G the activation energy for bulk etching and k is the Boltzmann constant.

2.8.5.2. Activation energy for track etching[124].

The variation of track etch rate V_T with etching temperature is also exponential. Here $V_T = B\exp(-E_T/kT)$ where B is another constant and E_T the activation energy for track etching.

2.9 Application of SSNTDs.

SSNTDs are extensively used in various disciplines of science and different branches of technology. Some of the important applications are follows.

2.9.1 Nuclear Physics[125].

Price and Walker were the poineers who has used the track detectors in nuclear physics studies. In experimental nuclear reaction studies, the most general requirement is to measure the yield and the spatial distribution of reaction products while their energy and type are simultaneously determined frequently in the presence of a high background due to various types of radiation. Especially in studying low yield nuclear processes, high efficiency and long term stability of the applied spectroscopic methods are highly desirable. In such situations various nuclear track detector method can be used very effectively and successfully. These are ideal when the resolving power ($\Delta E/E = 5 - 10\%$) required to separate the energy group is not too high.

In low energy nuclear reaction studies, the most important advantages of using plastic track detectors are the following.

(i) long term exposure can be performed due to high stability of the latent tracks,

(ii) selective particle detection can be realised even in high back ground radiation by properly chosen detector material and etching condition;

(iii) the whole angular range can be covered in one run using a detector strip bent around the target.

2.9.1.1 Track method in nuclear reaction studies [126]

The etch track methods applicable in nuclear spectroscopy can be classified according to the main track parameters to be measured. These are:

(i) the track diameter (for normally incident particles).

(ii) Track size method: Surface size parameters such as minor and major track axis at an arbitrary angle of incidence is measured and

(iii) Track shape method : Track shape parameters are measured from which the particle range can be determined.

In the early days these detectors were used mainly in fission physics studies. In Nuclear Physics, conventional detectors are nowadays replaced by track detectors, because of their high particle identifying capability. Depending upon the need minerals, glass and plastics are in use. As more and more sensitive track detectors were developed, their use in nuclear physics increased. Being very good threshold detector, SSNTD can record tracks of heavily ionising particles in a variety of adverse conditions such as intense background radiation and high temperature. They are very useful in low cross section studies. Owing to their passive nature, they can be exposed even for months or years together for low count rate measurements.

2.9.2 Cosmic ray physics.

In cosmic ray studies we require flexible, light weight track detectors that do not use electronic circuits. So SSNTDs are most suited for cosmic ray studies. Also, they have high charge resolution properties. The use of these detectors in payload experiments have provided valuable information regarding the presence of heavy and superheavy elements in the galactic cosmic rays:

Walker and Price[6] discovered in 1965 the presence of ultra heavy nuclei of $Z > 60$ in cosmic rays in the etched tracks in the meteoritic crystals. The studies of the

etched tracks of cosmic ray iron nuclei in many meteoritic crystals and in lunar rocks and soils were made by a number of centres in the world. In India, these studies have revealed many new facets of early history of the solar system. In 1975-80 TIFR-PRL group in India discovered in near earth space the anomalous cosmic rays in Lexan detectors flown in sky lab III mission of NASA. In 1985 the group flow CR-39 detectors in space shuttle space lab-3 mission of NASA and in 1990 made the first direct measurements of ionisation states of anomalous cosmic rays.

2.9.3 Dosimetry:

SSNTDs have some unique properties such as high spatial resolution and time integrity, good particle-particle and particle-gamma discrimination. So they are quite suitable for dosimetric applications[4]. They are easy to handle and have low price. So they are the apt detectors for large area survey. They register single nuclear tracks. Mass, energy and charge of incident radiation can be determined from track geometry and track and bulk etch rates. Track detectors etched after exposing to various radiation and gamma rays show considerable changes in optical transparency depending on the absorbed dose[127].

2.9.4 Radiography:

In medical and several other fields heavy particle radiography using plastic track detectors is widely used[128,129]. The residual energy or range of the mono-energetic charged particle beam after it has passed through the specimen is measured with a stack of plastic track detectors[130]. Whereas X-ray radiography is more suited to subjects having regions of highly varying atomic number, heavy particle radiography using track detectors is more appropriate in detecting abnormalities in subjects homogenous with respect to atomic number. Fast neutron radiography of extended or thick objects using plastic track detectors is used in non-destructive testing[131].

2.9.5. Nuclear track microfilters.

The nuclear track micropone filter(NTMF)[132] is a kind of novel material used successfully in various fields such as precise separation of biological cells, filtering of polluted air, stabilizing beverages, micro electronics, pharmaceutical and waste water recycling, filteration of bacteria from drinking water, measurement of viscosity of liquids such as heptane, xylene, toluene, water etc. Such applications will make them useful in chemical industries as well.

For the production NTMFs heavy ions ^{238}U, ^{209}Bi are best suited due to their high specific energy loss. We can also use high ions like ^{28}Si. Today various filters are avialable with desired range of porosity and dimensions, ranging from 10nm to 1mm, depending on the ion energy, type and thickness of SSNTD foil.

2.9.6 Earth Sciences:

In earth sciences, SSNTDs are used in the determination of spatial distribution and abundance of several elements on the earth crust. By this method, quite low as well as high concentration of various elements were determined[133]. Fission track dating is a very common method being used for the determination of the age and distribution of fissionable type of sediments[134]. Detecting the particles emitted by ^{222}Rn using track detectors is one of the standard methods in practice for radon monitoring in uranium mines and also for personnel monitoring[135].

The review gives the basic physics involved in the detection mechanism of SSNTDs. The detection and identification of various charged particles from protons to uranium are possible with track detectors. The latent tracks carry the signatures of the incident particles in suppressed form. They become eloquent on etching. Thus the identification of the incident particles finally reduces to the job of measuring the track parameters.

REFERECES

1. E.C.H Silk and R.S. Barnes, Phil Mag 4 (1959)970.
2. R.L.Fleisher and P.B. Price, Science 140(1963)1221.
3. B.E. Fischer and R. Sphor (1983) Rev. of Modern Phys. Vol55, 907-948.
4. B.G. Cartwright, E.K. Shirk and P.B. Price (İ978), Nucl. Inst. and Meth. Vol 53,457.
5. R.L.Fleisher and P.B. Price and R.M. Walker(1965) Journ Appl. Physics Vol.36,3645.
6. R.L.Fleisher and P.B. Price and Walker, Ann. Rev. Nucl. Sc. Vol 15,1(1965).
7. R. Katz and E.J. Kobetich(1968) Phys. Rev. Vol. 170,401.
8. J. Fain, M. Monnin and M.Montrat, Radiat. Res. 57(1974)379.
9. R.L.Fleisher and P.B. Price and R.M.Walker, Nuclear tracks in solids - principles and applications, University of California Press(1975).
10. E.V. Benton, USN RDL – TR – 67 – 80(1967).
11. E.V. Benton and W.D. Nix, Nucl. Instr. and Meth. 67(1969)343.
12. S.P. Tretyakova, Soviet J. Part. Nucl. 23(2), (1992) 156 – 186.
13. ICRU Report 16 "Linear Energy Transfer" (1970).
14. G. Bonfiglioli, A. Ferro and A. Majoni (1961) Journ. Appl. Phys.32,2499.

15. Herwing G Paratzke 'Solid State Nuclear Track Detectors' (1976) Proc. 9th Int. Nat. Conf. SSNTD, Newherberg/Munchen ed: F. Granzer, H. Paretzke and E. Schopper 1,87.

16. R.L. Fleischer and P.B. Price(1963) Journ. Appl. Phys. Vol. 34, 2903-2904.

17. J. Mory, 'Solid State Dosimetry' Gordon Breack Science Publishers, New York (1969).

18. R.D. Evan, The atomic Nucleus, Tata McGrawhill Publishing Co., (1955) New Delhi.

19. S.S. Kapoor and V.S. Ramamoorthy, Nuclear Radiation Detectors, Wiley Eastern Ltd., New Delhi(1993).

20. S.A.R. Al – Najir, R.K. Bull and S.A. Durrani, Nucl. Tracks. Vol. 3 PP 169-183.

21. T.V. Ramachandran, M.C. Subhramu and V.C. Mishra, Nucl. Tracks, Proc. Of the fifth Nat. Sem. on SSTD(1987) Ed: B.B.Baliga 140-160.

22. D.P.Bhattacharya, Sarbani Chakrabarti, Ruma Rukshit, Basudhara Basu and Pratibba Pal, Nucl. Instr. and Meth. in Phys. Res.B73(1993) 308-310.

23. J.S. Yadav, Nuclear Tracks, Proc. 4th Nat. Sem cum Workshop on SSNTD, Dehradun, India(1986) Ed: K.K.Sharma.

24. S.M. Farid and A.P. Sharma, Int. J. Appl. Radiat. Isot, Vol.35, No.18, 715-719(1984).

25. A Sandulescu, D.N. Poenaru and Greiner(1980) Soc. J. Part. Nucl. 11,528.

26. P.B. Price, O. Sullivan 'Solid state Nuclear Track Detectors' Ed: Fowler P.H. and Clapham V.M. Pergammon(1982) 929-932.

27. V.V. Rao, M.P. Hagan, and J. Blue, 'Solid State Nuclear Track detectors', Proc: 11th Int. Nat. Conf. SSNTD, Bristol, 7-12 sept 1981. Ed: PH. Fowler and U.M. Clapham, 921-924.

28. G. Somogyi, Ncul: Instr. Meth. Vol.173(1980)21.

29. Hameed A.Khan, Reinhard Brandi, Nacem A Khan and Khalid Jamil, Nucl. Tracks Vol7.No3 (1983)129-139.

30. H.A. Khan and S.A Durrani(1972) Nucl. Inst. Meth. Vol.92, 229-236.

31. R.N. Mukherji, B.B. Baliga, A.K. Ganguly and B. Chanduni, Nuclear Tracks, Proc. 5th Nat. Sem. on SSNTD 1987 Ed. B.B. Baliga 47-48.

32. Jolly Raju and K.K. Dwivedi Proc. 7th N. CPT 9-11 Oct 1991, Jodhpur, 200-208.

33. S.M. Farid and A.P. Sharma, Indian Journal of Pure and Applied Phys. Vol.21 sept. 1983 PP521-524.

34. S. M. Farid and A.P. Sharma, Indian Journal of Pure and Applied Phys. Vol.22 Mar. 1984 PP 133-137.

35. S. .M. Farid and A.P. Sharma, Indian Journal of Pure and Applied Phys. Vol.23, Mar. 1985. PP121-124.

36. S. Ghosh, J. Raju, P.P. Choubey and K.K. Dwivedi, Nucl. Tracks Radiation. Meas., Vol.19, Nos.1-4 PP 77-78. 1991.

37. Basudhara Basu, Shibaji Banerji, Amal Mazundar, Sibaji Raha, Satyajit Saha, Swapan K Saha, and Debapriyo Syam, Book of Abstracts 12th National Symposium on SSNTDs at Jalandhar conducted on Oct 29-31, 2001 PP34.

38. A. Battacharya, Jolly Raju, A. Saxena, K.K. Dwivedi. Proc. Seventh NCPT 9-11 Oct 1991, Jodhpur, 191-199.

39. A. K.Ganguly, Prathiba Pal, Basudhara Basu, S.C Mukherji and D.P. Bhatacharya : Indian J. Phys. 64A(3) 215-224(1990).

40. Hameed Ahamed Khan, Nuclear Instruments and Methods 173(1980) 43-54.

41. K. Becker, Solid State dosimetry (C.R.C. Press, 1973).

42. H.A. Khan and S.A. Durrani, Nucl. Instr. and Meth. 98(1972)229.

43. N.O. Lassen, Dan vid. Selsk Mat. Fys. Medd.25 No:11(1949).

44. R.L. Fleischer and P.B. Price, J. Geophys. Res.69(1964) 331.

45. H.A. Khan, unpublished resutlts(1979).

46. H.A. Khan, Nucl. Instr. and Meth. 173(1980)55-62.

47. H.A. Khan and S.A. Durrani, Nucl. Instr. and Meth. 113(1973)51.

48. K.M. Bukhari, M.H.Zauq and H.A.Khan, J. Nat. Sci. Math. 15(1975)113.

49. M. Nicolae, Rev. Rum. Phys. 15(1970) 881.

50. H.A Khan, J. Nucl. Sci. Technol.(Japan) 13(1976)100.

51. A.L. Frank and E.V. Benton, Rad. Eff.2(1970)269.

52. H.A. Khan, M.A. Atta, S.Yameen, M.R.Haroon and A.Hussain, Nucl. Instr. and Meth. 127(1975)105.

53. R.H. Boyett and K. Becker, J. Appl. Polymer Sci.14(1970)1654.

54. H.G.Partzke, E.V. Benton and R.P. Henke(1973) Nucl. Inst. and Meth. 108,73-80.

55. G. Somogyi, R. Scherzer, K. Grabisch and W. Enge(1977) Nucl. Instr. and Meth. 147,11

56. R.L. Fleischer, P.B. Price and R.T Woods(1969) Phys. Rev.88, 563-567.

57. G. Somogyi, B. Schlenk, M. Varanagy, L. Mesko and A. Valek(1968) Nucl. Instr. and Meth. 63, 189-194.

58. G. Somogyi, M. Varanagy and G. Peto(1968) Nucl. Instr. and Meth. 59, 299-304.

59. G. Somogy, M. Varanagy and L. Madevezky(1970) Rad. Eff. 5,111-116.

60. V. Hoppner, E: Konecny and G. Fiedler (1969) Nucl. Instr. and Meth. 74, 285-290.

61. G. Somogyi, B. Schlenk(1970) Rad. Eff. 5,61.

62. R.L. Fleischer, P.B.Price(1964) J. Geophys. Res.69,331.

63. G. Somogyi and S.A. Szalay(1973) Nucl. Instr. and Meth. 109,211-232.

64. H.B.Luck, Nucl. Instr. Meth. 202(1982) 497-501.

65. H.B. Luck, Nucl. Instr. and Meth. 131(1975) 105.

66. H.G. Paretzke, T.A Gruhn and E.V. Bentan. Nucl. Instr. and Meth. 107(1973)597.

67. W. Enge, K.Grabisch, L. Dallmeyer, K.P. Bartholoma and R. Beaujean, Nucl. Instr. and Meth. 127(1975)125.

68. T.A. Gruhn, W.A. Li, E.V. Benton, R.M. Cassou and C.S. Johnson, Proc. 10^{th} Int. Conf. on Solid State Nuclear Track detectors, Lyan(1979) P.291.

69. T.E. Rudakova, J.V. Moissev, V.I. Astrina, L.L. Rasumova, S.V.Vlassov and G.E.Zaykov, Vysokomal. Soed 17(1975) 1797.

70. G. Scatchard, J. Phys. Chem. 68(1964) 1056.

71. A. Parsegian, Nature 221(1969)844.

72. J.E. Anderson and H.W. Jackson, J. Phys. Chem. 78(1974)2259.

73. N.F. Miller and L.O. Case, J. Am. Chem. Soc.57(1935)810.

74. G.G. Cooper and B. Williams, J. Org. Chem.27(1962)3717.

75. K.L. Laidler and P.A. Landskroener; Trans. Faraday Soc.52(1956)200.

76. T.E. Rudakova, J.V. Moisseev, A.E. Tschalych and G.I. Zaykov, Vysokomal, Soed.14(1972)449.

77. H.B. Luck to be published.

78. M.L. Williams, R.F. Landel and J.D. Ferry, J. Am. Chem. Soc. 77(1955)3701.

79. A. Bernas and A. Chambaudet, Rad. Effects 22(1974)129.

80. S.D. Burow, D.T. Turner, G.F. Pezdirtz and G.D. Sands, J. Polym. Sci. A-1,4(1966)613.

81. R.H. Boyelt, D.R. Johnson and K. Becker, Radiat. Res.42(1970)1.

82. G. Somogyi, K. Grabisch, R. Scherzer and W. Enge, Nucl. Istr. and Meth. 134(1976)129.

83. H.B. Luck, Isotopenparaxis 14(1978)215.

84. R. Katz, B. Ackerson, M. Homayoonfar and S.C. Sharma, Radiat. Res.47(1971)402.

85. R. Katz, S.C. Sharma and M. Homayoonfar, Nucl. Instr. and Meth. 100(1972)13.

86. R. Katz and F.E. Pinkerton, Nucl. Instr. and Meth. 130(1975) 105.

87. J.C. Arthur, Jr. D.J. Stanonis, T. Mares and O. Hinojosa, J.Appl. Polym. Sci. 11(1967) 1129.

88. E. Kroh and M. Petschak, Chim. Vysok Energy. 4(1970)246.

89. W. De Sorbo, Nucl. Tracks 3(1979)13.

90. R.L. Platzman, Radiat. Res. 17(1962)419.

91. Y.N. Molim, I.I. Tchkeidze, A.A. Petrov, N.Y. Buben and V.V. Voevodsky, Doklady Akad. Nauk. S.S.S.R. 131(1960)125.

92. A. Mozunder, charge particle tracks and their structure, in Advances in radiation chemistry, eds: M. Burton and J. Magee Vol.1 (Wiley – Inter Science, New York, 1969).

93. R.S. Alger, Radiation effects in Polymers, in Physics and Chemistry of the organic Solid State, Ed: D.Fox (Inter Science, New York and London, 1965).

94. M. Dole, The radiation chemistry of macromolecules (Academic Press, 1972).

95. H.G. Partzke, 11th Int. Conf. on Solid state nuclear track detectors, Bristol (1981).

96. H.B. Luck, Nucl. Instr. and Meth. 114(1974) 139.

97. H.B. Luck, Rad. Annual Report zfk-367(1978)p.120.

98. H.B. Luck, Rad. Effects 29(1976)205.

99. D. Hilderbrand and E.V. Benton, Nucl. Tracks 4(1980)77.

100. H.B. Luck, Nucl. Instr. and Methods, 212(1983)483-487.

101. H.B. Luck and G. Pretzsch, to be published.

102. H.B. Luck, Nucl. Instr. and Meth. 198(1982)611.

103. H.B. Luck, Nucl. Instr. and Meth. 131(1975)105.

104. H.B. Luck, zfk-Report 301(1975).

105. S. Hayashi and S. Iwata, Rad. Effects 54(1981) 243.

106. A. Murakami, J. Phys. Soc. Jap.36(1974)923.

107. H.B. Luck, Nucl. Instr. and Meth. 212(1983)479.

108. H.B. Luck, Nucl. Instr. and Meth. 202(1983)497.

109. R.H. Boyett, D.R. Johnson and K. Becker, Radiat. Res. 42(1970).

110. K. Uberreiter, z. Phys. Chem. (B)48(1941)197.

111. F.A. Long and I.J. Thomson, J. Polym. Sci.15(1955)413.

112. T.J. Lewis, Polymer 19(1978)285.

113. R.M. Cassou and E.V. Benton, Nucl. Track Det. 2(1978)173.

114. D.L. Henshaw, S. Amin, V.M.Clapham, P. Fowler, D.J. Webster, A. Thomson and D. O'sullivan, Proc. 11th Int. Conf. on solid state nuclear track detectors, Bristol(1981).

115. G. Somogyi, Proc. 11th Int. Conf. on Solid state nuclear Track detectors, Bristol(1981).

116. G. Somogyi and I. Hunyadi, Proc. 10th Int. Conf. on Solid state nuclear track detectors, Leyon(1979)p.443.

117. D.L. Henshaw, N. Griftu, O.A.L Lander and E.V. Benton, Nucl. Instr. and Meth. 180(1981)65.

118. H.B. Luck, Isotopenpraxis, 14(1978) 215.

119. P.H. Fowler, S. Amin, V.M. Clapham and D.L Henshaw, Proc. 10th Int. Conf. on Solid State nuclear Track detectors, Lyon(1979)P.239.

120. E.V. Benton, G.C. Preston, F.H. Ruddy, R. Gold and J.M. Roberts, Proc. 10th Int. Conf. on Solid State Nuclear Track detectors, Lyon(1979) P.459.

121. E.V. Benton and N.M. Ceglio, Proc. 10th Int. Conf. on solid state nuclear track detectors, Lyon(1979)P.747.

122. Antoney Joseph and K.M. Varier, Radiation Measurements, Vol.24, No.2, PP111-114, 1995.

123. K.K. Sharma, Nucl. Tracks, Proc. Fourth Nat. Sem. cum workshop on SSNTD, Dehradun(1986).

124. W. Enge, K. Gabrisch, L. Dall Mayer, K.P. Barthaloma and R. Beau Jean, Nucl. Instr. and Meth. Vol.129(1975)225.

125. Paul Singh, N. Singh and S.K. Chakravarti, Indian J. Phys. Vol.644, 375-380(1990).

126. J. Mory, 'Solid state Dosimetry', Proc. NATO, Summer School, Bressels(1967). Ed: S Amalintx, B. Batz and R.Strumane-407.

127. M. Nikolac, Solid State Nuclear Track Detectors. Proc. Ninth Int. Conf. Neuherbeg/Munchen.

128. E.V. Benton, R.P. Henke and C.A. Tobias(1973) LBL 2016, Lawrence Berkeley Laboratory, Berkely, California.

129. E.V. Benton, R.P. Henke and C.A. Tobias, Science, Vol.182, 474.

130. E.V. Benton, C.A. Tobias, R.P. Henke and R. Cruty, Solid State Nuclear Track Detectors(1976) Proc. Ninth Int. Conf. Neuherberg/Munchen. Vol.2,739 Ed: F. Granzer, H. Paretzke and E. Schopper.

131. E. Bagge, E. Dulimke, W. Enge, H. Hirack Detectors(1976) Proc. Ninth Int. conf. Neuherberg/Munchen. Vol.2, 753. Ed: F. Granzer, H. Paretzke and E. Schopper.

132. S.K. Chakravarti, NISI Newsletter(1996) vol.2, No.2,7.

133. A.E. Liehu, Solid State Nuclear Track Detectors, Proc. Ninth Int. Conf. SSNTD, Neuherberg/Munchen(1976). Ed: F. Granzer, H. Paretzke and E. Schopper, Vol 1, 689-695.

134. R.L. Fleischer and M. Mogro Campero(1978) J. Geo Phys. Res. Vol 83, 3539.

135. R.A. Akbar, H.A. Khara, I. Ahmed and K. Jamil(1980), Nucl. Instr. Meth. Vol.173, 183-189.

CHAPTER III

PRELIMINARY STUDIES ON CR-39 TRACK DETECTOR

3.1. CALIBRATION OF CR-39 FOR LOW ENERGY ALPHA PARTICLES.

We have measured the track diameter distributions in CR-39 (NonDop) for alpha particles in the energy range 1.80 to 6.11MeV.

3.1.1. Details of the Experimental set up.

3.1.1.1. The Sources.

The alpha sources used in the present studies were 0.16 μCi ^{252}Cf with energy 6.11 MeV and 2.3 μCi ^{241}Am with energy 5.48 MeV. They were electroplated on a circular silver foil of diameter 3 cm and were placed inside an acrylic case .The sources were obtained from Bhabha Atomic Research Centre, Bombay.

The alpha particles of lower energies were obtained by passing 5.48 MeV particles from the ^{241}Am source through various thicknesses of degrader foils of mylar. The thicknesses of mylar foil needed to degrade the energy of alpha particles were evaluated using the energy loss values given by NorthCliff and Schilling [1].

3.1.1.2.CR-39 Detector

Non Dop CR-39 detector with the specifications given below in table 3.1 were used in this study.

Table 3.1. Specifications of CR-39 detector

Type	Thickness	Density	Refractive Index	Supplier
Non Dop	300 μm	1.35 gm/cc	1.505	Pershore Moulding, England.

Seven CR-39 sheets of dimensions 20 x 10 x 0.28 mm were used in this study.

3.1.1.3. The Irradiation Set up

To get a narrow beam of alpha particles, the source was covered with an aluminium lid of thickness 3.5 cm having a hole of diameter 1 mm at its centre. The track detector sheet along with the required thickness of mylar foil below it was placed over an acrylic sheet. Through a hole of 1mm diameter drilled in the acrylic sheet, alpha particles could reach and fall normally on the detector. The total distance of the detector from the source was 4 cm. The whole set up was placed in a scattering chamber made of perspex. As we wanted to use the same type of detector later in nuclear reaction studies also, with all the set up in vacuum, the effect of vacuum during irradiation has to be taken into account. Since the sensitivity of CR-39 has shown to decrease with the time of storage in vacuum before irradiation [2], the detector sheets were kept in vacuum for minimum time. Studies carried out by Jhan and Price [3] has shown that the presence of oxygen enhances track etching rate in polymers. A similar study carried out in 1987 by Drach et al [4] using CR-39 shows that the effect of oxygen pressure during irradiation decreases with charge Z of the incident ion. Benton et al [5] has shown that the presence of oxygen during irradiation has negligible effect on the track etch rate of low energy alpha particles. We have carried out all the irradiations in a rotary vacuum of 0.09 Torr.

The effect of temperature at the time of exposure on the etch rate of plastics was established by Drach et al [4]. Their study shows that as ionization energy decreases, the

effect also decreases. In order to minimize the variations in track etch rate due to changes in registration temperature, all the irradiations were done at room temperature(27^0C). Even though the exposure time was very short, for minimizing the ageing effects in the track detector [6,7], the chemical etching was done soon after the irradiation

Being a passive detector, CR-39 had to be shielded from the alpha rays except during the exposure time. An aluminium sheet having sufficient thickness to absorb the 6.11MeV alpha particles and which could be moved back and forth with the help of a small electrical motor kept inside the chamber was used for this purpose. The motor can be operated from outside the chamber. The diagram showing the irradiation set up is given in fig 3.1.

3.1.1.4. Set up for Chemical Etching.

The main part of the set up for chemical etching is a precisely controlled temperature bath. Transformer oil taken in a glass trough is heated with a 50 watt immersion coil. The coil is energized through a solid state thermostat control[8]. The temperature sensor used is a locally available thermistor immersed in the oil. The oil is stirred with an aluminium stirrer driven by a small motor. The glass trough is placed on a magnetic stirrer so that the etchant taken in a closed reagent bottle (250cc) and placed inside the oil bath is stirred by a teflon coated tiny magnet. Heating and temperature maintainance can be controlled reliably and consistently by the system. The temperature of the bath can be kept at any desired value between 30^0C and 100^0C and is stable to $\pm 1^0$C.

3.1.1.5 The etchant for Chemical Etching.

The etchant used is NaOH solution of concentration 6N and the etching was carried out at 70^0C.In a detailed study carried out by Green et al [9], it was shown that

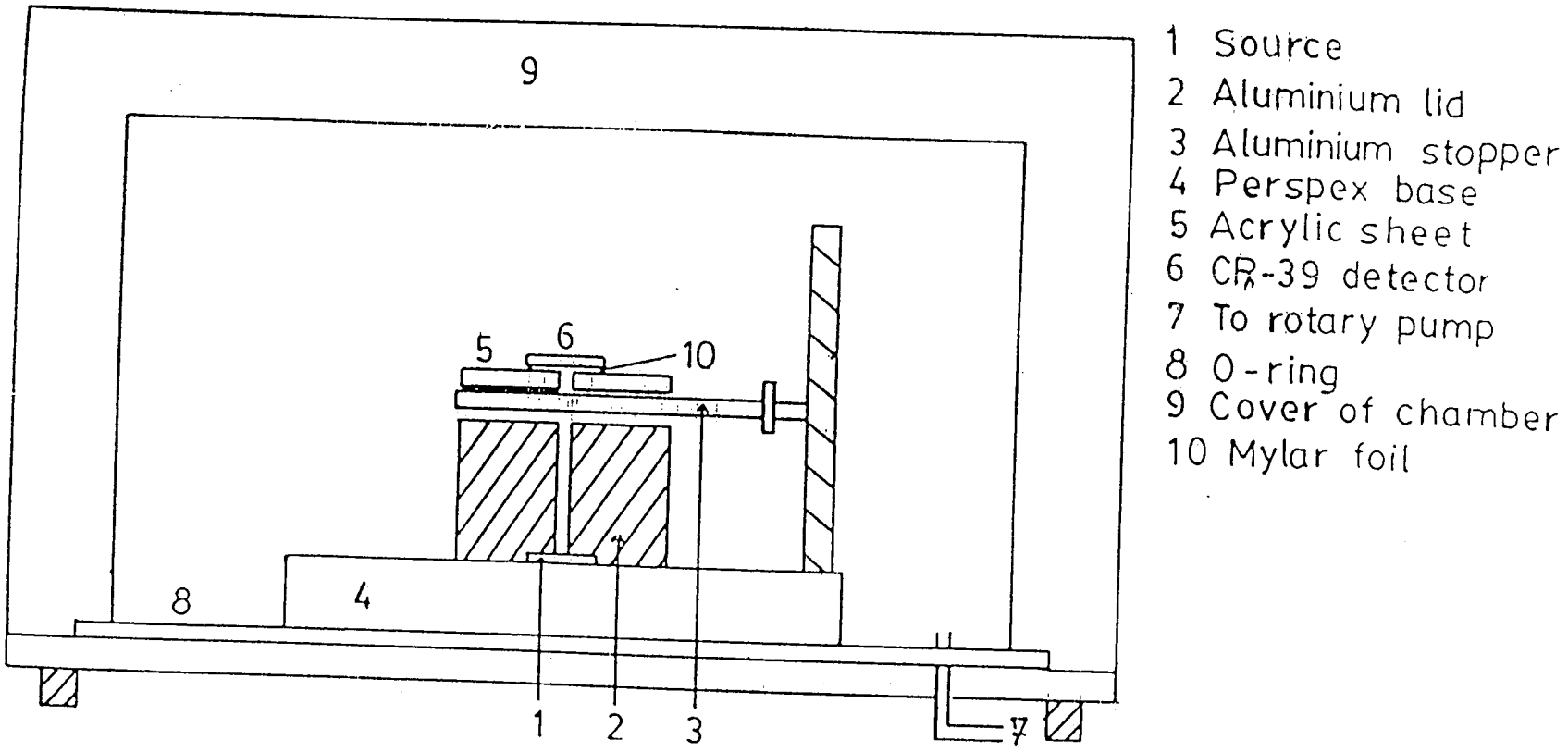

Fig 3.1. The setup used for α irradiation.

6N concentration and 70^0C is the optimum etching condition for alpha particles on CR-39.

3.1.1.6. Facilities for Measurements.

A Carl Zeiss Research optical microscope, attached to 10X filar micrometers were used for the track diameter measurements. The filar micrometers were calibrated using a stage micrometer. The least count of filar micrometer attached to microscope was 0.5 μm.

A Michelson Interferometer was used for measurement of thickness of the transparent detector sheets. A sodium vapour lamp was used as a standard source. The wavelength was taken as 5893 A^0. Achromatic fringes for reference were produced using a 100 watt incandescent bulb.

If the insertion of a transparent sheet of thickness t and refractive index μ in the path of a Michelson interferometer causes n fringes and d distance travelled to a reference line, the thickness t is then given by [10].

$$t = d / (\mu - 1) \qquad \ldots\ldots\ldots\ldots\ldots (3.1)$$

3.1.2. Experimental Procedure.

After carrying out the irradiation for 2 minutes with alpha particles from ^{241}Am and for 30 minutes with ^{252}Cf source, using the irradiation set up described in sec. 3.1.1.3, the detector sheets were etched for 5 hours and 10 hours in the etching set up described in sections 3.1.1.4 and 3.1.1.5. After 5 hours of etching, fresh etchant was used. On completing the etching for 5 hours and 10hours, the detector sheets were washed in distilled water and then left for drying. The diameters of nearly 350 tracks at the centre of the region of irradiation were then measured, using the microscope.

3.2. RESULTS

The distribution of alpha particle track diameters were plotted as histograms for different alpha particle energies and are given in figures 3.2 and 3.3 for the etching times of 5 hours and 10 hours respectively. It can be seen from these figures that for a given energy there is a distribution of track diameters. The smooth curves through the histogram gives the average trend of the distribution. Each of these curves can be considered as a gaussian with a tail. The width of the distribution may be due to the following three factors.

1. The alpha particles from the source may have inherent energy distribution due to the source thickness and backing.

2. The energy deposition process is statistical in nature and this will be reflected in the track diameter also.

3. The energy degradation in mylar is statistical in nature.

The track diameter corresponding to each energy is taken as the mean value of the track diameter distribution. The track diameter decreases with increase in the energy of the alpha particles as observed earlier [11]. The measured track diameters for alpha particles in the energy range 1.80 to 6.11MeV are given in table 3.2. The errors are the standard deviations of the diameter distributions.

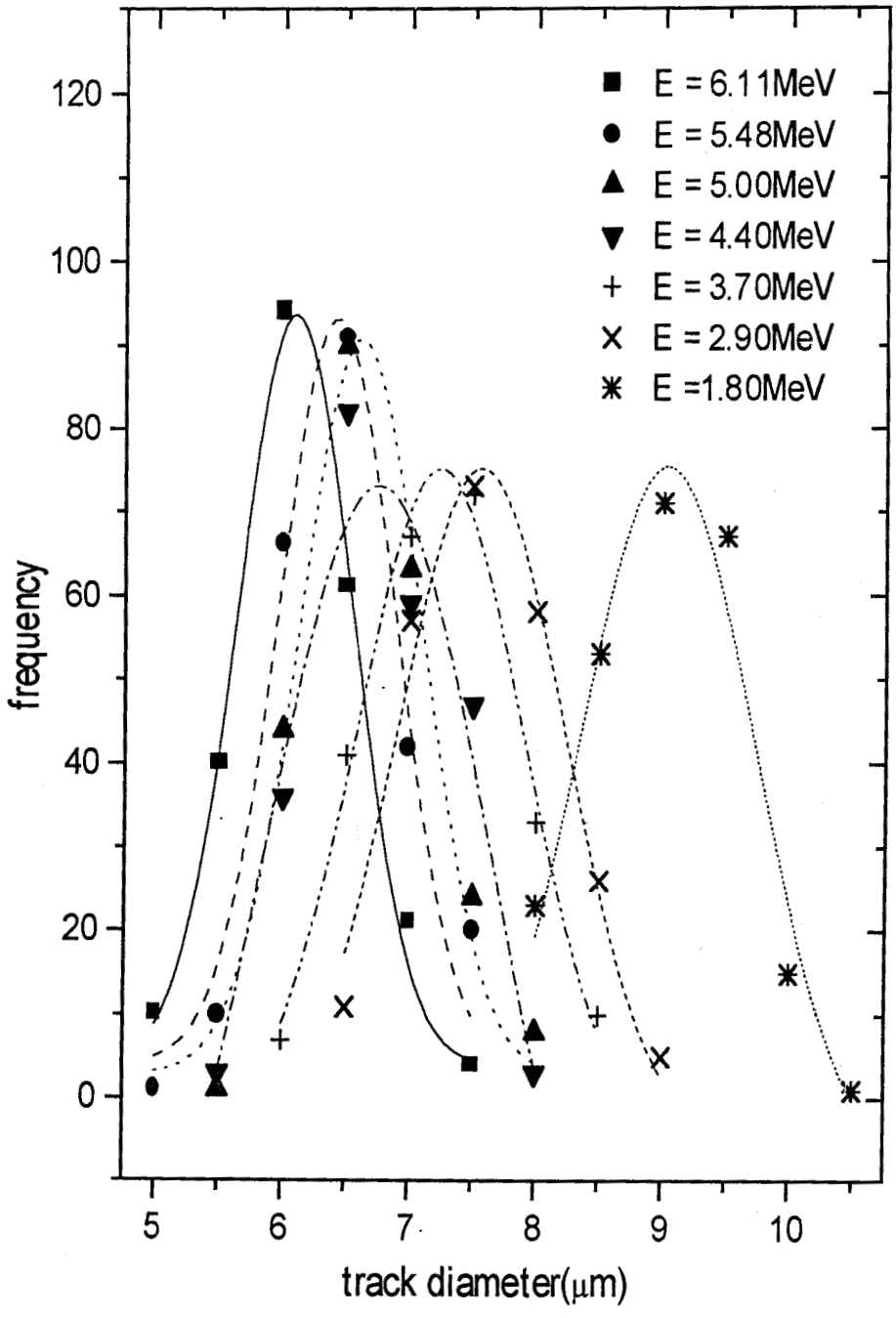

Fig 3.2 Track diameter distribution of α particles after 5 hrs of etching

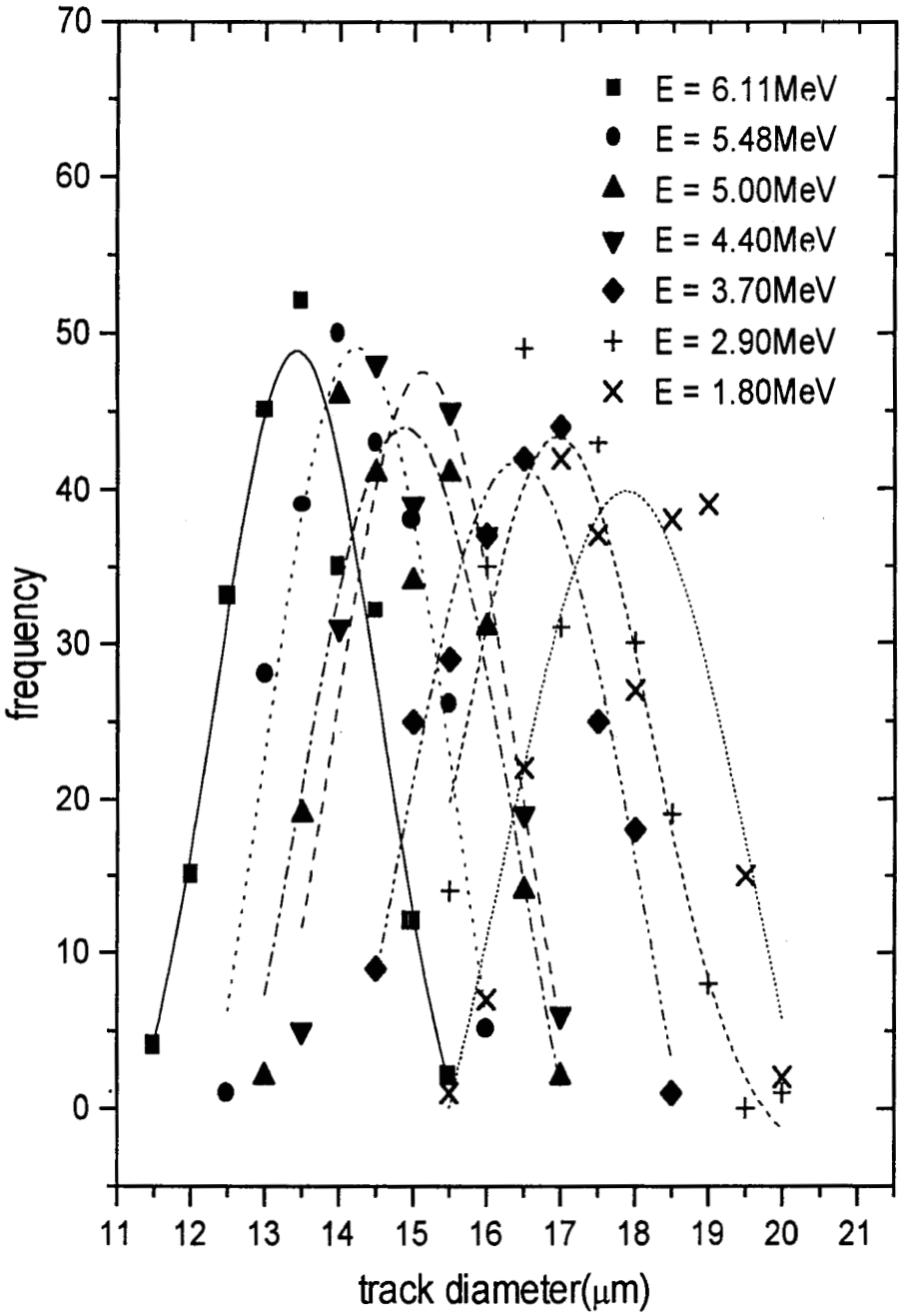

Fig 3.3 Track diameter distribution of α particles after 10 hrs of etching

Table 3.2. Measured track diameters for various alpha energies

Energy (MeV)	Track diameter (μm) after etching for 5hrs	10hrs
6.11	6.16 ± 0.55	13.46 ±1.10
5.48	6.41 ± 0.57	14.25 ±1.15
5.00	6.71 ± 0.60	14.94 ±1.23
4.40	6.75 ± 0.61	15.23 ±1.25
3.70	7.25 ± 0.71	16.38 ±1.40
2.90	7.66 ± 0.70	17.02 ±1.45
1.80	9.06 ± 0.73	17.86 ±1.51

References

1. L.C.Northcliff and R.F.Schilling(1970) Nucl.Data Tables 7
2. G.Somogyi, M.Toth-Szilagy, I.Hunyadi and A.F.Hafis(1986) Nucl.Tracks 12, 97.
3. J.H.Jhan and P.B.Price(1975) Phys.Rev.Lett 35,539
4. J.Drach, M.H.Salamon, M.Solarz and P.B.Price(1987) Nucl.Instr.and Meth. in Phys.Res.B.23,367-368.
5. E.V.Benton, T.Gruhn, M.Tran and R.Spohr, 'Solid State Nuclear Track Detectors',Proc.11th Int.Conf.SSNTD,Bristol(1981) ed:P.H.Fowler and U.M.Clapham 155-157.
6. T.Portwood,D.L.Henshaw and J.Stejney(1986) Nucl.Tracks 12,109-112.
7. J.Drach, M.Solarz, R.Gluoxiao and P.B.Price(1987) Nucl.Instr.and Meth.in Phys.Res.B 28,364-368.
8. Anil.V.Borkar,Science today(1978 Jul) 58.
9. P.F.Green, A.G.Ramli, S.A.Najjar, F.A.Jarad and S.A.Durrani(1982) Nucl.Instr..and Meth.203,551.
10. N.Subrahmanyam and Brijlal 'A Text Book of Optics'S.Chand and Co.Ltd.(1980) New Delhi P.309.
11. P.Wuhnsen,W.Enge and R.Beaujean(1984) Nucl.Track.Radiat.Meas.8,179-182.

CHAPTER IV

SOME NUMERICAL CALCULATIONS ON ETCHED TRACK PROPERTIES IN SSNTDs

4.1. INTRODUCTION

Over the past few decades, Solid State Nuclear Track Detectors (SSNTDs) have become a versatile tool for detection, counting, and in some cases, identification of charged particles. Their usefulness as detectors emerge from the damage tracks left by the charged particles as they traverse the detector medium. These 'latent' tracks are made visible by several techniques. Chemical etching is one of the important techniques for track revelation or visualization. This useful technique depends on the fact that specific chemical reagents attack the material of the detector more easily along the tracks than on the bulk material. The latent tracks are thereby amplified and can be made visible by means of a microscope [1]. Consequently two etching velocities are to be considered: bulk etch rate V_G and track etch rate V_T. Both these quantities depend on the type of the material medium of the track detector, the normality of the etchant solution and the temperature of etching. In addition, V_T depends on the type and energy of the incident ions. Given the etching conditions, the track parameters((track diameter and track length) will depend on the particle type and energy through the damage responses. Thus the track parameters give information on the particle parameters for identifying them.

The basic model had earlier been developed by Antony Joseph and Varier [2]. Details of this model are given in section 4.2 below. In the present work some modifications/improvements have been incorporated into the basic model. The details are discussed in sec.4.3.

4.2 THE MODEL.

In the basic model, it was assumed that the bulk etch rate V_G is a constant throughout the etching process, equal to the measured value of 1.2μm/hr (0.027mg/cm^2/min).At any point on the etched detector surface, as well as on the track profile, the subsequent etching proceeds normal to the surface. The track etch rate V_T is assumed to vary along the track of the incident ion.

The initial detector surface, before the start of etching, is taken as the XY plane. Only normal incidence is considered. The Z axis is along the axis of the track.
Two types of variations have been tried. In the first case, referred to as id = 1,the etch rate along the axis of the track is assumed to be proportional to a power of the specific energy loss de/dz of the ion. Thus

$$V_T(x = 0,z) = V_G[1 + a_0(de/dz)^{a1}] \qquad \text{----- } 4.1$$

where a_0 and a_1 are parameters to be adjusted for obtaining agreement with measurements. A similar relation has been used by Farid and Sharma [3] in the calculation of the range of ^{20}Ne ions in Lexan detector. In the second case (id = 2), the variation of V_T along the track is assumed to follow the equation given below

$$V_T(x = 0,z) = V_G + \{a_0(r - z)(de/dz)_{max}^{a1} / [a_2^2 + (r - z)^2]\} \qquad \text{------ } 4.2$$

where (r – z) is the difference between the range of the incident ion in CR-39 and the distance along the track from the point of incidence,$(de/dz)_{max}$ is the stopping power at the Bragg peak and a_0 is the spatial separation of the Bragg peak and the end of the track. Here again, a_1 and a_2 are parameters to be adjusted.

At points away from the axis of the track, the track etch rate is assumed to follow a Gaussian variation with distance from the axis. ie. ,

$$V_T(x,z) = V_G + [V_T(x = 0,z) - V_G]\exp(- x^2 / 2a_3) \quad \text{-----} \quad 4.3$$

Here a_3 is another parameter which has to be optimized for good agreement with experiments. As it appears in the above equation, a_3 is equal to the square of the standard deviations. It can be physically interpreted as an effective width of the central plasma zone [4].

In the numerical calculations, a convenient X – grid is assumed. At time t = 0, the detector surface is assumed flat and etching is normal to the surface at all points. The etch rate V_T is evaluated for all x. The etching interval dt is initially taken as 0.1 minute and t > 1, it is 1 minute. The value of Z of track profile after the interval dt is calculated as

$$Z(dt) = Z(0) + V_T dt \quad \text{--------} 4.4$$

After each time interval, the energy of the incident particle is reduced to

$$E_{n+1} = E_n - \Delta E_n \quad \text{-------} \quad 4.5$$

where

$$\Delta E_n = (dE_n / dx).dr_n \quad \text{------} \quad 4.6$$

is the energy loss of the particle in traversing through the distance $dr_n = V_T dt$. The required stopping powers dE_n/dx are calculated by interpolation between the interpolated values from standard tables[5].

Next, the slopes tan(θ) of the normals to the etched surface are obtained at the various (X,Z) points. The etching in the next interval dt is assumed to proceed along these normals (as already mentioned). Thus, the point(X,Z) on the etched surface will move to (X_n,Z_n) after the next etching interval dt, where X_n and Z_n are given by

$$X_n = X_{n-1} + V_T(X_{n-1},Z_{n-1})dt \cos(\theta_{n-1}) \quad \text{-------} \quad 4.7$$

$$Z_n = Z_{n-1} + V_T(X_{n-1},Z_{n-1})dt \sin(\theta_{n-1}) \quad \text{-------- 4.8}$$

The Z co-ordinates corresponding to the original X-grid points are obtained by interpolation. Then, the new points $(X_n,Z_n)$for the subsequent etching interval dt are found using equations 4.7.and 4.8. This procedure is repeated until the required maximum etching time is reached.

After each 30 minutes of etching, the diameters of the track profile is obtained by finding the point along the track profile at which Z becomes numerically equal to the thickness of the etched out layer (ie., $h = V_G t$).The corresponding visible track length l is obtained as the difference [Z(x = 0) – h].The above calculations are repeated for id =1 and id = 2.

A FORTRAN code was earlier developed by Antony Joseph and Varier for calculating the track diameter evolution as a function of etching time. In this code, a trial set of initial values of the parameters a_i was assumed and the track diameter evaluated at different etching times using the above numerical method. The parameters were varied in small steps and the calculations repeated. The optimum set of parameters giving best agreement between experimental and calculated track diameters were arrived at.

4.3. MODIFICATIONS/IMPROVEMENTS OF THE MODEL IN THE PRESENT WORK

1. In the earlier model due to Antony Joseph and Varier, the track diameters for only low energy alpha particles had been calculated. In the present work we have applied the model to calculate track diameters of protons, alpha particles, deuterons and other heavy ions.
2. We have extended the calculations to Makrofol-E apart from CR-39.

3. The earlier work used FORTRAN for the calculation. We have used 'C' language. Provision for graphical display of the etched track profile has also been incorporated in the present work.

4. In the earlier work, an initial set of parameters a_i was assumed and an optimum set arrived at by successive calculations using parameters which had been varied by finite steps in an ordered way. In the present work a reliable least squares procedure has been adopted. Starting with the initial guess values for the parameters a_i, the chi-squared was evaluated as follows:

$$\chi^2 = \sum_{i=0}^{n} [\{d(i) - d_{fit}(i)\} / d(i)]^2 \qquad \text{--------- 4.9}$$

where d(i) is the experimental track diameter for the i^{th} data point and $d_{fit}(i)$ is the value calculated by the numerical method described in section 4.2.This will be a function of the parameters a_i:

$$\chi^2 = f(a_0, a_1 .....) \qquad \text{------- 4.10}$$

The parameters are then varied one by one, keeping all the others constant, to obtain c^2 values for a_i - > $a_i + da_i$,(i = 0,1,.....n).From these results the derivatives $d\chi^2 / da_i$ are evaluated These derivative values are used in the code to arrive at the net proper set of parameters, required to decrease the value of χ^2.This procedure is repeated until the optimum set of a_i, giving minimum value of χ^2 is obtained.

5. We have used more accurate stopping power data using SRIM Code[6].

4.4 RESULTS

4.4.1 Track Etch Rates Along The Ion Trajectory

The variation of the track etch rates along the trajectories of low energy protons (0.11 MeV to 1.17 MeV), higher energy protons (1 MeV to 10 MeV), low energy

deuterons (0.11 MeV to1.15 MeV), low energy α particles (2.28 MeV to 5.3 MeV), 40 to 64 MeV $_8O^{16}$ ions, 36 to 162 MeV $_{10}Ne^{20}$ ions,6.5 to 75.6 MeV $_{36}Kr^{84}$ ions and120 to 358 MeV $_{26}Fe^{56}$ ions are done. The graphical representations of track velocities of these some of these charged particles are shown in figures 4.1 to 4.4. These track etch rate values have been used in the numerical calculations to obtain the etched track profile at various etching times. It is seen that V_T approaches the value of the bulk etch rate as the particle approaches the end of its track. This is used to determine the track length in the code.

4.4.2 Track Profiles

The graphics facility in the code has been used to reproduce the etched track profile at different etching times. Figures 4.5 to 4.7 gives the development of the track profiles with etching time for the case of 1 MeV protons, 5.3 MeV α particles and 36 MeV $^{20}{}_{10}Ne$ ions. The visible change in the shape of the etched track profile when the etching time exceeds the time required to etch out the entire track length of the incident ion is obvious from the above figures.

4.4.3. Track Diameters

The calculated and experimental values of protons [7,8,9] on CR-39 of different energies are given in table 4.1 and that of deuterons [7] in table 4.2 and that of a particles[7,10] in table 4.3.The track diameters of heavier ions such as $_{10}Ne^{20}$, $_{26}Fe^{56}$ and $_{36}Kr^{84}$ on Makrofol-E are calculated with reference to experimental values [11]. They are also given in Tables 4.4,4.5 and 4.6 respectively. The graphical representations are given in figures 4.8 - 4.11.

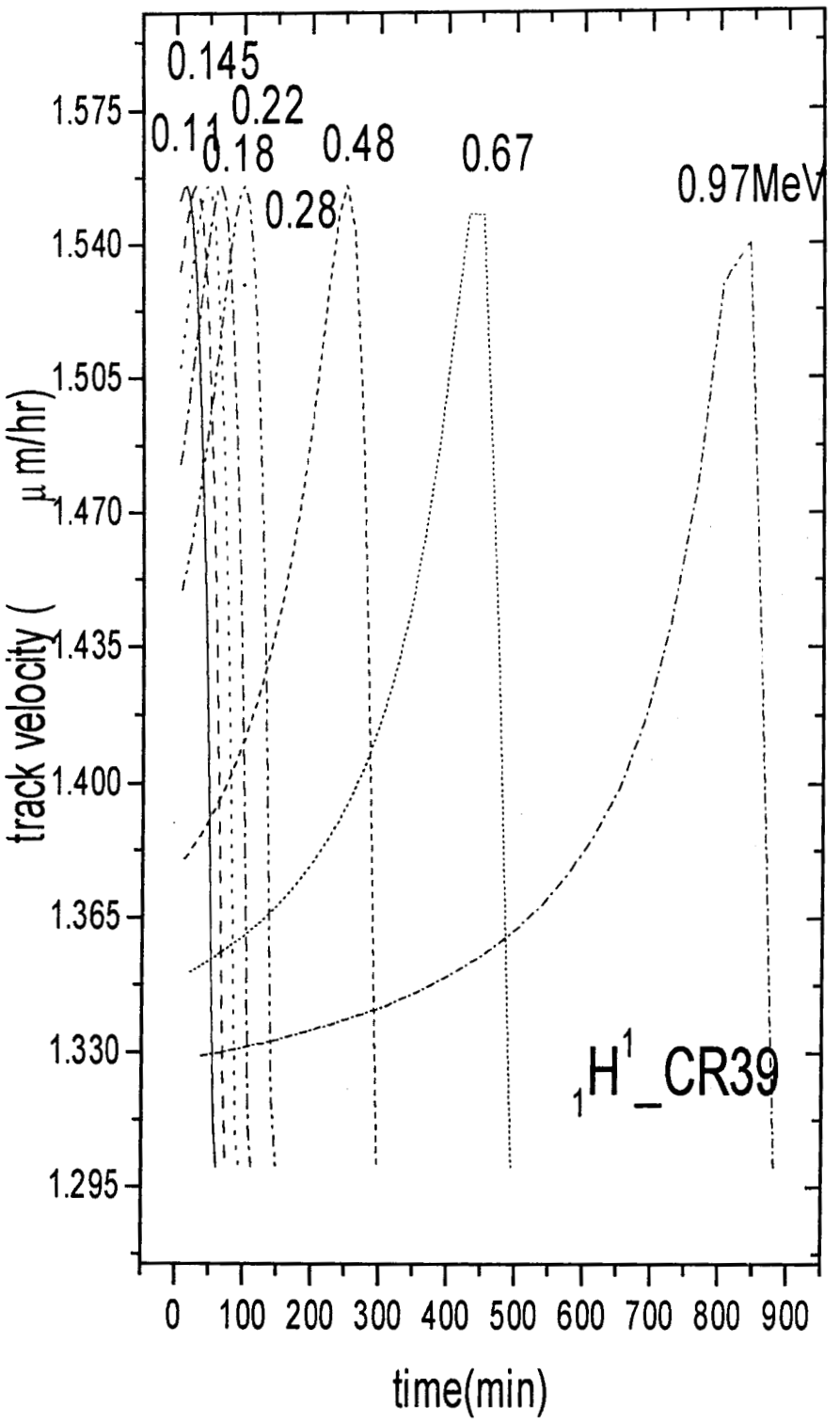

Fig 4.1 Track velocity of protons on CR-39 as a function of tir

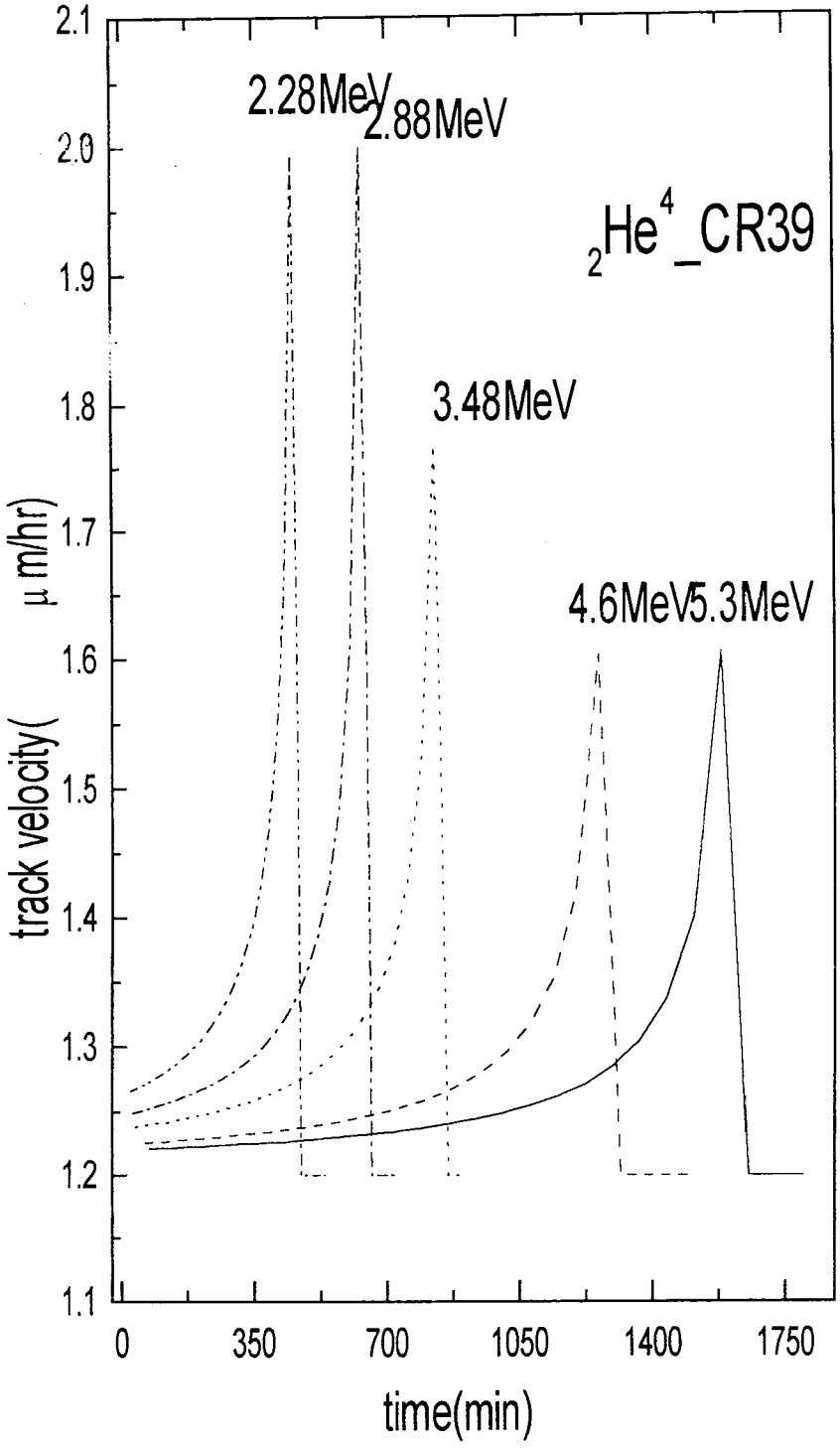

Fig 4.2 Track velocity of α paticles on CR-39 as a function of time

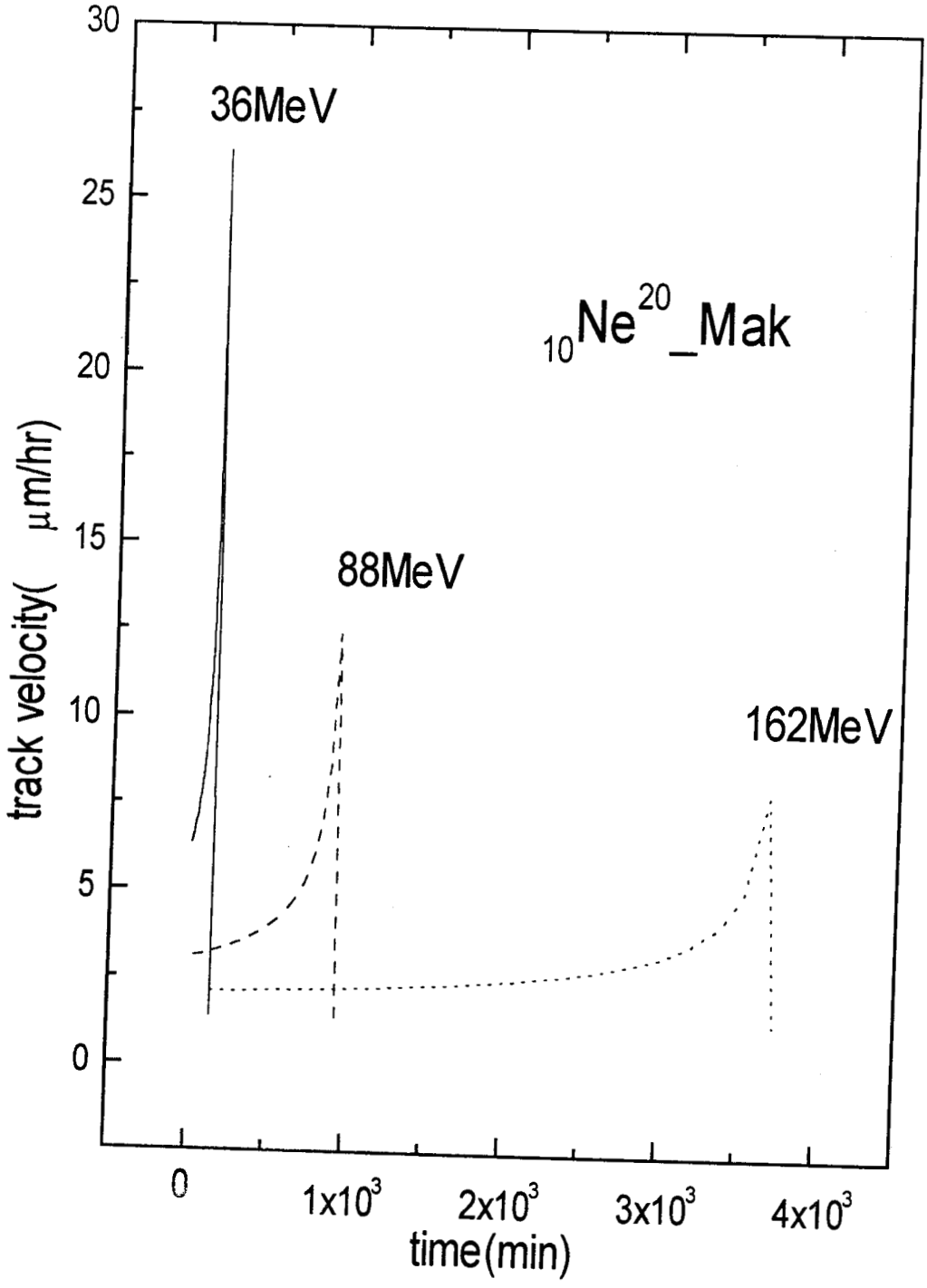

Fig 4.3 Track velocity of $_{10}Ne^{20}$ on Makrofol-E as a function of time.

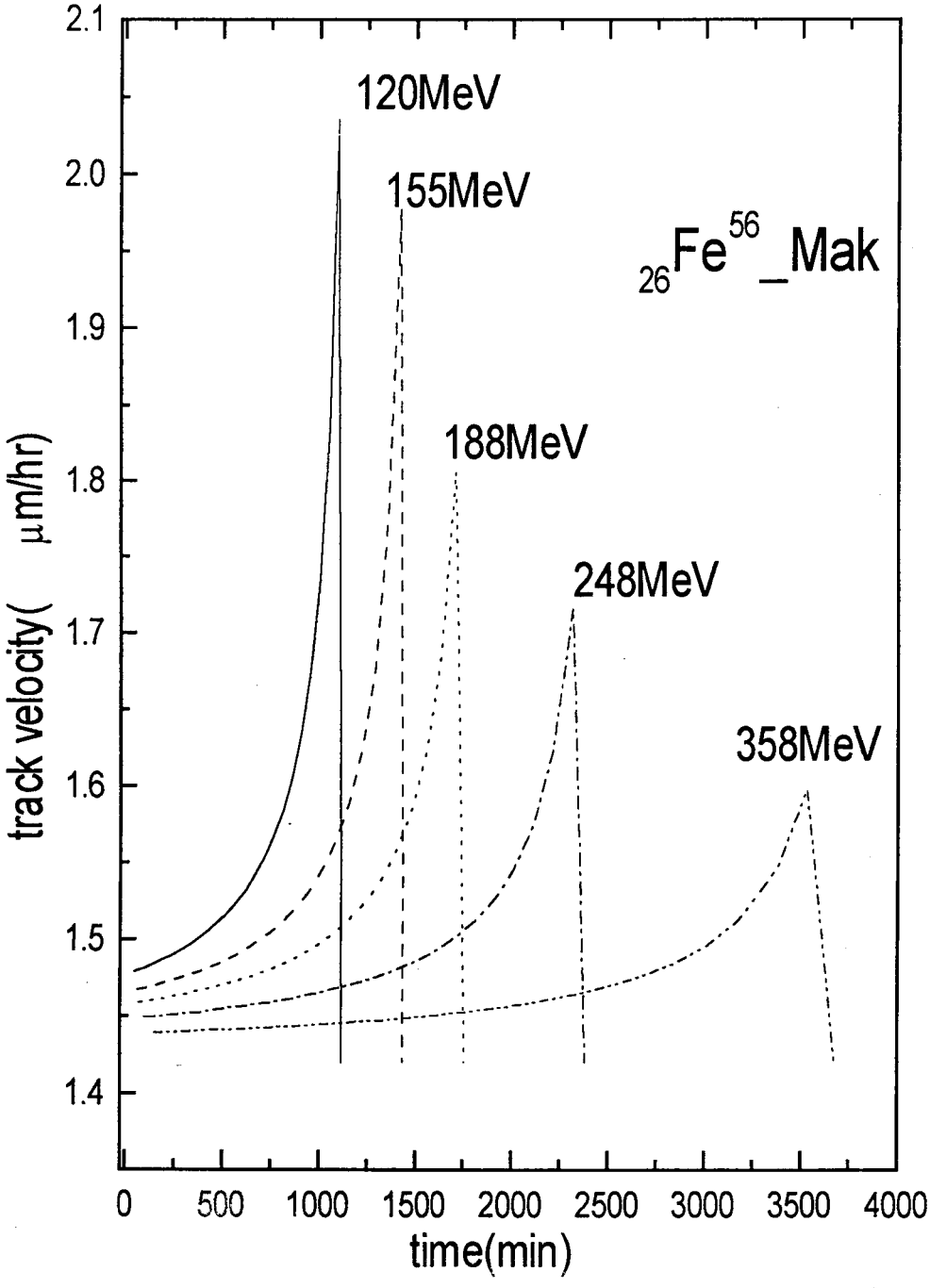

Fig 4.4 Track velocity of $_{26}Fe^{56}$ on Makrofol-E as a function of time.

1_MeV_H_1

Bulk etch Rate = 1.20 microns / hour

No. of track	Etch time Hours	Track Diameter Microns	Track Length Microns	Range Microns
1	4.00	3.00	1.64	21.05
2	8.00	6.90	3.38	21.05
3	12.00	10.50	5.30	21.05
4	16.00	14.40	5.71	21.05

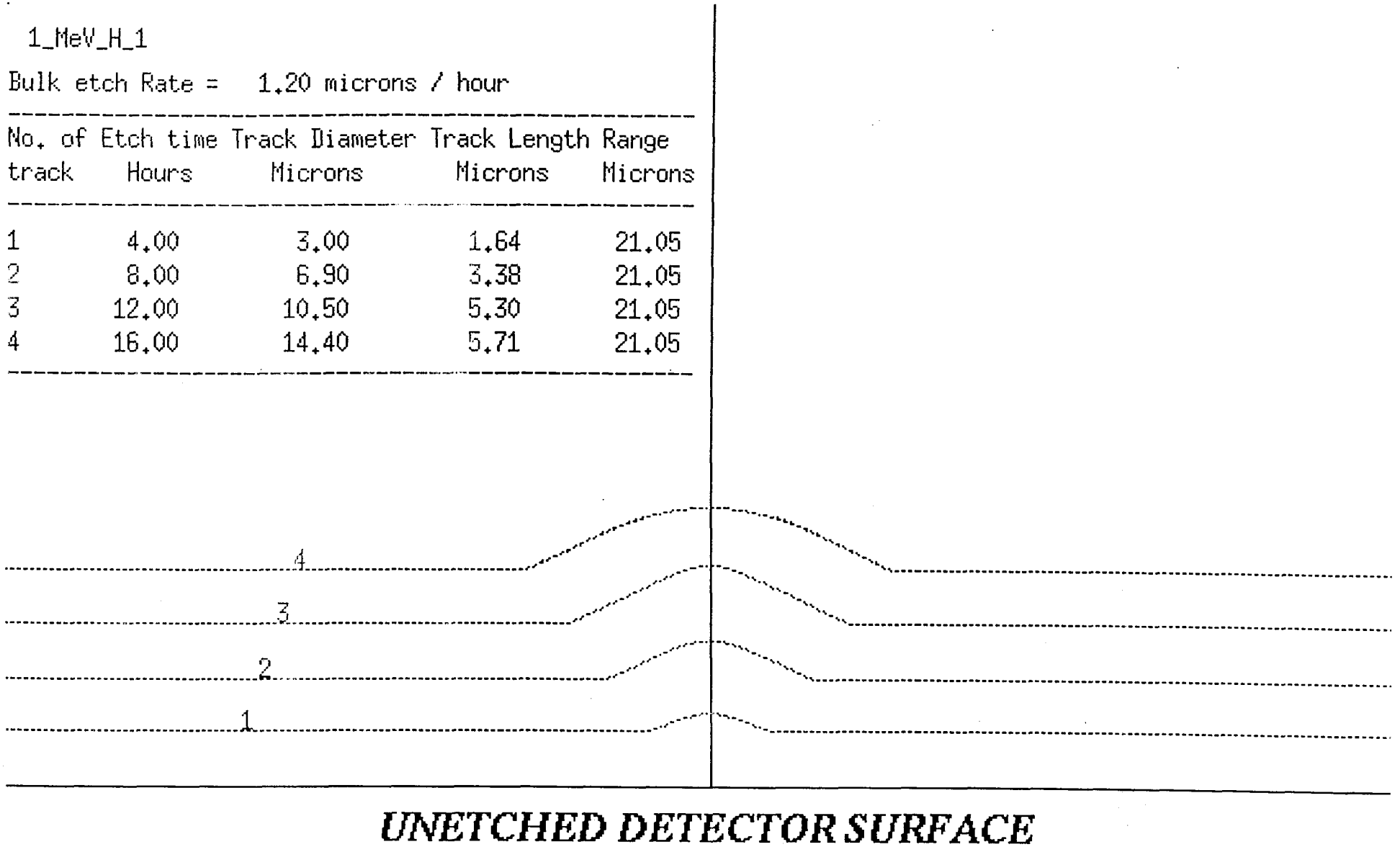

Fig 4.5 Track profiles at various etching times for 1 MeV protons in CR-39 track detector

5_MeV_He_4

Bulk etch Rate = 1.20 microns / hour

No. of track	Etch time Hours	Track Diameter Microns	Track Length Microns	Range Microns
1	5.00	5.10	4.47	32.01
2	10.00	11.40	9.06	32.01
3	15.00	17.70	13.80	32.01
4	20.00	24.00	13.89	32.01

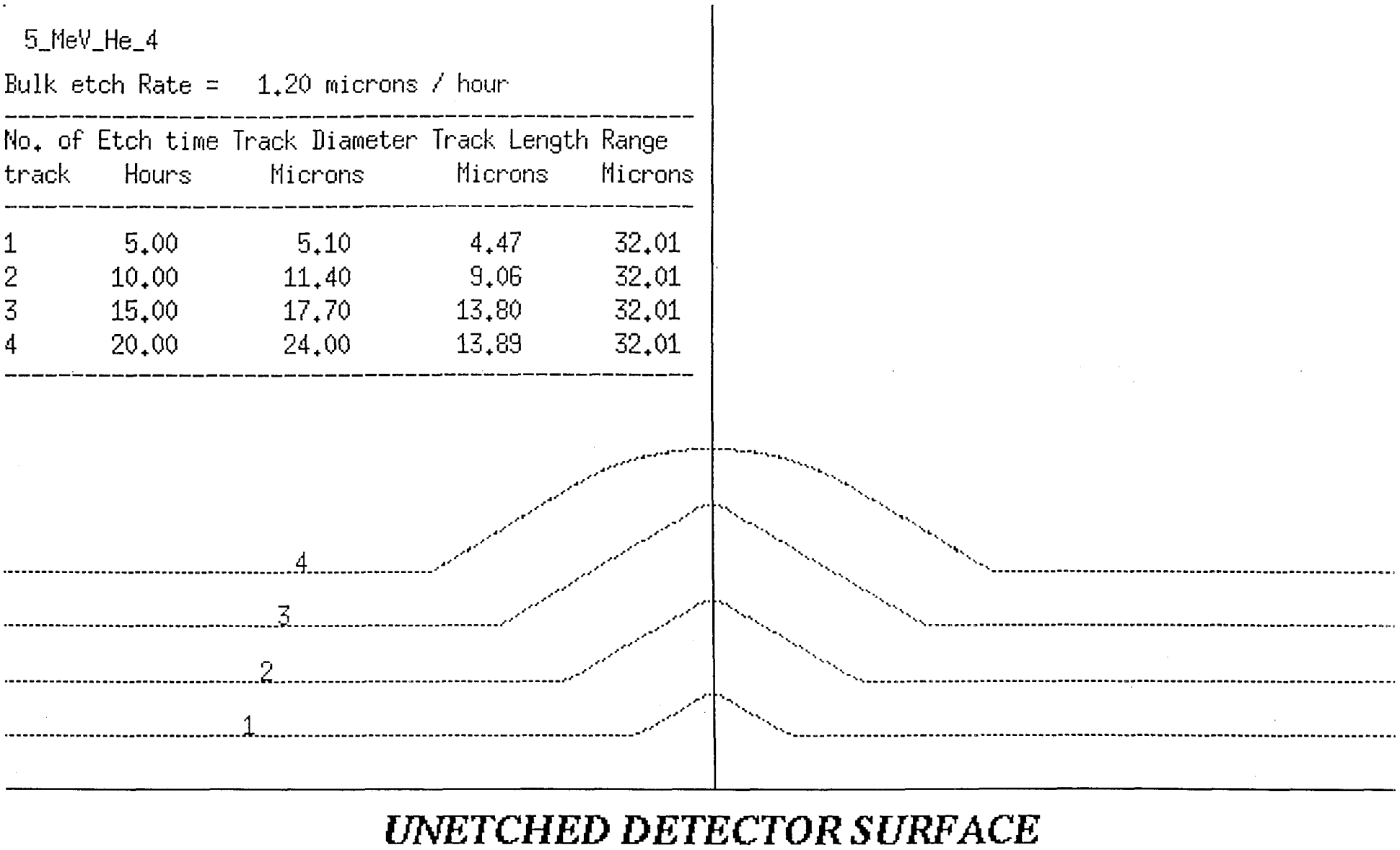

Fig 4.6 Track profiles at various etching times for 5 MeV Alpha particles in CR-39 track detector

36_MeV_Neon_20

Bulk etch Rate = 1.38 microns / hour

No. of track	Etch time Hours	Track Diameter Microns	Track Length Microns	Range Microns
1	2.00	3.60	5.01	27.66
2	4.00	7.50	10.11	27.66
3	6.00	11.10	15.27	27.66
4	8.00	15.00	18.00	27.66

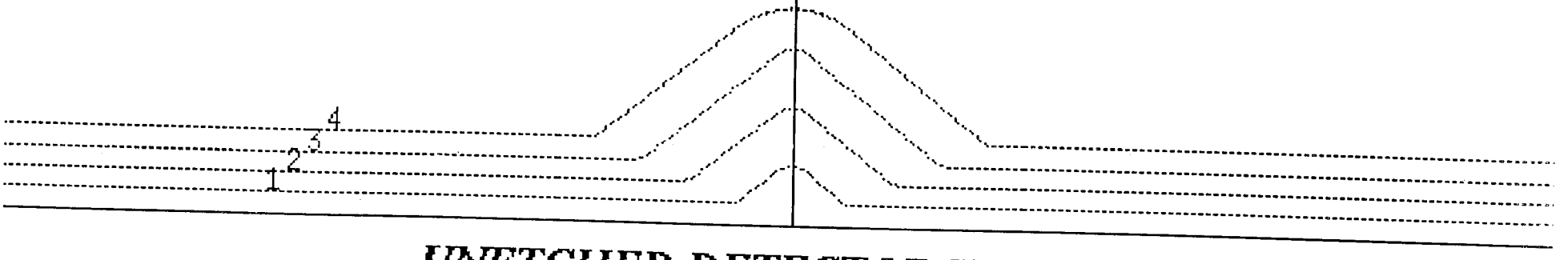

Fig 4.7 Track profiles at various etching times for 36 MeV 20Ne ions in Makrofol track detector

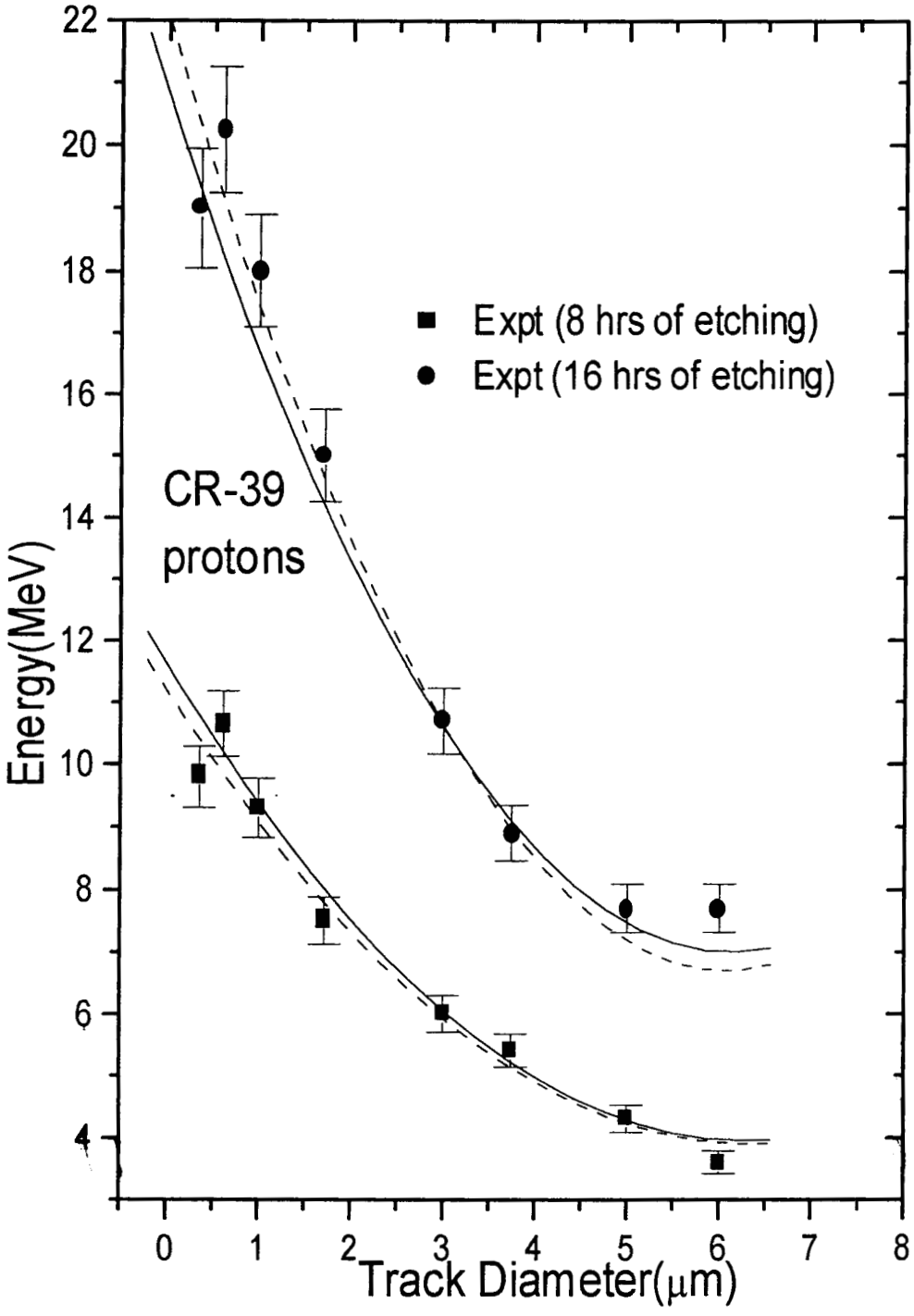

Fig 4.8 Track Diameter of Protons on CR-39 having different energies : solid curves id = 1; dashed curves id = 2.

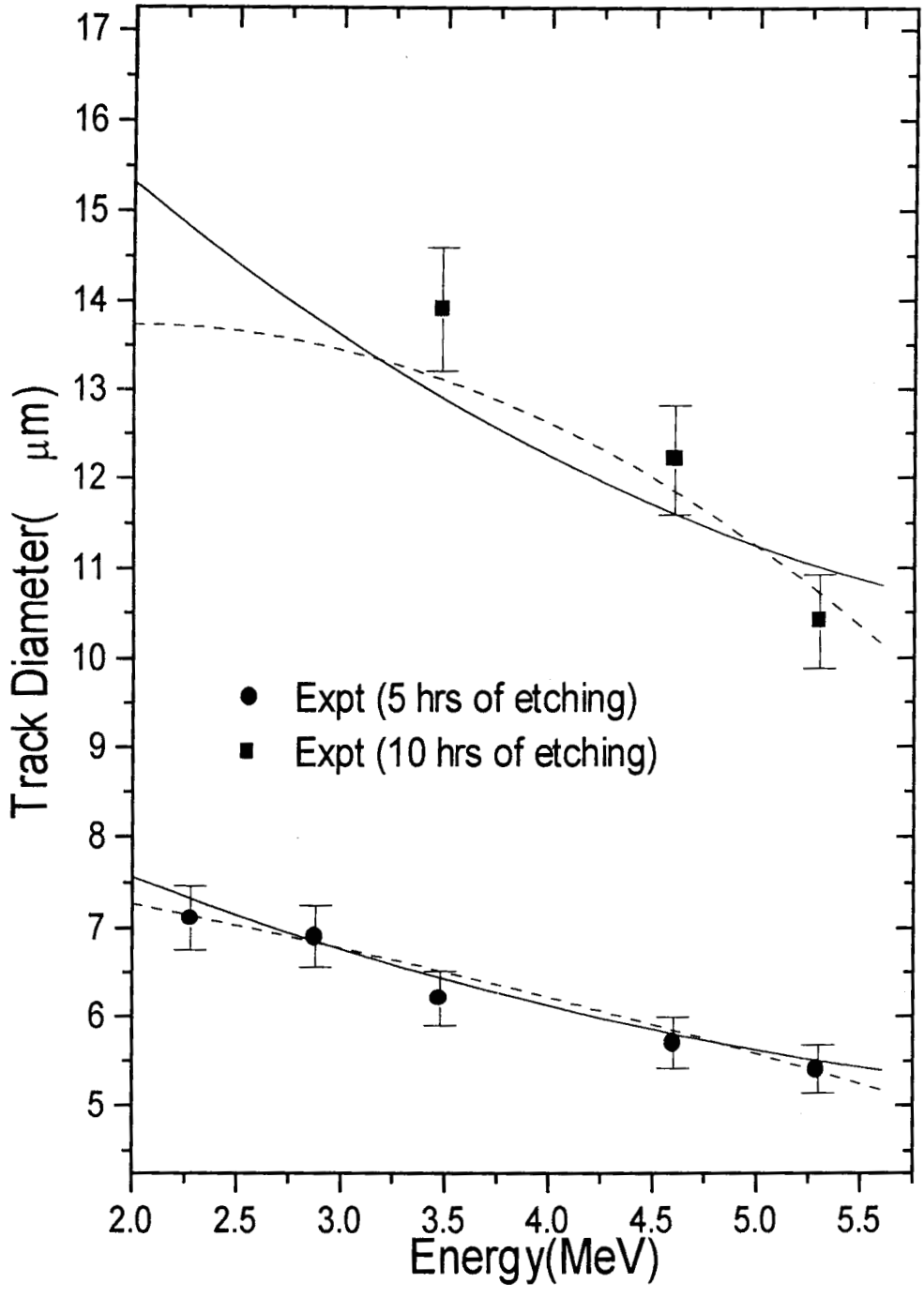

Fig 4.9 Track diameter of α particles on CR-39: solid curves: id = 1; dashed curves: id = 2

NIS H570
539.77 TH LIL/T

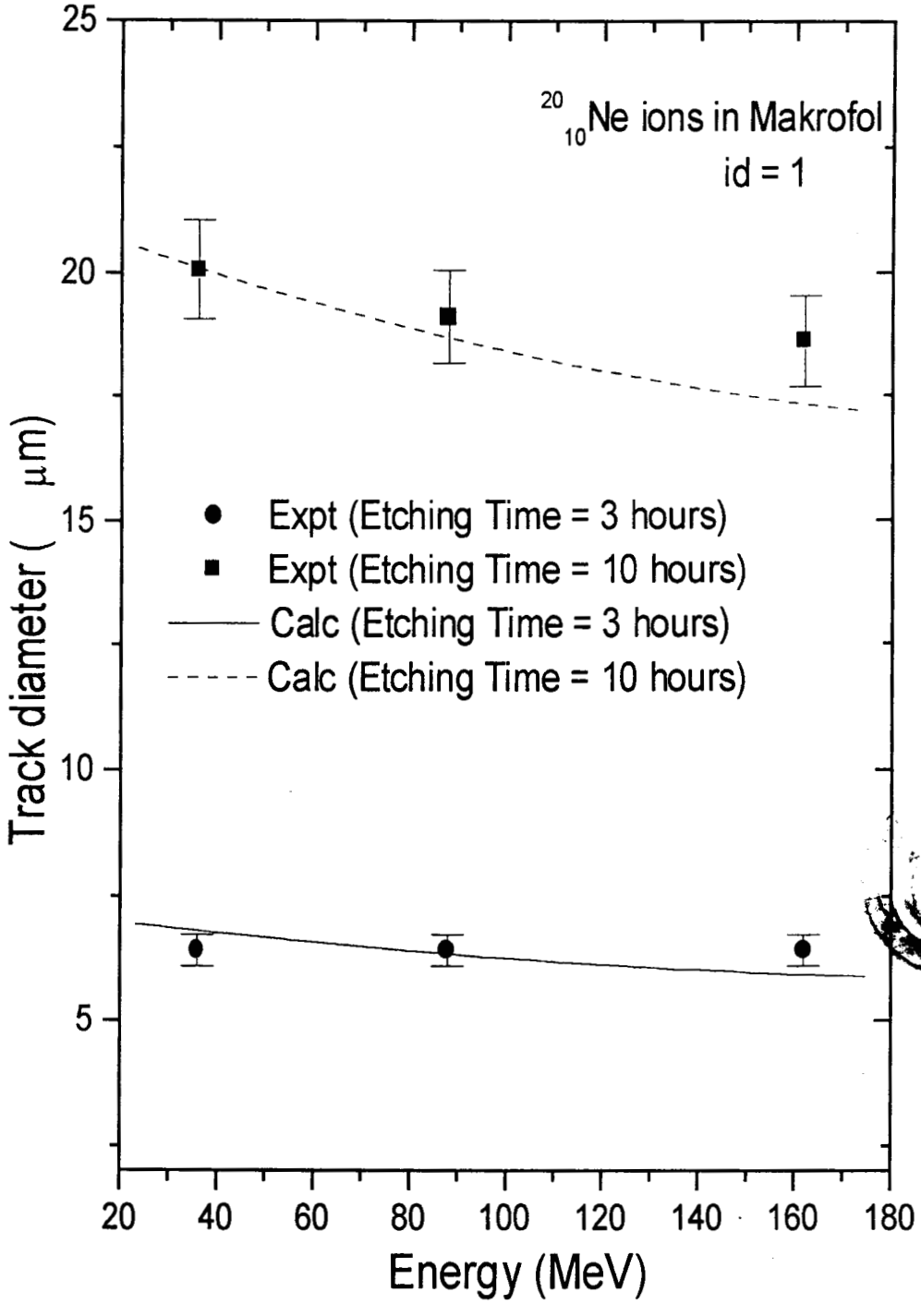

Fig 4.10 Track diameters of $_{10}Ne^{20}$ on Makrofol-E

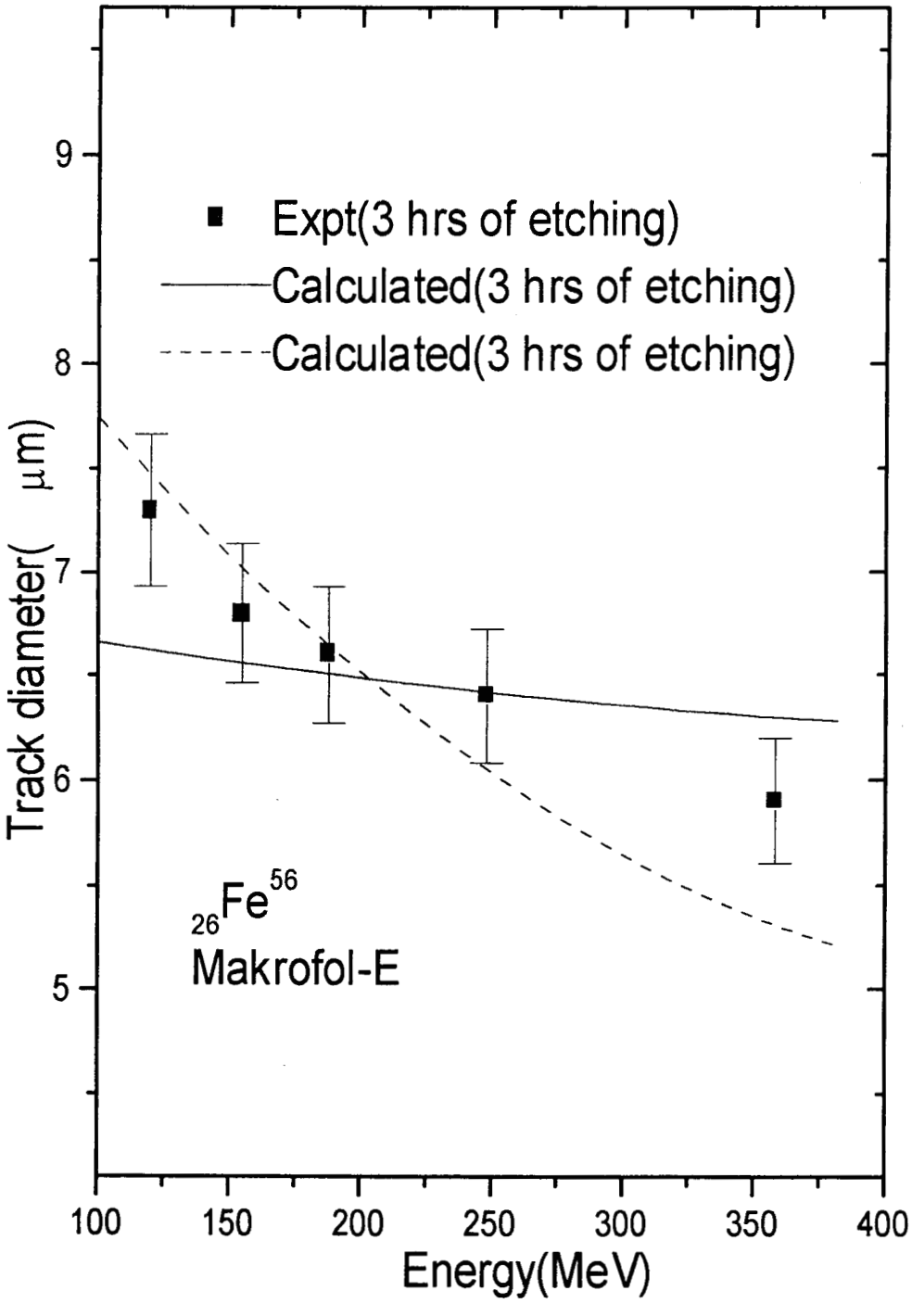

Fig 4.11 Track diameters of $_{26}Fe^{56}$ on Makrofol-E: solid curves id =1; dashed curves: id = 2.

Table 4.1a-Calculated and experimental track diameters for protons on CR-39.

Energy (MeV)	Time of etching	Calculated track diameter (μm) with id = 1	with id = 2	Experiment [7]
0.110	4hrs	3.5	3.3	3.6
"	5 "	4.1	4.4	4.0
0.145	2 "	3.4	3.9	3.6
"	3 "	3.8	4.2	4.3
"	4 "	4.6	4.2	4.5
"	5 "	5.4	5.2	5.2
0.182	2 "	3.7	3.7	3.7
"	3 "	4.3	4.3	5.0
"	4 "	5.3	5.0	5.3
"	5 "	6.1	6.3	5.9
0.220	2 "	3.7	3.8	3.8
"	3 "	4.8	5.2	5.4
"	4 "	6.0	6.3	5.7
"	5 "	7.2	7.2	7.2

Table 4.1b-Calculated and experimental track diameters for protons on CR-39

Energy (MeV)	Time of etching	Calculatedtrack diameter(μm) with id = 1	with id = 2	Experiment [8]
0.280	2 hrs	4.5	4.3	4.0
"	4 "	4.5	4.6	5.0
"	8 "	6.3	5.9	6.75
"	12 "	8.4	8.6	8.5
"	16 "	10.3	10.8	10.5
"	20 "	12.2	12.8	12.0
0.480	4 "	3.4	3.7	3.5
"	8 "	6.6	6.9	7.0
"	12 "	9.8	9.6	9.0
"	16 "	12.5	11.5	12.0
"	20 "	15.0	15.4	15.5
0.670	4 "	1.6	2.1	1.5
"	8 "	3.5	4.3	3.5
"	12 "	7.9	7.8	8.5
"	16 "	11.6	10.9	12.5
"	20 "	14.5	13.1	16.0
0.970	8 "	1.8	2.2	1.8
"	12 "	2.9	3.2	2.5
"	16 "	5.8	4.4	8.0
1.17	12 "	1.8	1.8	1.5
"	16 "	2.5	2.5	2.5
1.35	16 "	1.7	1.6	1.5
"	20 "	2.3	2.1	2.5
1.55	20 "	1.5	1.5	1.5

Table 4.1c-Calculated and experimental track diameters for protons on CR-39.

Energy (MeV)	Time of etching	Calculated track diameter(μm) with id = 1	with id = 2	Experiment [9]
0.350	8hrs	10.4	9.5	9.8
"	16 "	18.0	19.0	19.0
0.610	8 "	10.7	10.8	10.65
"	16 "	19.4	20.0	20.25
1.00	8 "	9.5	9.4	9.3
"	16 "	17.0	18.2	18.0
1.71	8 "	7.7	7.5	7.5
"	16 "	14.1	14.6	15.0
3.00	8 "	6.1	5.7	6.0
"	16 "	10.9	10.2	10.7
3.74	8 "	5.2	5.1	5.4
"	16 "	8.4	8.9	8.9
5.00	8 "	4.4	4.5	4.3
"	16 "	7.6	7.2	7.7
6.00	8 "	3.9	3.8	3.6
"	16 "	7.1	6.8	7.7

Table 4.2-calculated and experimental track diameters for deuterons on CR-39.

Energy (MeV)	Time of etching	Calculated track diameter(μm) with id = 1	with id = 2	Experiment [7]
0.110	2hrs	3.0	3.0	3.0
"	3 "	4.0	3.9	4.0
0.160	1 "	2.6	2.1	2.5
"	2 "	2.7	2.9	3.0
"	3 "	3.6	3.8	3.9
"	4 "	4.4	4.5	4.2
0.212	1 "	2.6	2.1	2.5
"	2 "	3.5	3.4	3.5
"	3 "	4.8	4.6	4.4
"	4 "	6.1	5.8	5.9
0.270	1 "	2.4	2.1	2.5
"	2 "	3.9	3.7	3.4
"	3 "	5.5	5.5	5.6
"	4 "	7.1	7.0	8.0
0.390	2 "	2.4	2.4	2.1
"	4 "	4.6	4.6	5.2
0.560	2 "	2.1	2.2	2.0
"	4 "	4.0	4.2	4.4
0.760	2 "	2.1	2.1	2.2
"	4 "	4.0	3.8	3.8
0.960	2 "	1.8	1.8	1.8
"	4 "	3.3	3.1	3.1

Table 4.3a-Calculated and experimental track diameters for a particles on CR-39.

Energy (MeV)	Time of etching	Calculated track diameter(μm) with id = 1	with id = 2	Experiment [7]
0.083	2hrs	3.8	3.9	3.8
"	3 "	3.8	3.9	3.8
"	4 "	3.8	3.7	3.8
0.110	2 "	3.8	3.7	3.7
"	3 "	3.8	3.7	3.9
"	4 "	4.3	4.3	4.2
0.140	2 "	3.6	3.9	3.6
"	3 "	4.0	4.2	4.2
"	4 "	4.7	4.6	4.6
0.170	2 "	3.7	3.9	3.7
"	3 "	4.0	4.2	4.4
"	4 "	4.7	4.4	4.6
0.295	2 "	3.6	3.6	3.4
"	4 "	6.1	5.9	6.3
0.745	2 "	3.8	3.8	3.5
"	4 "	6.7	7.3	7.6
1.090	2 "	4.0	3.7	3.5
"	4 "	7.0	7.5	8.5

Table 4.3b-Calculated and experimental track diameters for a particles on CR-39.

Energy (MeV)	Time of etching	Calculated track diameter(μm) with id = 1	with id = 2	Experiment [10]
5.3	5 hrs	5.5	5.4	5.4
"	10 "	11.0	10.8	10.4
4.6	5 "	5.8	5.8	5.7
"	10 "	11.6	11.7	12.2
3.48	5 "	6.4	6.5	6.2
"	10 "	12.9	13.1	13.9
2.88	5 "	6.9	6.9	6.9
2.28	5 "	7.3	7.1	7.1

Table 4.4-Calculated and experimental track diameters $_{10}Ne^{20}$ ions on Makrofol-E.

Energy (MeV)	Time of etching	Calculatedtrack diameter(μm) with id = 1	Experiment [11]
36	3 hrs	6.8	6.4
"	10 "	20.1	20.0
88	3 "	6.3	6.4
"	10 "	18.6	19.1
162	3 "	5.9	6.4
"	10 "	17.3	18.6

Table 4.5-Calculated and experimental track diameters for $_{26}Fe^{56}$ ions on Makrofol-E.

Energy (MeV)	Time of etching	Calculated track diameter(μm) with id = 1	with id = 2	Experiment [11]
120	3 hrs	6.6	7.5	7.3
155	"	6.6	7.0	6.8
188	"	6.5	6.6	6.6
248	"	6.4	6.1	6.4
358	"	6.3	5.3	5.9

Table 4.6-Calculated and experimental track diameters for $_{36}Kr^{84}$ ions on Makrofol-E.

Energy (MeV)	Time of etching	Calculated track diameter(μm) with id = 1	Experiment [11]
6.5	3 hrs	7.0	6.5
33	"	8.2	8.5
75.6	"	8.4	9.5

4.4.4. Track Length

The calculated and experimental values of $_8O^{16}$ ion on Makrofol-E [12] are given in Table 4.7. The graphical representations are given in figure 4.12

Table 4.7-Calculated and experimental track lengths for $_8O^{16}$ ions on Makrofol-E.

Energy (MeV)	Time of etching	Calculated track length(μm) with id = 1	with id = 2	Experiment [12]
40	3.0 hrs	12.2	10.7	12.0
"	3.5 "	14.3	13.1	14.4
"	4.0 "	16.3	15.8	16.6
"	4.5 "	18.4	18.9	18.4
"	5.0 "	20.5	23.1	19.8
64	3.0 "	18.4	16.6	15.0
"	3.5 "	21.5	20.0	20.0
"	4.0 "	24.7	23.6	23.6
"	4.5 "	27.8	27.5	28.2
"	5.0 "	31.0	31.9	32.7

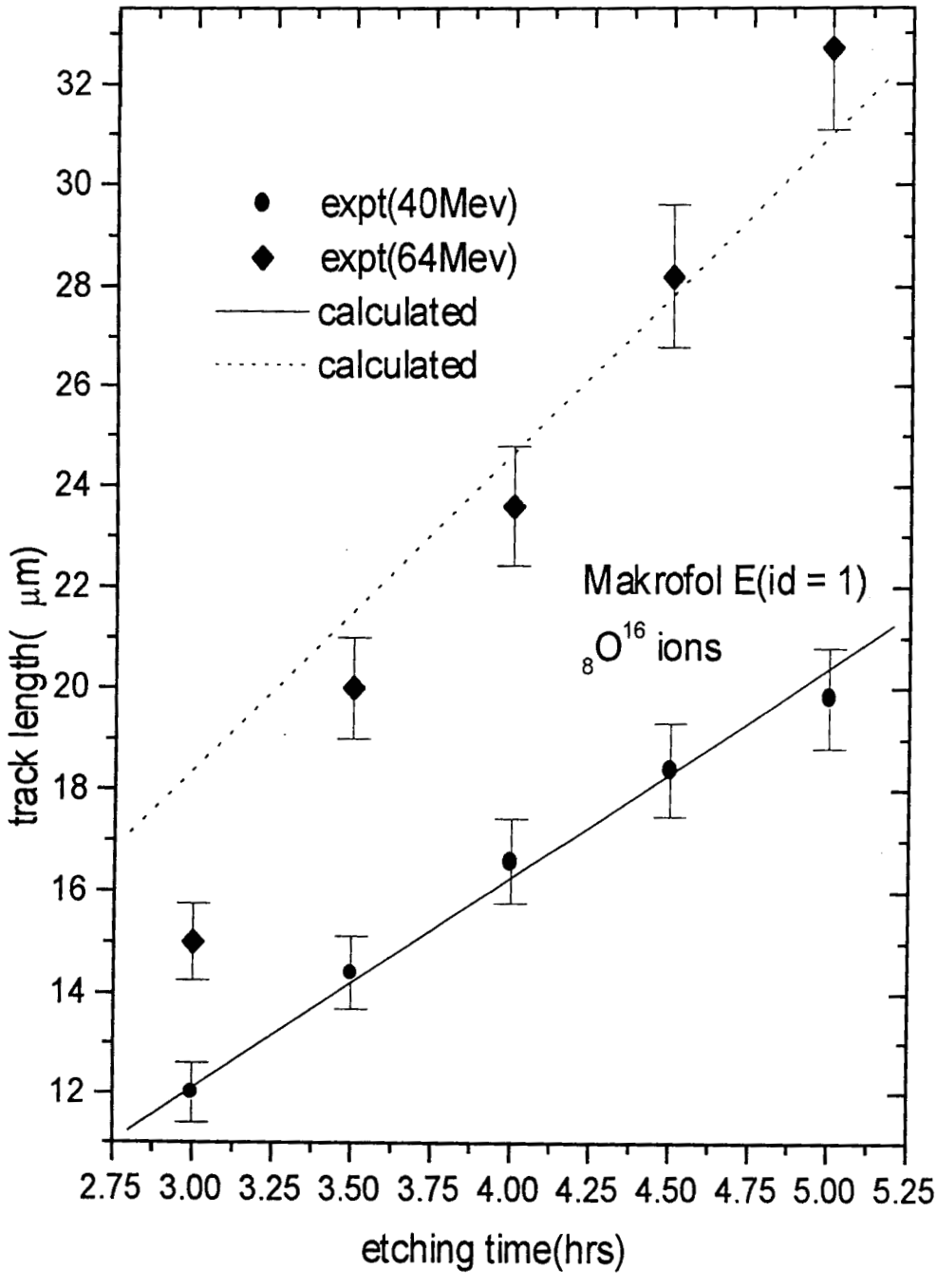

Fig 4.12 Track lengths of $_8O^{16}$ on Makrofol-E

4.4.5. Discussion

It is seen from the tables and figures given in the earlier sections that the present calculations reproduce reasonably well most of the experimentally measured track diameters and track lengths for CR-39 and Makrofol. There are no clear indications in the calculated results which would help to choose between the two options id = 1 and id = 2.

References

1. R.L.Fleischer, P.B.Price and R.M. Walker(1975) Nuclear Ttracks in Solids-Principles and Applications, University of California press.
2. Antony Joseph and K.M.Varier, Radiation Measurements vol.24,No.2, pp111-114, 1995.
3. S.M.Farid and A.P.Sharma, Int.J.Appl.Radiat.Isot.,vol 35,No.18,715-719(1984)
4. R.L.Fleischer, P.B.Price and R.M. Walker(1965) Jour.Appl.Physics vol.36,3645
5. L.C.Northcliff and R.F.Schilling(1970) Nucl.Data Tables 7
6. J.F.Ziegler, J.P.Biersack, Logical"SRIM 2000",Pergamon, New York,2000.
7. A.Szydlowski, M.Sadowski, T.Czyzewski, M.Jaskola and A.Korman, Nuc.Instr. and Meth.B149(1999)113 –118.
8. M.Sadowski, E.M.Al-Mashbadani, A.Szydlowski, T.Czyzewski, L.Gglowacka, M.Jaskola and M.Wielunski, Nuc.Instr. and Meth.B86((1994)311-316.
9. Hameed A.Khan and Reinhard Brandt, Nuc.Tracks vol.7,No.3,pp129-139(1983).
10. Antony Joseph, Ph.D.thesis(unpublished), Calicut University(1993).
11. S.M.Farid and A.P.Sharma, Int.J.Pure andAppl.Phys.23(1985)121
12. S.M.Farid and A.P.Sharma, Int.J.Pure andAppl.Phys.,21(1983)521 and22(1984)133.

CHAPTER V

NEUTRON SLOWING DOWN STUDIES IN PARAFFIN USING CR-39 TRACK DETECTOR

5.1. INTRODUCTION

CR-39, a very versatile nuclear track detector has been used in the present work for some studies using fast neutrons from a neutron Howitzer. Determination of the slowing down length in paraffin is one such study. Fast neutrons produced by the $^{9}Be(\alpha,n)$ reaction are slowed down in paraffin medium. In order to determine the slowing down length in the material, one needs to estimate the thermal neutron flux distribution in the medium. Joy Stephen[1] in his measurements irradiated indium foils at various distances and determined the thermal neutron flux by measuring the induced beta activity in the foils. Another method is to detect the charged particles, viz: α particles and lithium ions produced in the reaction $^{10}B(n,\alpha)$ and indirectly estimate the neutron flux from the observed yield of the α particles or lithium ions or both. We have studied the slowing down length in paraffin by this second method, using CR-39 track detector for detecting the α particles produced in the above reaction. The experimental details and the results obtained are described in the following sections.

5.2. EXPERIMENTAL DETAILS.

5.2.1. The Neutron Source.

The source of fast neutrons for the present investigations was a neutron Howitzer (Model NH 11) procured from Electronics Corporation of India, Hyderabad. In this howitzer neutrons are generated from a 250 mCi ^{241}Am-^{9}Be source. The neutron emission rate is estimated to be around 5.5×10^{5} per sec. The howitzer has a cylindrical geometry with the neutron source at the centre of its axis. Paraffin wax surrounds it all around. The energy distributions of the emitted neutrons varies from zero to a maximum energy of about 12 MeV. There are several irradiation ports.

5.2.2. The Detector.

Ten sheets of CR-39 (Non Dop) detector of dimensions 2cm x 1cm x 0.028cm were used for the irradiations.

5.2.3. The Target.

The boron targets for the $^{10}B(n,\alpha)$ reaction have been prepared using Boric acid powder (H_3BO_3). Pellets of diameter 1 cm and thickness 0.1cm were prepared.

5.2.4. Experimental Procedure.

The experimental set up is given in fig 5.1.A cylindrical paraffin block of height 40 cm and diameter 10 cm was moulded, with slots along the axis at intervals of 4cm each. The boric acid pellets were kept in these slots, along with CR-39 sheets. CR-39 track detector is used for detection of the α particles and lithium ions. The paraffin block, along with the pellets and detectors, was kept in the central irradiation port of the neutron Howitzer. The irradiation time was 21 days. After the irradiation, the track detector sheets were taken out and etched. Etching was done using 6N NaOH solution at 70 ± 1^0C in a temperature controlled water bath described in section 3.1.1.4 and 3.1.1.5. After 5 hours of etching, the alpha tracks were counted by means of Carl Zeiss research microscope. The diameters of the charged particle tracks were measured accurately by means of a micrometer eyepiece.

5.3. RESULTS

The measured diameter distributions of the charged particles is given in figure 5.2. It consists of two broad peaks, which can be identified as belonging to alphas and

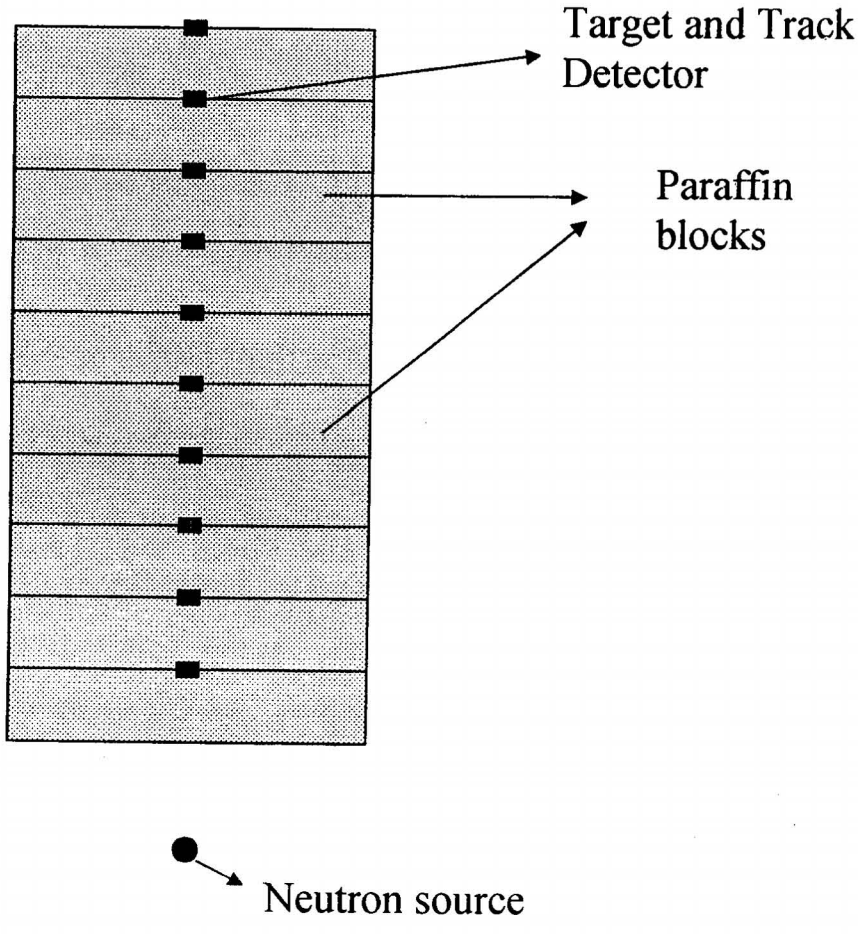

Fig 5.1 Experimental setup for neutron irradiation

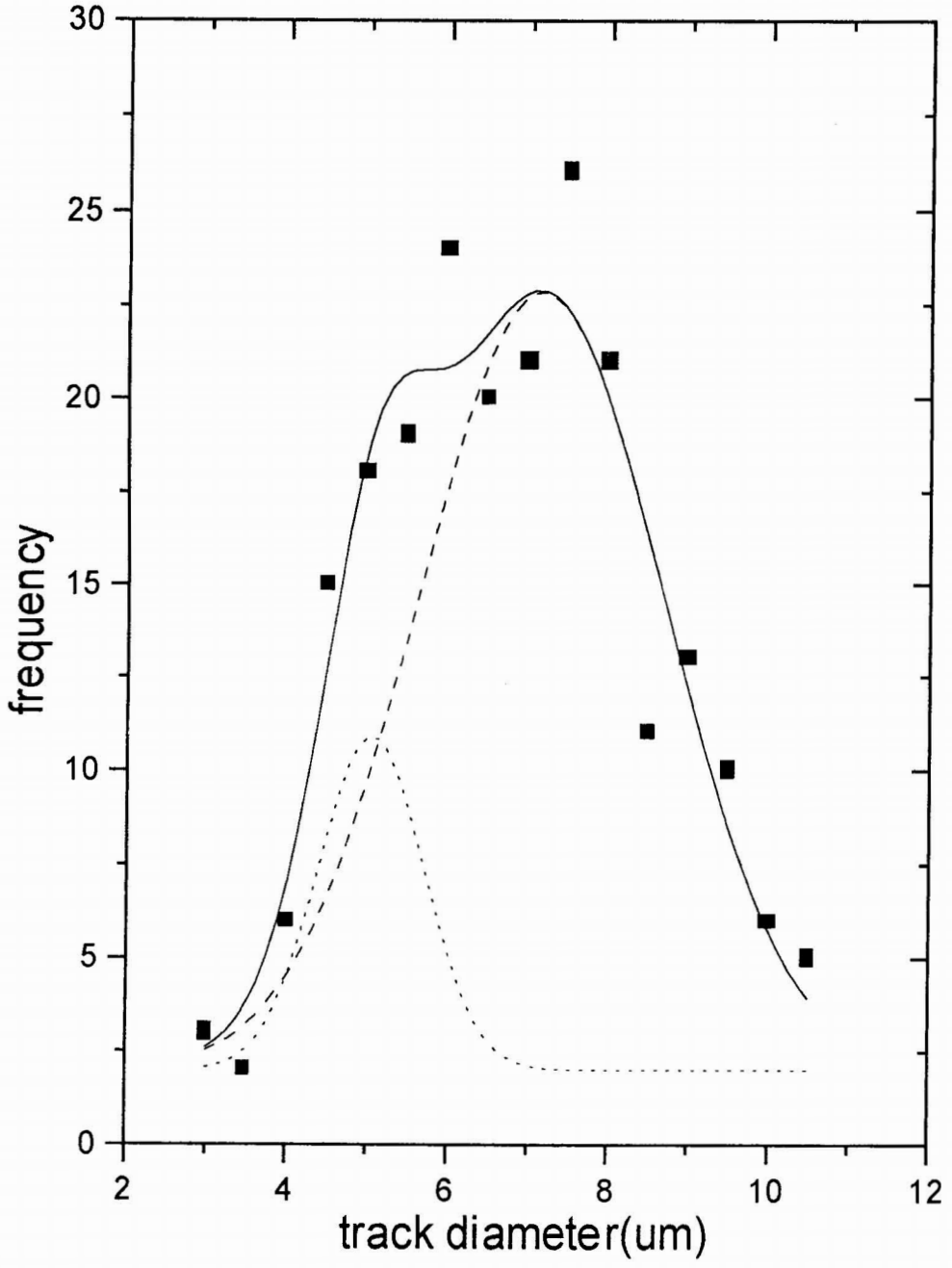

Fig 5.2 Track diameter distributions of the charged particles from the $^{10}B(n,\alpha)$reaction

lithium ions. The measured yield as a function of distance from neutron source has been plotted in figure 5.3.

The thermal neutron flux distribution Φ will also be of similar relative shape. Using this curve, plots of $r^4\Phi$ and $r^2\Phi$ are made which is given in figure 5.4. The total areas under these plots were determined and mean square average radius was calculated by finding the ratios of these areas. The slowing down length was calculated as one-sixth of this radius. The slowing down length was also calculated from the slope of the linear portion of the log Φ vs r^2 graph, which is shown in fig 5.5.

The results obtained in the present study are compared in table 5.1.with those obtained earlier by Joy Stephen [1] earlier using the beta measurements.

Table 5.1. Neutron Slowing down lengths

Parameter	from $^{10}B(n,\alpha)$ reaction		from induced
	$r^4\Phi$ and $r^2\Phi$ graph	log $\phi - r^2$ graph	beta activity[1]
neutron slowing down length	5.81 cm	6.40 cm	5.90 cm

References

1. Joy Stephen "Slowing down length of neutrons in Parraffin", M.Phil. dissertation (unpublished)University of Calicut,1982.

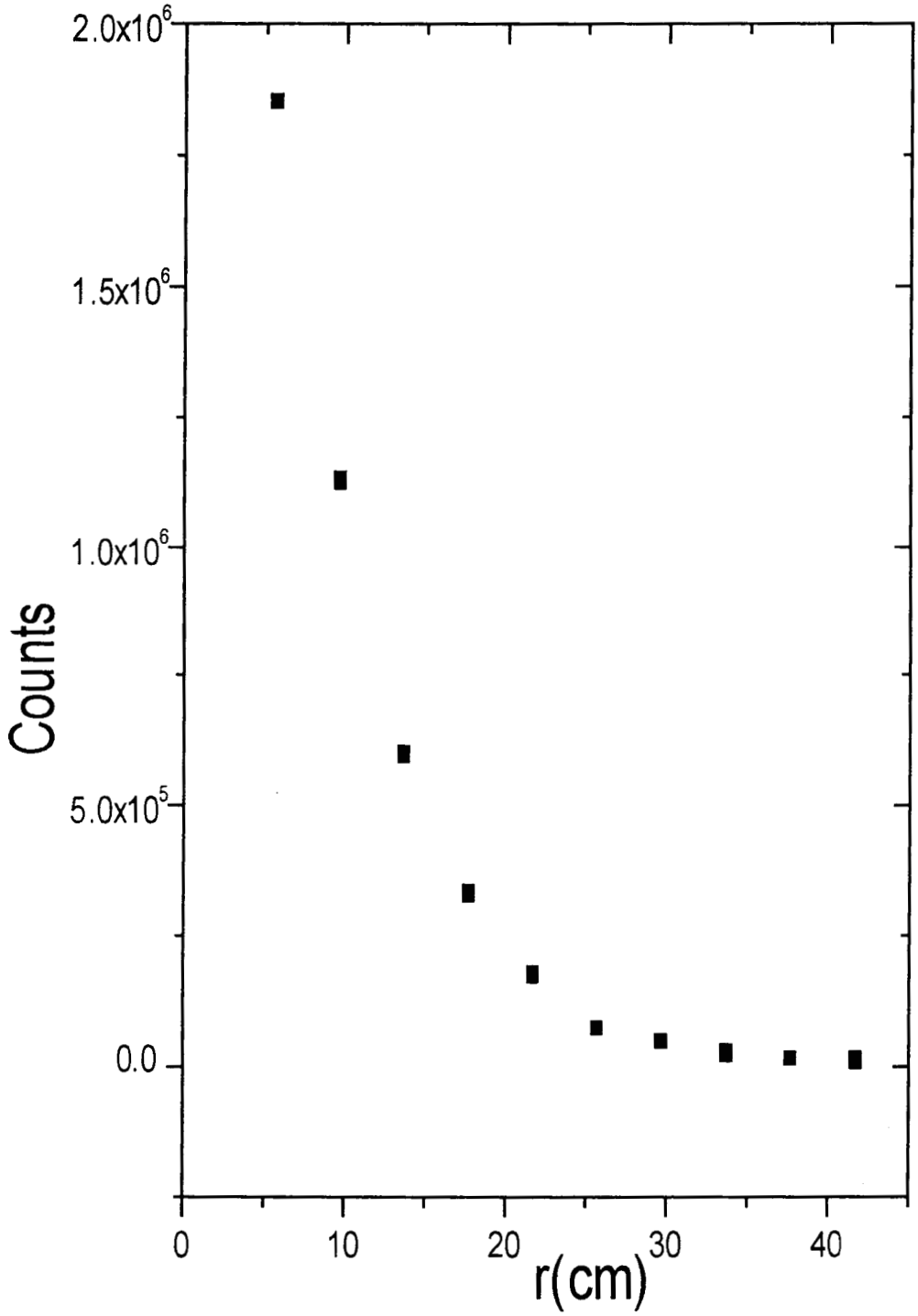

Fig 5.3 Thermal neutron flux distribution

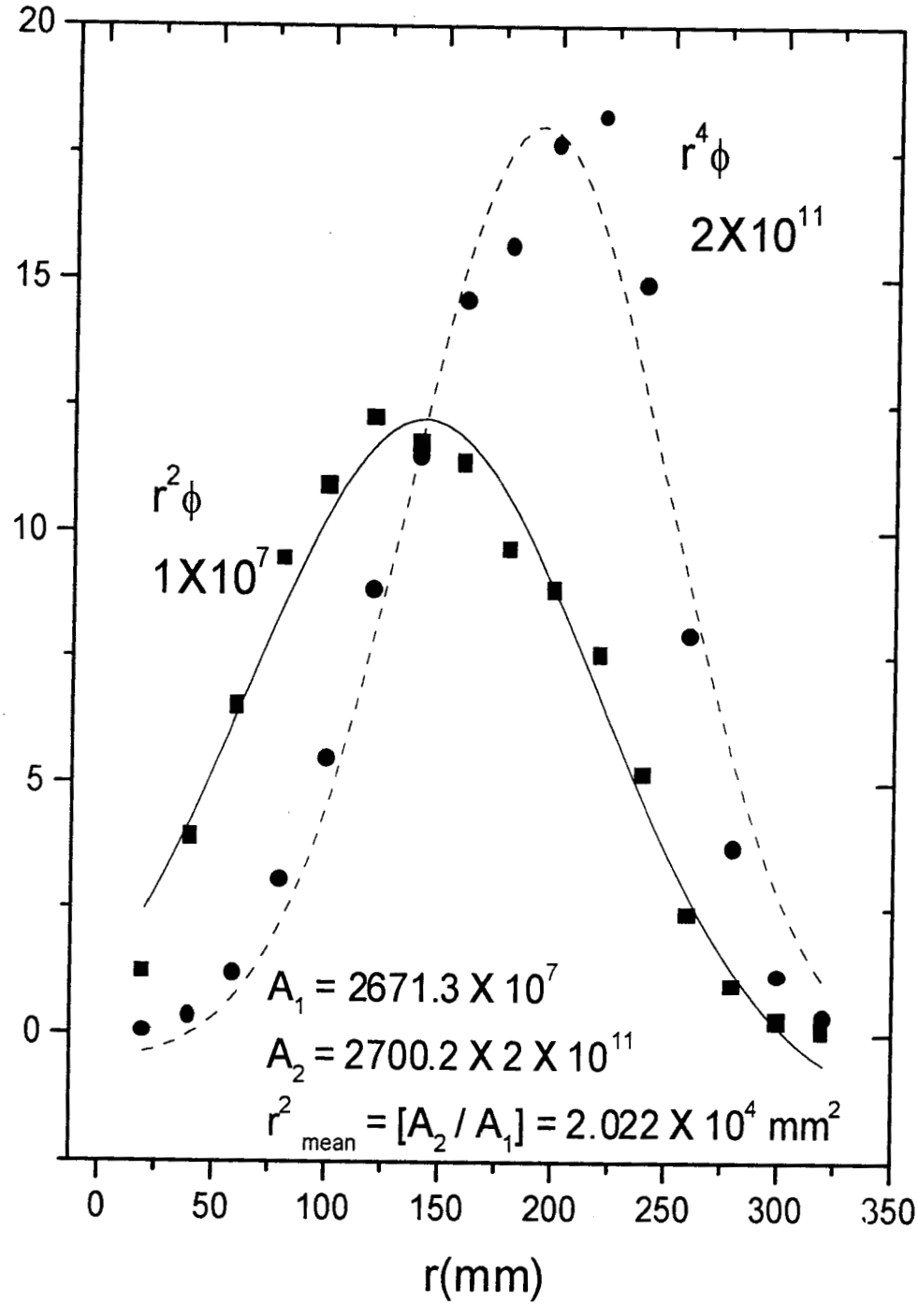

Fig 5.4 Plots of $r^4\phi$ and $r^2\phi$

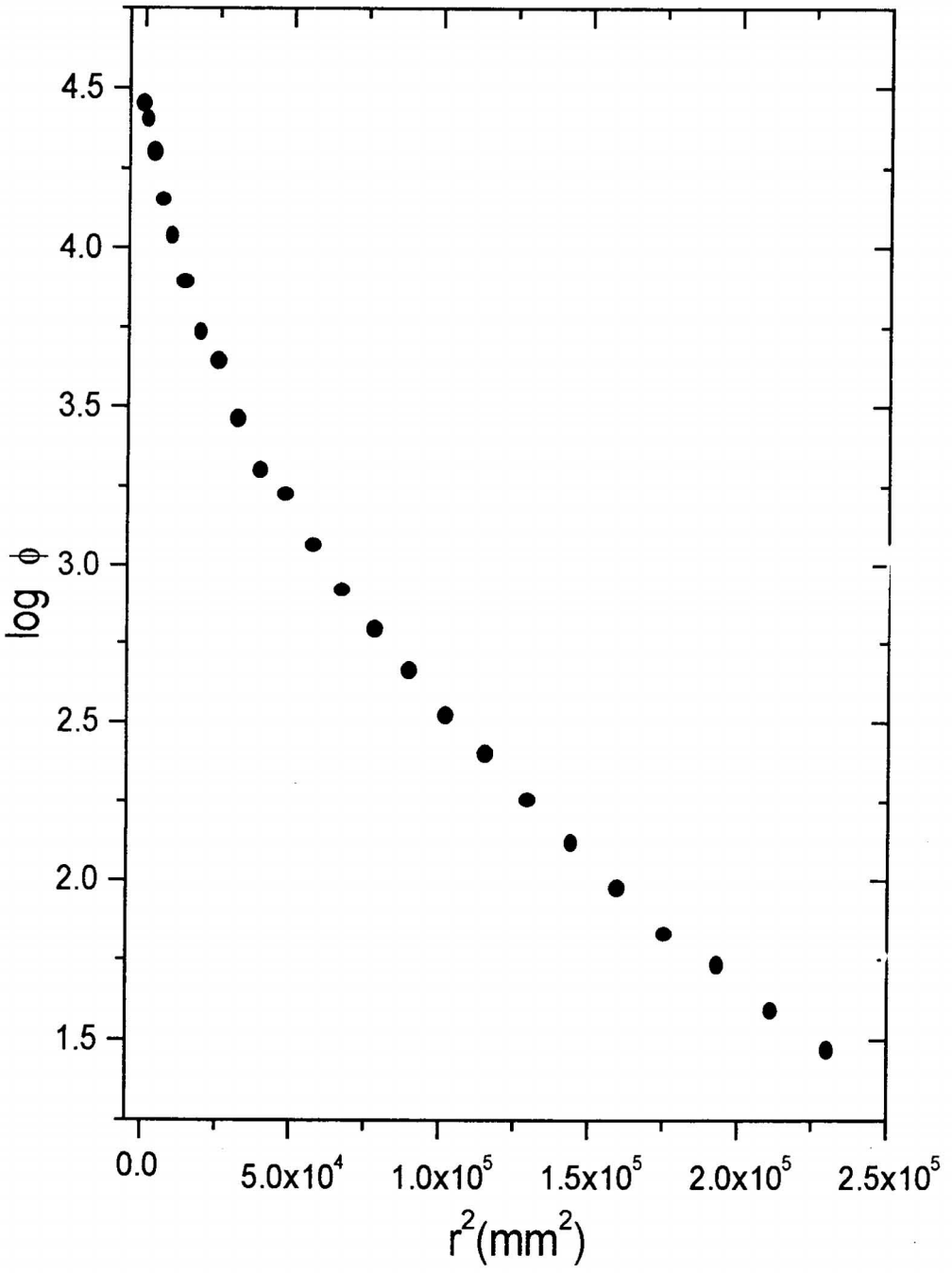

Fig 5.5. Log ϕ vs r^2 graph

CHAPTER VI

NEUTRON INDUCED REACTION STUDIES IN BORON AND COPPER USING CR-39 TRACK DETECTOR

6.1. INTRODUCTION

CR-39 is a very efficient track detector for both light charged particles like protons and alphas as well as heavy ions. One important application of this track detector is in nuclear reaction studies. A combination of a neutron Howitzer as a source of neutrons and the CR-39 as a charged particle detector offers some advantages over accelerator based experiments for neutron induced reaction studies. One obvious advantage is the simplicity of the set up. Of course the rather low intensity of the incident neutrons poses certain problems. However, this can be overcome by extending the measurements over long periods of time, especially since no electronic online data acquisition is required.

We have carried out studies on (n,α)reactions on Boron and Copper using CR-39 detectors. The details of the experiment and the results obtained are presented below.

6.2. EXPERIMENTAL DETAILS

6.2.1. The Neutron Source.

The same source was used as explained in section 5.2.1.Here the central portion was used for fast neutron irradiation and farther ones were used for thermal neutrons.

6.2.2. The Targets.

Targets for the $^{10}B(n,\alpha)$ reaction have been obtained from the target laboratory of the Nuclear Science Centre, New Delhi. They were with thickness of around 200 $\mu g/cm^2$. Copper target had a thickness of 1 mm.

6.2.3. The Detector.

Three separate sheets of CR-39 (Non Dop) detector of dimensions 2cm x 1cm x 300 μm were used.

6.2.4. Experimental Procedure.

The combination was fixed to a horizontal paper sheet kept at a convenient distance above the central port of the Howitzer (for fast n irradiations) so that the target faces the neutron beam. Also, the paper sheet had a clear hole above the area of the target so that no charged particles fall on the top face of the detector sheet due to reactions with the nuclei of the paper sheet. In the case of slow neutron irradiations, the target-detector set up was kept with their planes vertical, so that they face the neutron source. The target was irradiated with neutrons typically for about 4 days. After the irradiations, the detector sheets were etched using 6N NaOH solution at (70 ± 1^{0})C in a temperature controlled water bath as described in chapter 3. The etching was carried out for 5 hours in order that the etched charged particle track grow to sufficient size to be measured with reasonable precision. Track measurements were carried out by means of a Carl Zeiss research microscope, fitted with a micrometer eyepiece with about 0.5 μm accuracy.

6.3. RESULTS

The measured diameter distributions of charged particles detected by the track detector are shown in fig 6.1 for copper target. Fig 6.2 gives the measured diameter distributions of charged particles detected in the case of ^{10}B target.

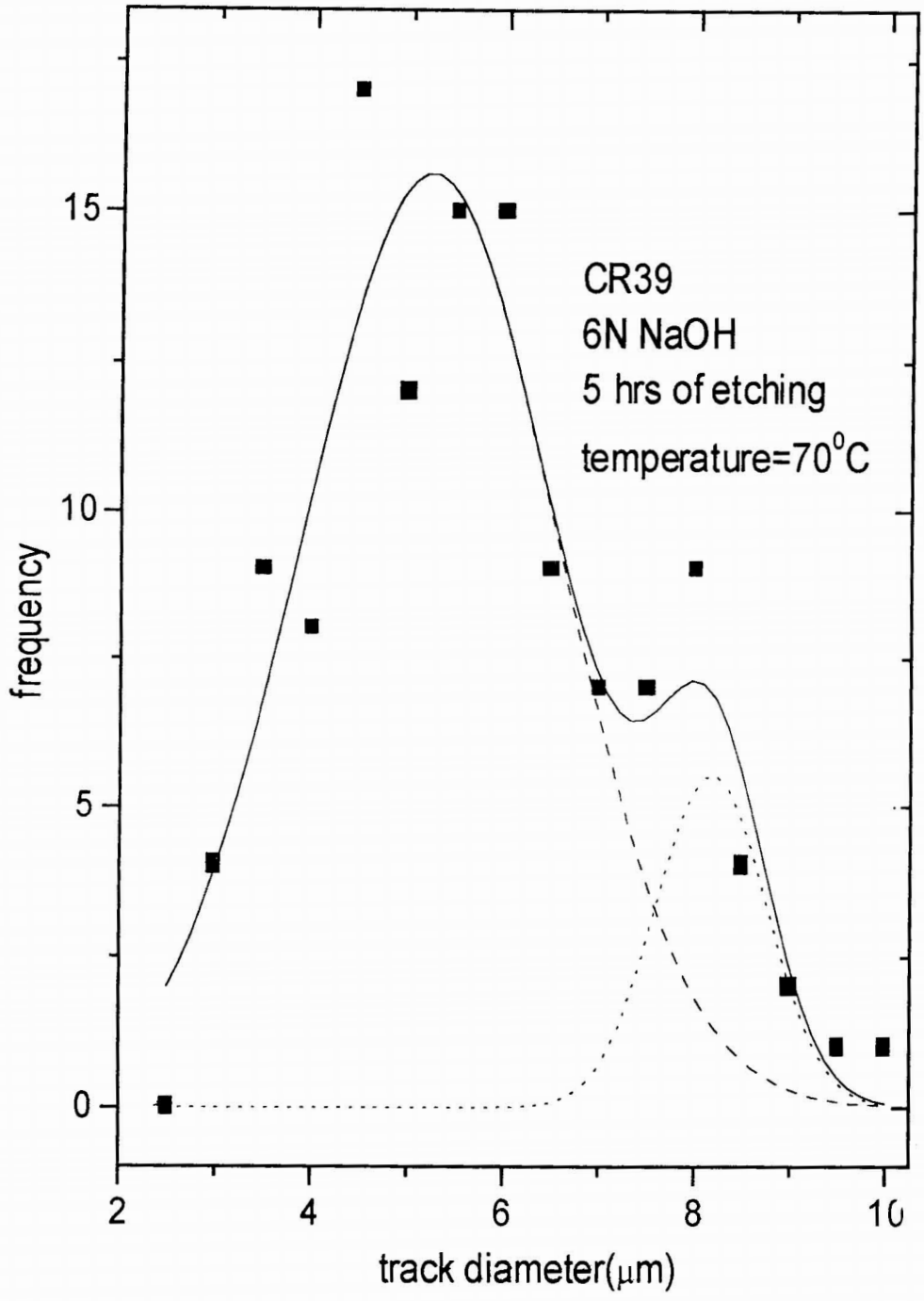

Fig 6.1 Track diameter distributions of charged particles from neutron induced reaction on copper.

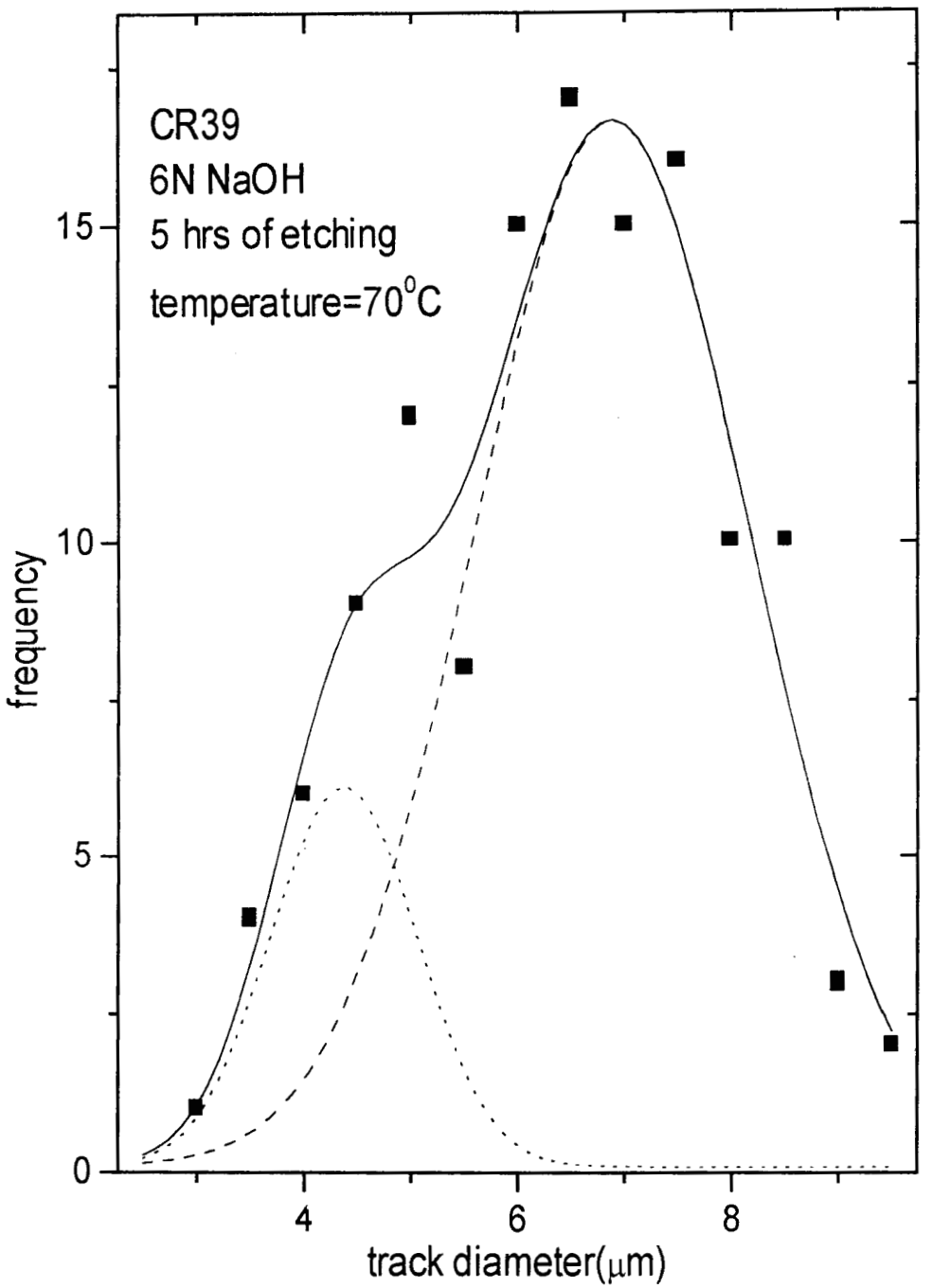

Fig 6.2 Track diameter distributions of charged particles from $_0n^1$ induced reaction on ^{10}B sheet

CHAPTER VII

USE OF OVERHEAD TRANSPARENCY SHEET AS A HEAVY ION TRACK DETECTOR

7.1 Introduction

In an earlier paper, Ghosh et al. [1], had subjected overhead projector transparency sheets (OPT) to some studies in order to characterize it as a track detector. They determined the elemental composition and found it to be a triacetate. The optimum etching conditions were arrived at and the bulk etch rate V_b and the activation energy E_a were measured. They used 14.5 MeV/u and 5.9 MeV/u ^{132}Xe ions as well as ^{252}Cf fission fragments for these studies. Subsequently, Basu et al. [2] observed α particles and fission fragment tracks in a particular type of OPT film. The fission tracks were quite distinguishable with larger diameters as compared to the α particle tracks. In a more recently reported work [3], they experimented with yet another type of OPT sheet and measured the diameter distributions and V_t / V_b ratios for the two types of OPT films.

We have made similar measurements on a locally available OPT sheet, using ^{252}Cf fission fragments. The following sections discuss the experimental details and the results obtained.

7.2 Experimental details

The OPT sheets used in the present studies were Garware make with a thickness of 100 μm. Pieces of dimensions 2 cm X 1 cm were cut from the sheets. They were exposed to alpha particles from ^{241}Am source and to alpha particles and fission fragments from the ^{252}Cf source for about 30 minutes at normal incidence. The detector sheets were etched in a constant temperature water bath [4]. We have used NaOH etchant with concentrations of 4N, 5N, 6N and 7N. These etchings were carried out at 70 $\pm$ 1°C. At

6N concentration, different temperatures were used for the etching, for the purpose of determination of the activation energy. The etching was carried out for 3 hours, 6 hours and 9 hours. After each etching, the track diameter distributions were measured using a Carl Zeiss Research microscope. A suitable magnification was used whereby an accuracy of 0.5 μm was obtained in the diameter measurements. For determining the bulk etch rate, un-irradiated detector sheets were etched for 3 hours, 6 hours and 9 hours and the masses measured using a sensitive electronic balance. The bulk etch rates were calculated therefrom.

7.3 Results

The value of the bulk etch rates obtained from the mass measurements are given in table 7.1 for different etchant concentrations at 70 °C and in table 7.2 for various temperatures of etching for 6N NaOH etchant.

Fig 7.1. gives a plot of log V_b vs. 1 / T. This is a straight line. From the slope of this line, the activation energy E_a for bulk etching is calculated to be 103 kJ mol^{-1} compared to the value of 59.3 kJ mol^{-1} obtained by Ghosh et al.[1] earlier for a different brand of OPT.

Examination of the etched, irradiated sheets showed conclusively that these sheets are insensitive to alpha particles of the energies used (upto 6.11 MeV). The sheets irradiated with ^{241}Am alpha particles also did not yield any etchable tracks.

Fig. 7.2. gives the diameter distribution of the etched tracks for fission fragments for etching times of 3 hours, 6 hours and 9 hours. The etching conditions were 6N NaOH at 70°C.

Fig 7.3. shows the diameter distributions for 6N NaOH for 6 hours of etching at various temperatures from 50°C to 80°C and fig 7.4. for NaOH concentrations of 4N, 5N, 6N and 7N at 70°C . All the distributions show a characteristic double peaked structure,

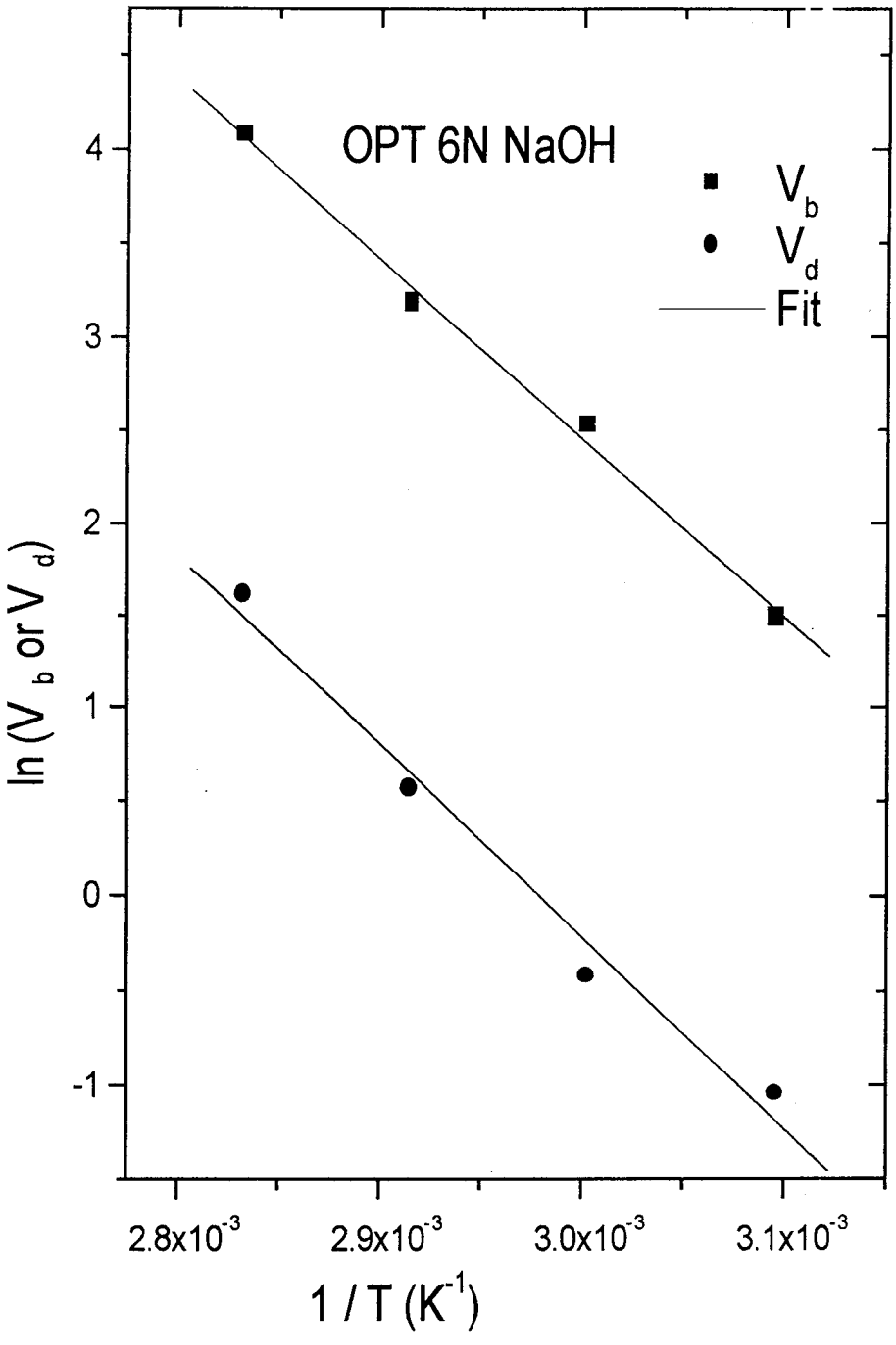

Fig 7.1 Variation of bulk etch rate V_b and velocity of track diameter evolution vs. 1 / T

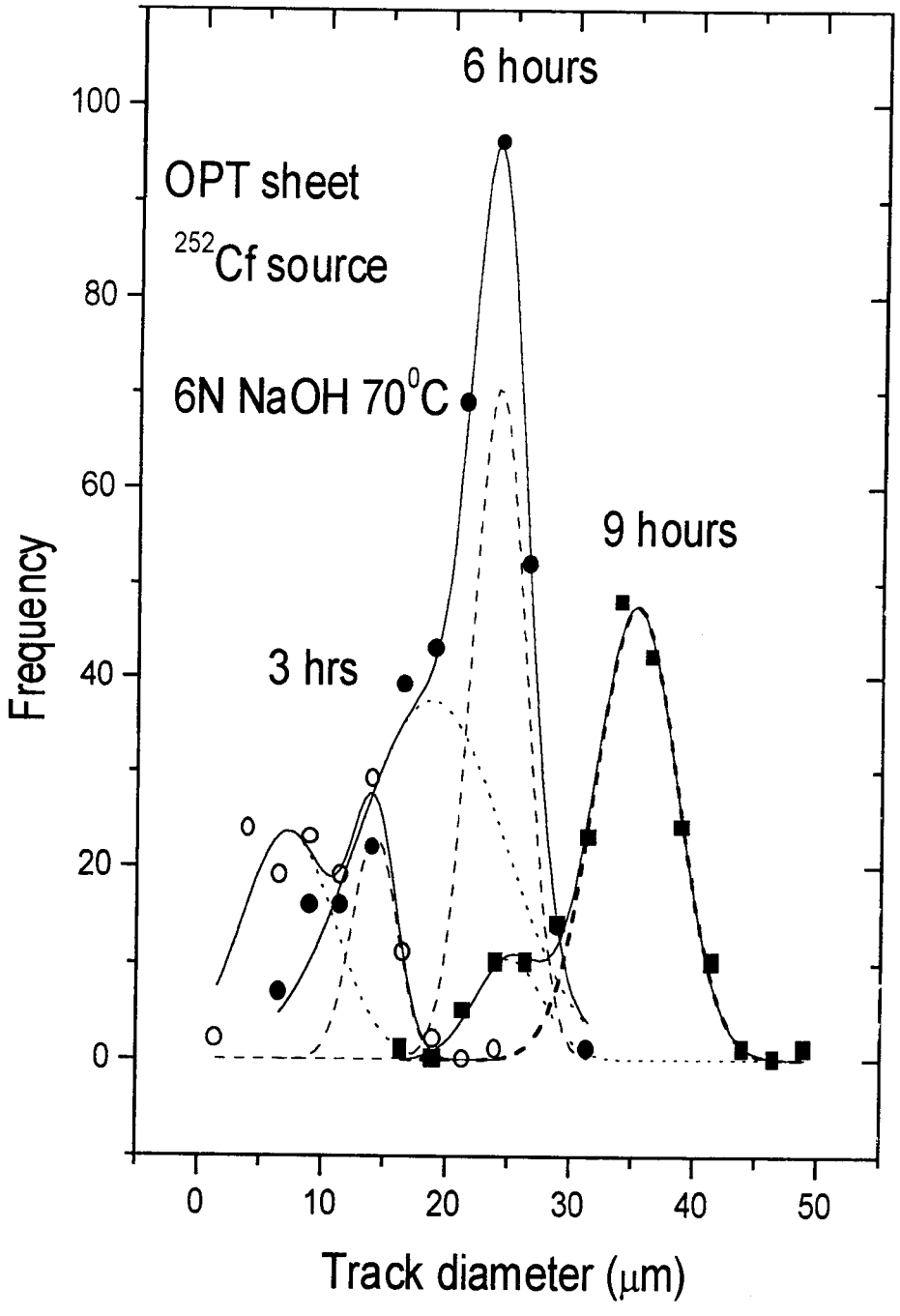

Fig 7.2 Track diameter distribution for 252Cf fission fragments in OPT sheet

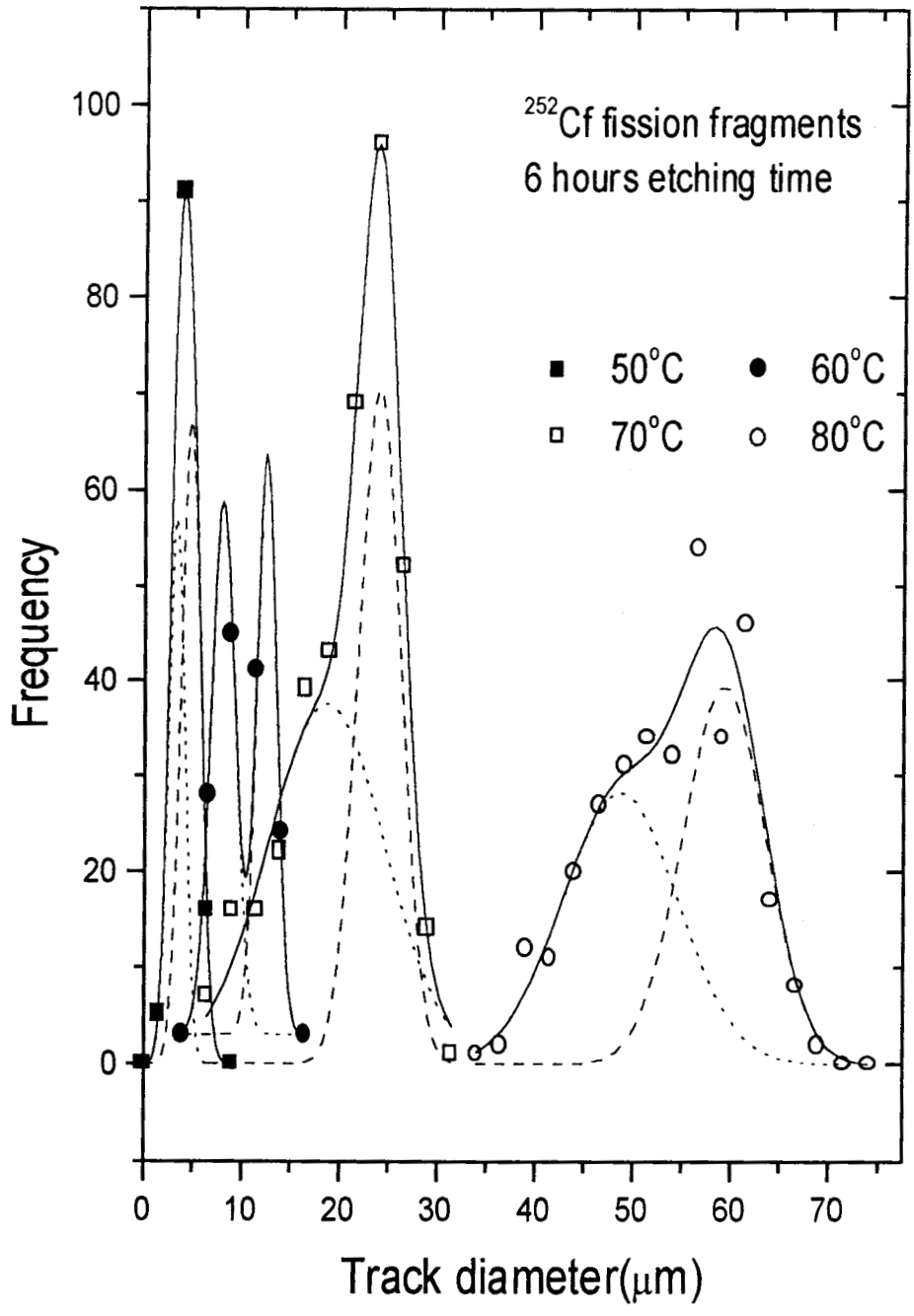

Fig 7.3 Track diameter distribution for ^{252}Cf fission fragments in OPT sheet. Etchant 6N NaOH

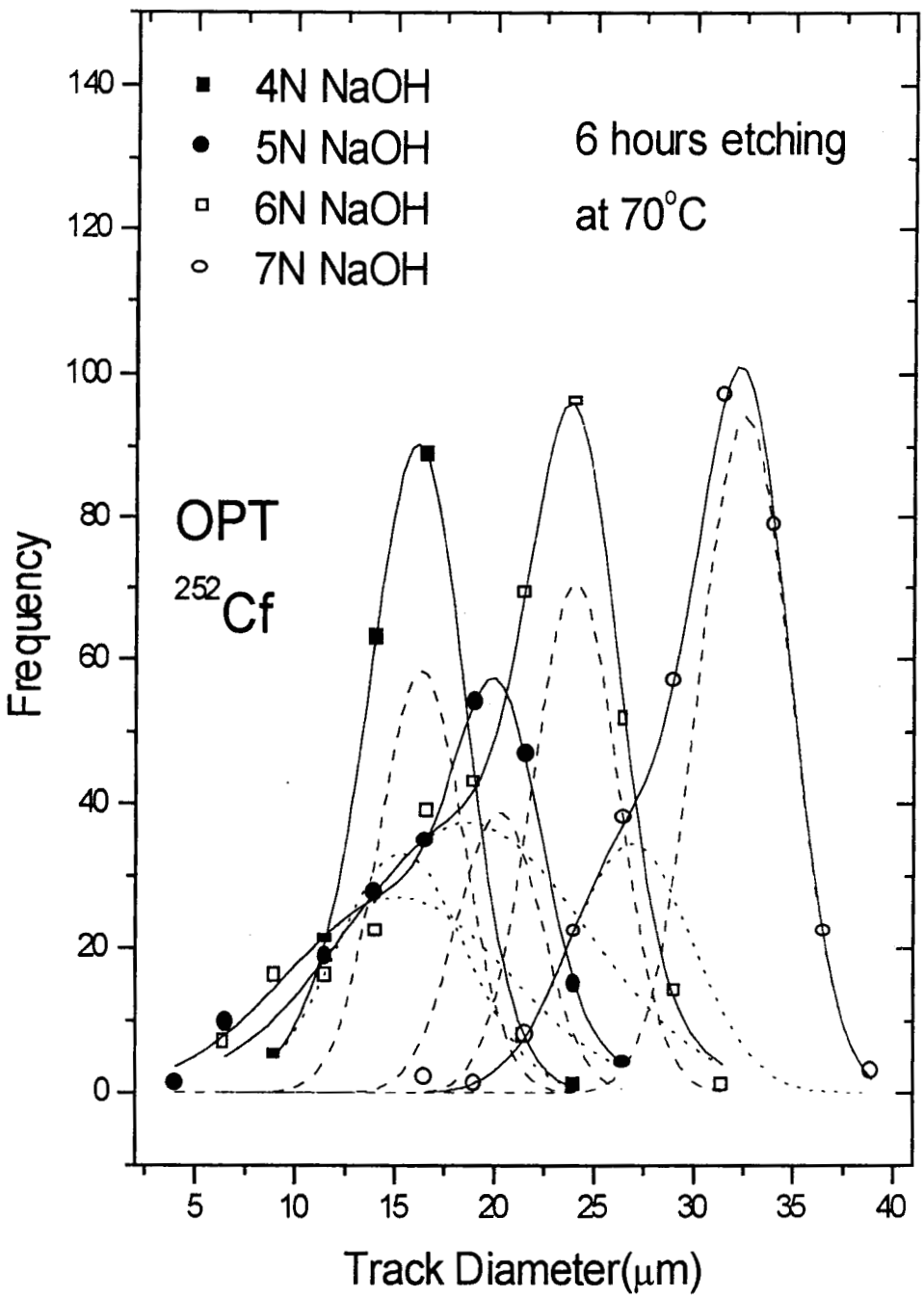

Fig 7.4 Track diameter distributions of ^{252}Cf fission fragments in OPT sheet for various etchant concentrations

most probably corresponding to the double humped mass distribution of the fission fragments. The lower peak cannot be due to 6.11 MeV alphas since their number far exceeds that of the fission fragments. Simple two peak Gaussian fitting was attempted. The results are indicated in the above plots by the solid curves for the fit and by the dashed curves for the individual peaks.

From the figures 7.2 & 7.3, we have extracted the velocity of track diameter evolution (V_d) at the higher maximum. These values have been also plotted in fig 7.1. as a function of 1 / T for 6 hours of etching in 6N NaOH. An effective activation energy for track etching the detector surface has been extracted from the plot. The value is 79 kJ mol^{-1}.

We have also compared the performance of the OPT sheets with that of CR-39 for fission fragments. Fig. 7.5 shows the track diameter distribution for the CR-39 detector, for similar etching conditions of 6N NaOH at 70°C, but for 10 hours of etching. Comparison with fig. 7.2. for OPT sheet reveals the better performance of the OPT sheets. However, the OPT sheets show interfering background for large etching times. In comparison, the etched tracks in CR-39 stand out against a clear background even at large etching times.

7.4. Investigations on X-ray film.

Some studies have been carried out on X-ray films also. Here, the X-ray films were first etched for half an hour in 6N NaOH at room temperature in order to remove the photosensitive coating. Then they were irradiated for 30 minutes with fission fragments from ^{252}Cf source. Then they were etched in 6N NaOH at 60^0C and70^0C for 3 hours, 6 hours and 9 hours. The bulk etch rates were determined by gravimetric method to be 0.88μm/hr and 1.69μm/hr respectively at 60^0C and 70^0C.The observed track diameter distributions are shown in fig 7.6 and 7.7 for the two etching temperatures.

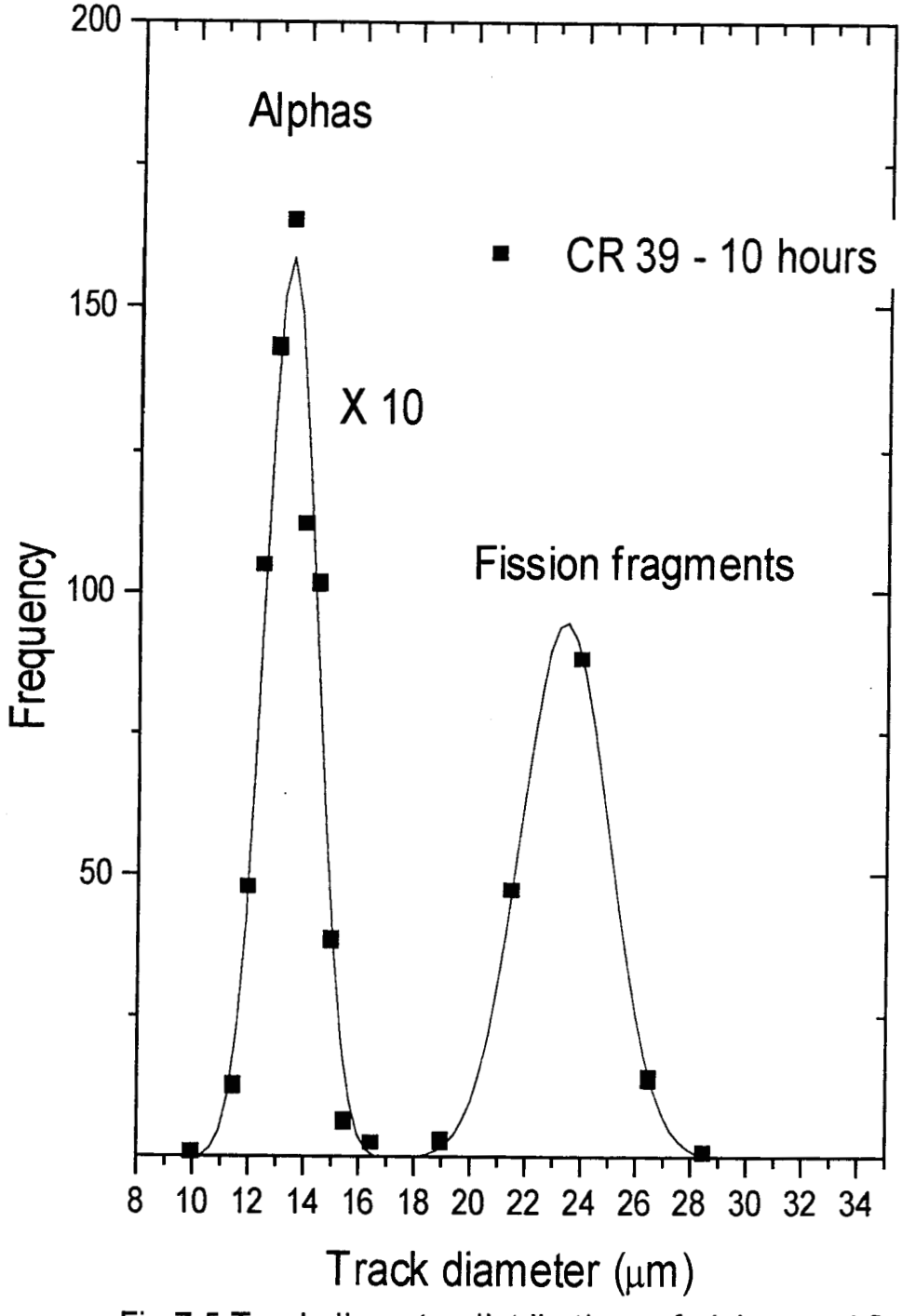

Fig 7.5 Track diameter distributions of alphas and fissio
fragments from ^{252}Cf in CR-39

Table 7.1 : Bulk etch rate variation with NaOH concentration (at 70°C)

Etchant concentration	Bulk etch rate (V_b) – μm/hour
4 N	1.13
5 N	1.37
6 N	1.75
7 N	2.70

Table 7.2 : Bulk etch rate variation with temperature of etching for 6N NaOH

Temperature of Etching (°C)	Bulk etch rate (V_b) – μm /hour
50	0.35
60	0.68
70	1.75
80	5.00

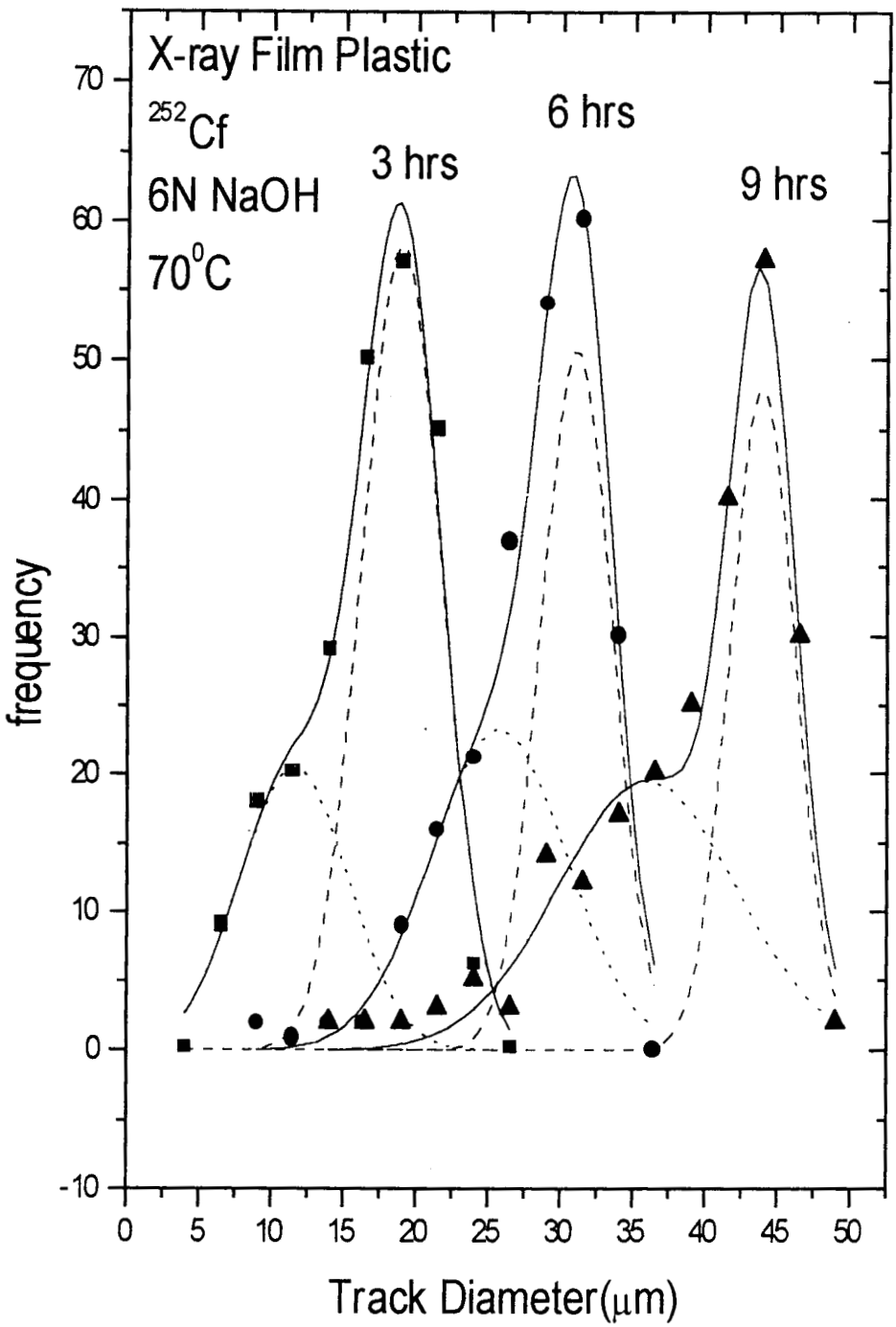

Fig 7.6 Track diameter distribution at different etching times for ^{252}Cf fission fragments in X-ray film.

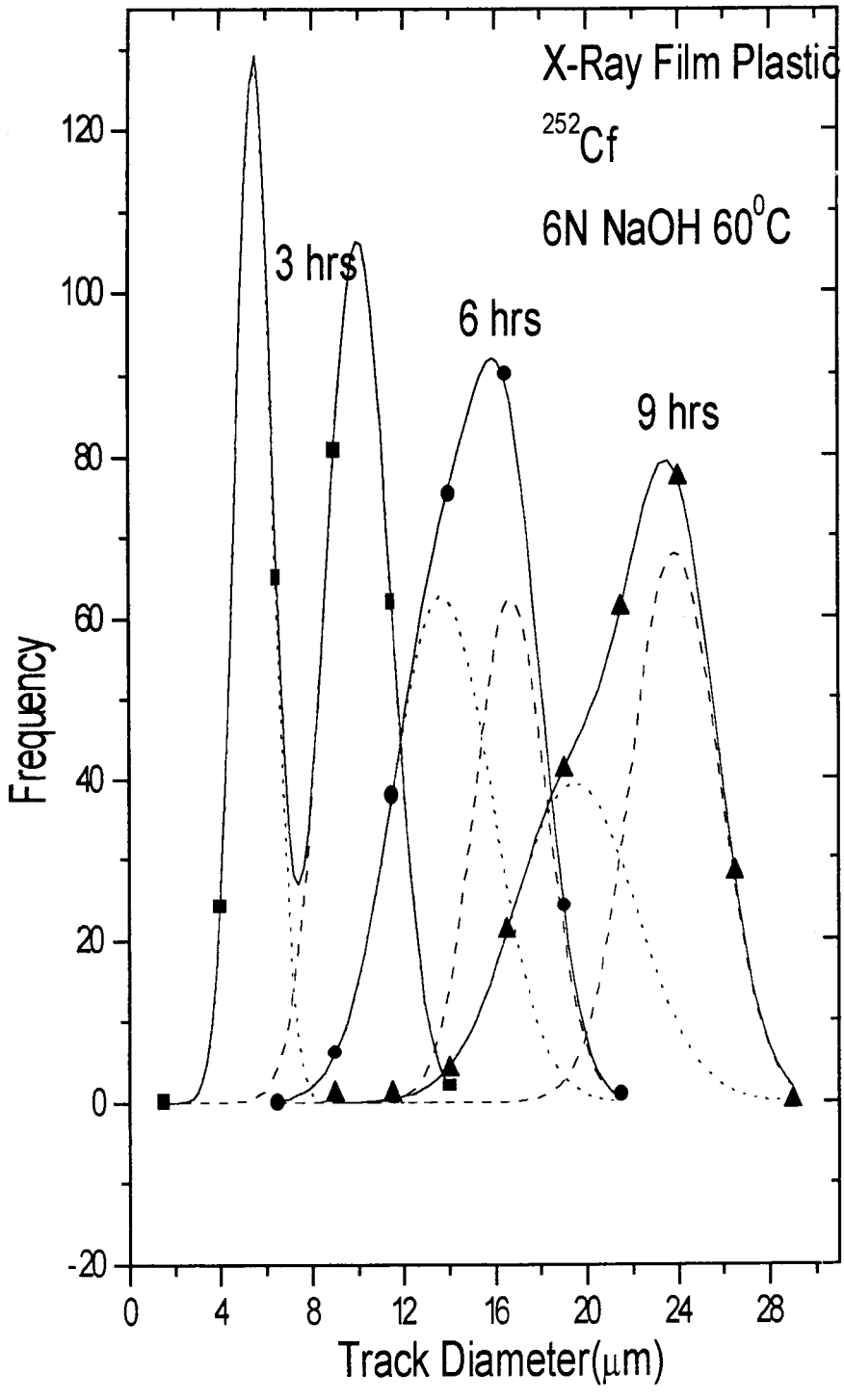

Fig 7.7 Track diameter distribution for ^{252} Cf fission fragments in X-ray film

References:

1. S.Ghosh, J.Raju, P.P.Choubey and K.K.Dwivedi, Nucl. Track Rad. Meas., 19 (1991)77
2. B. Basu, S. Banerjee, A. Mazumdar, S. Raha, S.K. Saha and D. Syam, Proceedings of 12th National Symp. On SSNTDs, Jalandhar (2001)
3. B. Basu, S. Banik, A. Mazumdar, S. Raha, S. Saha, S.K. Saha D. Syam and P. Vater, Proceedings of International Conference on SSNTDs, New Delhi (2002)
4. Antony Joseph, Ph.D.Thesis (1993 - Unpublished), University of Calicut, Kerala

NIBH510